Modelling the effect of wave action on sediment transport, morphological evolution and vegetation dynamics in coastal mangrove systems

(Barloventomagico, 2008)

Remco Belonje

Utrecht University

Modelling the effect of wave action on sediment transport, morphological evolution and vegetation dynamics in coastal mangrove systems

By

Remco Belonje

In partial fulfilment of the requirements for the degree of Master of Science in Marine Sciences at Utrecht University

October 2019

Utrecht

Contact rgbelonje@gmail.com
Supervisors Danghan Xie MSc.
Dr. Timothy Price
Dr. Barend van Maanen
Dr. Christian Schwarz

Utrecht University

Preface

This thesis is part of my Master of Science education in Marine Sciences at the Faculty of Geosciences at Utrecht University in Utrecht, the Netherlands. This research took place between August of 2018 and October of 2019 at the Department of Physical Geography. I would like to thank Danghan Xie for his supervision during the entire research and for showing me all the intricacies of Delft3D and his vegetation model. I would like to thank Barend van Maanen and Christian Schwarz for their supervision during the first phase of this research, and Timothy Price for his supervision during the final phase of this research.

Abstract

Mangrove forests are dominant ecosystems covering the intertidal zone of shorelines at tropical and subtropical latitudes. They provide valuable ecosystem services and functions, such as carbon sequestration and coastal protection. However, mangrove forests are being threatened by human activity and climate change, reducing the resilience of the ecosystem. Gaining further understanding about the hydro-morphodynamic processes and vegetation dynamics governing mangrove systems will prove essential in governing and protecting these ecosystems.

As mangrove forests are located on the coast, they are subject to wave action. While much research has gone into how mangroves attenuate waves, little research has gone into how wave action affects the development of mangrove coasts. Wave action has a significant effect on the coastal hydro-morphodynamics, which affect mangrove forest resilience and development. Therefore, research on the interactions between wave action and mangrove system development will prove beneficial in gaining further understanding on the functioning of mangrove ecosystems.

A hydro-morphodynamic model is used to study the effect of wave action on mangrove coasts. The model simulates bio-geomorphic feedbacks between mangrove vegetation and coastal hydro-morphodynamic processes. The approach uses the Delft3D-FLOW hydro-morphodynamic model including the roller model simulating waves, and a dynamic vegetation model in MATLAB.

Forty model scenarios are run, with three variables changing between model runs: wave height, vegetation presence and sea level rise. Four different wave height scenarios are included: no waves, small waves with a significant wave height of 0.3 m, medium-sized waves with a significant wave height of 0.5 m and large waves with a significant wave height of 1.0 m. For each of these wave heights, two scenarios are run with varying vegetation presence. One scenario is run including vegetation and one scenario is run excluding vegetation. To conclude, five different sea level rise scenarios are considered for each wave height and vegetation presence scenario. These scenarios consist of no sea level rise, slow linear sea level rise, fast linear sea level rise, slow exponential sea level rise and fast exponential sea level rise.

The results show that wave action has a significant effect on the hydro-morphodynamics and vegetation dynamics of the mangrove system. Waves increase the bed shear stress and the suspended sediment concentration, which enhance the erosion and sedimentation, respectively. They also transport sediment from the seaward boundary towards the coast through Stokes drift. The balance between erosion and sedimentation is influenced by the wave height. Small waves cause coastal progradation, medium-sized waves can cause either coastal progradation or coastal regression, while large waves cause coastal regression.

Mangrove vegetation affects the hydro-morphodynamics through two processes. Firstly, the vegetation traps sediment through the dampening of currents, which enhances sedimentation within the mangrove forest. Secondly, it influences the tidal asymmetry. This increases the ebb-tidal dominance, which enhances erosion. Which of these processes is dominant depends on the wave height. While without waves the presence of vegetation inhibits coastal progradation, it has the opposite effect when medium-sized waves are introduced to the system.

Mangrove vegetation only survives within a specific relative hydroperiod, which is governed by the amount of time a location is inundated relative to the amount of time it is dry. Because waves cause increased coastal progradation, the bed level at a location changes faster than without waves, and the relative hydroperiod changes with it. This causes vegetation to get less time to mature while a location contains its optimal hydroperiod. Through this mechanism, waves put additional stress upon growing vegetation, with higher waves causing lower vegetation number and total vegetation biomass. However, this affects small trees relatively more than large trees, since smaller trees are more vulnerable. This causes the average vegetation biomass to increase under the influence of wave action.

Sea level rise influences the coastal hydrodynamics by increasing the water depth. The faster the sea level rises, the more it affects the morphological change, increasing the peak bed level. Whether the sea level rise is linear or exponential influences the final shape of the bed profile, changing the curvature of the plateau. In the current model set-up, the sediment supply is sufficient for the mangrove system to keep up with all tested sea level rise scenarios, which means the vegetation is not significantly affected by sea level rise.

In conclusion, wave action, mangrove vegetation and sea level rise all affect the development of the coastal system. However, their contributions are not equal. Wave action affects the coastal dynamics the most, followed by the mangrove vegetation and finally sea level rise. Waves also have a significantly larger effect on the vegetation parameters than sea level rise. This information can be used to improve management strategies for coastal mangrove systems, both in the present and when devising strategies for the future, when climate change will become more important.

Table of Contents

List of figures

List of tables

1 Introduction

1.1 Problem description

Mangroves are woody plants that can survive in brackish waters, living on the coasts at tropical and sub-tropical latitudes, where they inhabit the intertidal zone. Mangrove systems provide valuable ecosystem functions and services, including their ecological value (Kathiresan & Bingham, 2001), their economic value (Leong et al., 2005), carbon sequestration (Alongi, 2012; Laffoley & Grimsditch, 2009) and coastal protection (Alongi, 2008; Thampanya et al., 2006). Since hard coastal defense structures are proving to be damaging to ecosystems (Airoldi et al., 2005) and becoming unsustainable to maintain, a shift to the use of natural "soft" coastal defense systems like mangroves is being advised (Temmerman et al., 2013). However, these ecosystems are currently being threatened in multiple ways. Human activity is destroying large amounts of mangrove systems in order to make room for aquaculture, agriculture and urbanization, reducing their global area by approximately 35% between the early 1980s and 2000s (Valiela et al., 2001). Climate change is also a threat to mangroves, with sea level rise threatening to drown the systems if sediment accretion does not keep up with the rising water levels (Schuerch et al., 2013). Apart from sea level rise, climate change also causes changing wave climates (Hemer et al., 2013), changing the hydrodynamics within mangrove systems. Further research into the sediment dynamics, morphodynamics and vegetation resilience of mangrove systems will prove to be essential in proper management and conservation of these precious ecosystems.

Coastal mangrove vulnerability is highly dependent on the hydro-morphodynamics, which are affected by the vegetation dynamics. There are multiple different aspects to sediment dynamics, morphodynamics and vegetation within mangrove systems. Tidal currents (Anthony, 2004), river supply (Hopkinson et al., 2018), waves, anthropogenic influences (Willemsen et al., 2015) and vegetation dynamics (Furukawa & Wolanski, 1996) all influence the sediment dynamics in these systems, and understanding their individual roles will prove vital in understanding the entire system. Vegetation influences the hydrodynamics through flow attenuation, while mangrove colonization, growth and mortality are determined by environmental factors such as the inundation regime and resource availability. While the effects of most of these factors have been studied extensively, there is a noticeable knowledge gap on the effect of waves on mangrove systems. In order to fill this knowledge gap and to further increase understanding of the interaction between wave action and mangrove systems, this study will focus on the effect of waves on mangrove systems.

Waves influence the hydrodynamics, sediment transport and morphodynamics of coastal systems. These factors influence the vegetation dynamics of mangroves, so understanding the role of wave action in mangrove systems on the hydrodynamics, sediment transport and morphodynamics will increase our knowledge about the development of mangrove systems. Since waves threaten wetland coasts, more information about the effect of waves on mangrove systems will prove helpful in developing mangrove preservation and governance strategies. Prior studies on waves and mangroves have shown that mangroves reduce the wave height and thus the amount of energy as waves travel through them, because of the friction between the water and the mangrove roots, trunks, leaves and branches (McIvor et al., 2012). However, most of these studies only studied waves with a wave height lower than 70 cm. This means that there is a significant knowledge gap on the interaction between mangroves and waves with a wave height higher than 70cm. Mazda et al. (1997) found that young mangroves hardly reduce wave energy, while mature mangroves have a significant effect.

Most these studies have focused on the effect of mangroves on waves, while the effect of waves on mangrove development is less studied. The effect of waves on coastal profile evolution has been studied for salt marsh systems, where waves have been shown to drive lateral retreat and vertical accretion (Best et al., 2018). However, the effect of waves on coastal profile evolution in mangrove systems is less studied. Previous research has shown that disturbance due to waves has a negative effect on vegetation cover (Riis & Hawes, 2003). However, this has not been studied for mangroves in particular. These gaps in knowledge show that further research on the effect of waves on hydro-morphodynamics in mangrove systems is needed to improve the knowledge base for proper management of coastal mangrove systems.

1.2 Research aim

The primary aim of this research is to determine the effect of wave action on sediment dynamics, morphology and vegetation dynamics in coastal mangrove systems. The secondary aim of this research is to explore the underlying processes dictating the relations between waves, sea level rise and coastal mangrove systems. Bio-geomorphic feedbacks between mangroves, coastal morphodynamics, tides, waves and sea level rise will be studied by using a comprehensive bio-morphodynamic model.

To study the interactions between waves and the mangrove system, model simulations will be run featuring different scenarios with varying wave height, vegetation presence and sea level rise. Gaining more understanding on the response of mangrove systems to waves in different situations can provide new insights on the biophysical feedbacks in such systems. This will prove useful in assisting the development of long-term sustainable coastal wetland management, taking climate change and sea level rise into account. As mangroves serve an important role in the ecosystems and protection of tropical and sub-tropical coasts, gathering more knowledge about how wave action affects them could prove beneficial for the governance of mangrove systems.

1.3 Research questions

During this research, answers to the following research questions will be developed:

1. How does wave action affect the hydro-morphodynamics in mangrove systems?
    a. How does wave height affect the hydrodynamic processes?
    b. How does wave height influence the sediment transport?
    c. How does wave height affect the coastal evolution?
2. How does wave action affect the vegetation dynamics in mangrove systems?
    a. How does wave height affect the amount of mangrove trees?
    b. How does wave height affect the vegetation biomass?
    c. How does wave height affect the changing vegetation dynamics of a mangrove forest through time?
3. How does wave action affect a coastal mangrove system in the presence of sea level rise?
    a. How does wave action affect the hydro-morphodynamics in a mangrove system in the presence of sea level rise?
    b. How does wave action affect the amount of mangroves and the vegetation biomass in the presence of sea level rise?
    c. How does wave action affect the resilience of a mangrove system influenced by different rates and types of sea level rise?

2 Background

2.1 Mangroves

Mangroves are woody plants that inhabit tropical and sub-tropical shorelines across the world (Figure 1), where they are subjected to continuous flooding (Hogarth, 2015). They have adapted to this environment through aerial roots, which allow them to obtain oxygen from the atmosphere and to distribute it to the waterlogged roots. Another function that these roots serve is to provide physical support (Steffens & Rasmussen, 2016).

Figure 1: Distribution of the world's mangrove forests in the year 2000. (Giri, et al., 2011)

The different species of mangroves can be distinguished in twelve genera belonging to eight different families (Waisel, 1972). Different mangrove species have different distinguishing features. One of the most important features that differs between mangrove species is the type of roots. Mangrove roots appear in various different shapes (Ng & Sivasothi, 2002):

- Pneumatophores. These are upward, erect appendages of the underground root system.
- Prop roots. These are roots that extend from the trunk and lower branches of the tree.
- Kneed roots. These are horizontal roots that periodically grow upwards and then loop downwards again.
- Plank roots. These are thick, wavy roots radiating out from the trunk base.

In Figure 2, a schematic example of different types of roots and the genera they belong to can be seen.

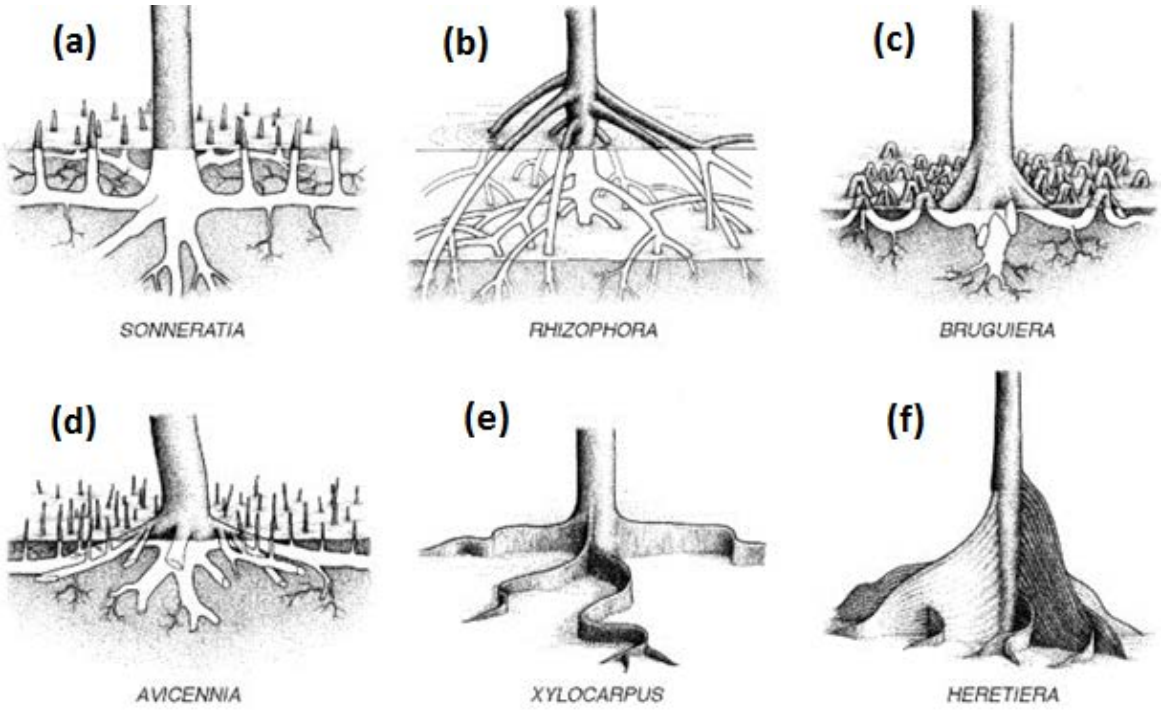

Figure 2: Different types of mangrove roots, with the genera to which they belong. Pneumatophores (a and d), prop roots (b), kneed roots (c), plank roots (e and f). (Göltenboth & Schoppe, 2006)

Different mangrove species have different properties, and thrive in different environments. These different preferences include salinity, soil type, nutrient content and predation. Since many of these preferences depend on the location on the coastal slope, zonation of mangrove species occurs. Zonation of mangrove species means that different parts of the coastal slope are dominated by different mangrove species, based on their optimal conditions (Alongi, 2002; Liu et al., 2018). Among these factors, the optimal environment for a specific species relies on the relative hydroperiod, which is the ratio between the amount of time a mangrove is inundated and the amount of time it is dry. The preferred relative hydroperiod differs between mangrove species. Since the relative hydroperiod in an intertidal environment depends on the location on the coastal slope, with higher locations being inundated less often, zonation occurs on the coastal slope, even if the other factors do not change. Changes in the sea level or in the coastal slope can cause these zones to shift.

The geomorphic setting of mangrove systems depends on three dominant features, namely rivers, tides and waves (Yuvaraj et al., 2014). These geomorphic settings can be classified in five major types, which can be seen in Table 1.

Table 1: Classification of mangrove geomorphic settings. Adapted from Yuvaraj et al. (2014).

Geomorphic setting	**Dominant feature(s)**	**Resulting structure**
River dominated, allochthonous	Rivers	Abandoned distributaries, finger-like mangrove protrusions.
Tide dominated, allochthonous	Tides	Numerous tidal creeks with funnel-shaped main river channel, subtidal shoals on river mouth.
Wave dominated barrier lagoon	Waves	Sand barrier with beach ridges and lagoons in the river mouth.
Composite-wave and river dominated	Waves, rivers	Adjacent lagoons near main river channel with sand beach ridges and salt tolerant species.
Drowned bed rock valley	Waves, tides	Open estuarine system, drowned bedrocks in coast, mangroves in river head.

Mangroves have been shown to influence the geomorphology. They influence the pattern of sedimentation, promoting accretion in order to create more favorable living conditions for themselves (Bird, 1986). This ability to trap sediment is affected by environmental factors, with mangroves being able to trap more sediment during the wet season than during the dry season (Van Santen et al., 2007). Sediment dynamics are important for the vegetation survival, with seedling survival showing to be extremely sensitive to surface erosion (Balke et al., 2013). Mangrove systems have shown to be very sensitive, showing noticeable mortality after only minor variation in their hydrological or tidal regimes (Blasco et al., 1996).

In this study, we consider the species *Avicennia germinans*, which is known by the common name "black mangrove". *Avicennia germinans* can reach a maximum height of 35 m, a maximum diameter of 140 cm at breast height and can live to be 300 years old (Chen & Twilley, 1998). It features pneumatophores (Figure 2d), and can have up to 10,000 pneumatophores per tree (Hogarth, 2007), with the pneumatophores having a diameter of 1 cm and a height of 15 cm (van Maanen et al., 2015). Its distributional range covers three continents: North America, South America and Africa (Figure 4). It typically occurs in the mid to high intertidal region of the coast. On intertidal slopes, *Avicennia germinans* survives best around mean water, and has trouble surviving around highest high water and lowest low water (Ellison & Farnsworth, 1993). Coastal profiles of *Avicennia* dominated coasts have shown to be similar to those of marshes, with a flat platform and a steep seaward edge (Bryan et al., 2017) (Figure 3).

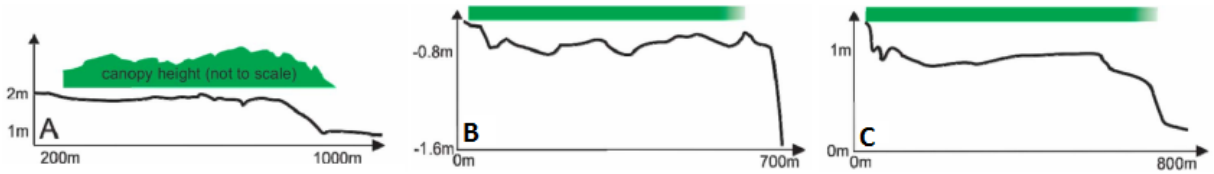

Figure 3: Examples of Avicennia-dominated coastal profiles. A: Firth of Thames, New Zealand. B: Hang Hai, Vietnam. C: Queensland, Australia. Adapted from Bryan et al. (2017).

Figure 4: The distribution of Avicennia germinans as of 2007. (Ellison et al., 2010)

2.2 Waves and tides

Wind and swell waves have shown to impact sediment dynamics in the coastal zone, suspending and transporting sediment. Wave-induced transport processes differ between non-breaking and breaking wave conditions. In general, net onshore sediment transport dominates in non-breaking wave conditions, while net offshore sediment transport dominates in breaking wave conditions (van Rijn, 1993). Under non-breaking waves, two transport components of the same order of magnitude affect the sediment transport: a high-frequency transport component, which is directed onshore, and a low frequency transport component, which is directed offshore. Under breaking waves, more processes are involved in sediment transport. Whether onshore or offshore sediment transport is dominant depends on the location in the surf zone and the type of breaking wave (van Rijn, 1993). Waves also cause sediment transport through Stokes drift, which transports water particles forwards in the direction of wave propagation (Stokes, 1847; van den Bremer & Breivik, 2017). In muddy coasts, waves weaken the bed, decreasing its erosion resistance and facilitating erosion. This generates a thin layer of fluid mud, with a very high suspended sediment concentration. Above this fluid mud layer, there is a significantly lower suspended sediment concentration (Maa & Mehta, 1987). Muddy bottoms have a larger rate of wave attenuation than rigid bottoms by an order of magnitude. The effect of the current on the rate of wave attenuation, in which opposing currents increase wave attenuation and following currents decrease wave attenuation, is larger for a muddy bottom than for a rigid bottom (Zhao et al., 2006).

Waves are important to include in morphodynamic models for a variety of reasons. The effects of waves include enhancing vertical mixing processes due to turbulence, inducing a net mass flux, generating long-shore currents and cross-shore set-up and enhancing the bed shear stress (Deltares, 2014). Wave action can be a significant source of coastal erosion, causing coastal regression (Pye & Neal, 1994). Large waves have shown to cause erosion on a macro tidal mudflat, while calm conditions have shown to cause accretion (Christie et al., 1999). Phuoc & Massel (2006) found wave intensity and tidal current velocity to be the most important drivers of suspended sediment concentrations in mangrove systems. However, they did not study the transport of this suspended sediment.

Most research considering the interactions between waves and mangroves focuses on the ability of mangroves to reduce wave height and energy in order to protect the coast. Mazda et al. (1997) found reductions of wave energy due to mangrove forests by up to 20% (Figure 5). Mangrove pneumatophores can dissipate the turbulent kinetic energy under waves, especially under breaking waves (Norris et al., 2017). However, dense pneumatophore canopies have also been found to enhance turbulence, enhancing sediment transport within mangrove systems (Norris et al., 2019). Mangroves have also shown to protect against more extreme events such as storm surges (Montgomery et al., 2019), cyclones (Das & Vincent, 2009) and tsunamis (Danielsen, et al., 2005; Kathiresan & Rajendran, 2005).

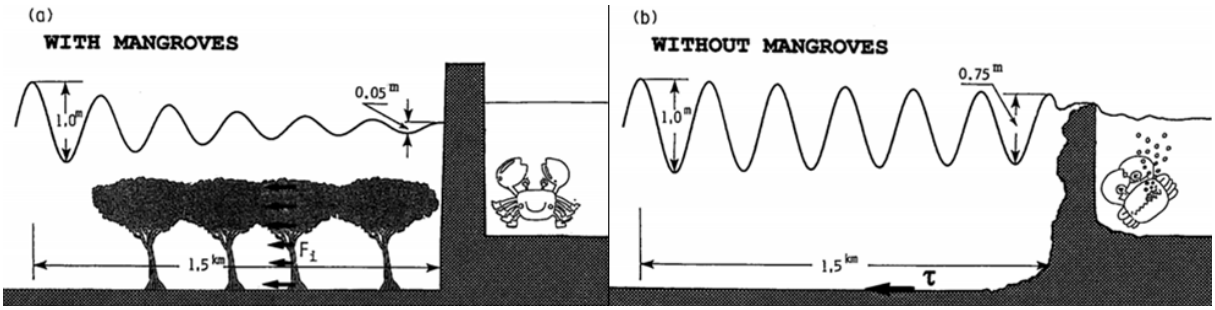

Figure 5: Differences in the effect of wave reduction between scenarios (a) with and (b) without mangroves (Mazda et al., 1997).

Another major factor influencing sediment dynamics in mangrove coasts is tides. Tidal currents transport sediment, with the net direction of this sediment transport being largely determined by the asymmetry of the tidal flows. This asymmetry can be flood- or ebb-dominated (Héquette et al., 2008). Tidal asymmetry is produced by the distortion of the tidal wave by the morphology (Dronkers, 1986). Tidal asymmetry affects the residual sediment transport mainly through a difference between the slack water periods before ebb and flood and a difference between the maximum currents during ebb and flood. The former mainly affects the fine fraction of the suspended load, while the latter mainly affects the coarse fraction of the suspended load (Dronkers, 1986).

Mangroves trap a significant amount of the sediment brought in by tidal currents (Furukawa et al., 1997). Sediment gets trapped by mangroves because of mangroves reducing tidal flows at low tide, and sites with two mangrove species have been shown to trap sediment more effectively than sites with only one species (Kathiresan, 2003). Removal of mangrove forests can cause enhanced erosion due to increased tidal flows after mangrove removal. This also affects coastal areas where no mangroves are present, which are adjacent to the area with the mangrove forest (Mazda, et al., 2002). Mangroves can attenuate tides (Horstman et al., 2019), but the degree to which mangroves are capable of attenuating tidal waves is dependent on the channelization. When there are many channels for the water to flow through, the vegetation does not significantly contribute to the flow resistance. However, even in such a situation mangroves can prove helpful, such as during flood events where the amount of water exceeds the capacity of the channels, forcing flow through the mangroves (Montgomery et al., 2018). Mangroves also affect tidal asymmetry in mangrove creek systems, with the drag force due to mangroves increasing the ebb flow dominant tidal asymmetry (Horstman et al., 2019), causing more sediment to be transported away from the coast in mangrove creeks (Mazda et al., 1995). However, neither of these studies included the effect of waves.

2.3 Climate change

Climate change will cause the sea level to rise in the near future (Intergovernmental Panel on Climate Change, 2014). Sediment accretion within mangrove coasts is important for keeping up with sea level rise. Mangroves need a higher rate of accretion than the rate of sea-level rise, which depends, among other factors, on the supply of sediment (Krauss, et al., 2010). For the "business-as-usual" RCP8.5 climate change scenario, the IPCC expects a rate of sea level rise of 8 to 16 mm yr^{-1} between 2081 and 2100, compared to 2.0 mm yr^{-1} between 1971 and 2010 (Intergovernmental Panel on Climate Change, 2014).

This means that mangrove systems will have to build soil elevation in order to survive under a faster rising sea level. Elevation gain depends on a combination of biological and physical feedbacks (Kirwan & Megonigal, 2013) (Figure 6). These feedbacks include the slowing down of water velocities by vegetation, which increases mineral sedimentation, and the captured minerals promoting vegetation growth. Because sediment needs to be present in the system to be captured, the response of mangrove systems to rising sea levels depends on the input of sediment. If there is enough sediment input to keep up with the rising sea level, then mangroves are able to survive, while they risk drowning if this is not the case (Woodroffe, 1990). The ratio between sediment accretion and the relative sea level change is very important for mangrove systems, and this sediment can either be mineral or biotic material (Krauss, et al., 2013). This ratio determines whether the bed level of the mangrove system keeps up with sea level rise, or lags behind. If the mangrove system cannot keep up with sea level rise, the relative hydroperiod of the system will change. Mangrove systems in which the sediment accumulation cannot keep up with sea level rise suffer a reduction in the mangrove cover with rising sea level (Ellison, 1993). Because of declining sediment delivery, many mangrove systems are expected not to be able to keep up with sea level rise (Lovelock, et al., 2015). However, process-based models predict that mangroves and other marsh systems are less vulnerable to sea level rise than predicted by current assessment methods. There are two reasons for this overestimation of vulnerability. Static landscape models tend to fail to consider biophysical feedback processes between tidal inundation and increased vertical accretion that accelerate soil building with sea level rise, in which increased tidal inundation causes more frequent and longer periods of mineral sediment settling and enhanced vegetation growth. Meanwhile, point-based assessments ignore the potential of inland migration of marshes into adjacent uplands (Kirwan et al., 2016). When enough sediment is available to allow mangrove systems to keep up with sea level rise, and the mangrove systems are relatively undisturbed from human activities, climate change can cause expansion of mangrove forests. This expansion can be in either a seaward or a landward direction, with seaward expansion occurring due to an increase in river discharge causing an increase in sediment delivery to the nearshore environment, while landward expansion occurs due to an increase in rainfall and sea level rise (Asbridge et al., 2016).

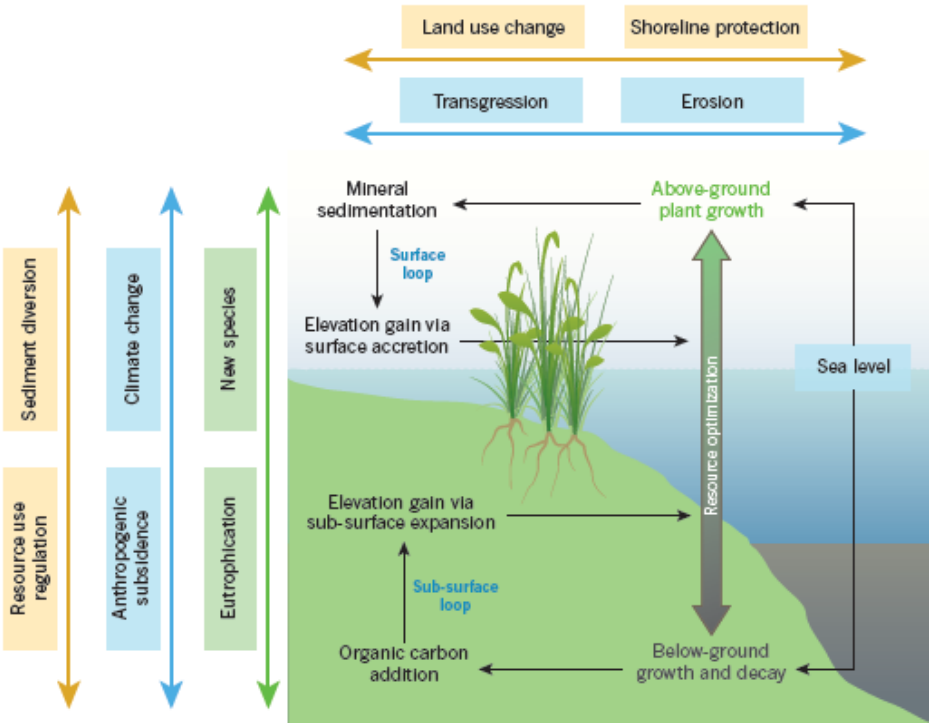

Figure 6: Feedbacks on vertical elevation change in wetlands. These feedbacks are affected by local factors (green), large-scale factors (blue) and political, social and economic factors (orange) (Kirwan & Megonigal, 2013).

Climate change also affects waves, showing a consistent projected decrease in annual mean significant wave height for over 25% of the global ocean area and a projected increase for over 7% of the global ocean area (Hemer et al., 2013). While the area of projected increase is mostly located in the Southern Ocean, the area of projected decrease is located in the other ocean basins, particularly at subtropical latitudes (Figure 7). This change in wave climates means that mangrove systems will be subjected to less wave action, possibly having significant effects on mangrove system development. The decrease in wave height is related to changes in the wind climate (Charles et al., 2012), the specific changes of which will differ on a regional scale. Conversely, other research has shown an increase in wave height, caused by sea level rise (Vu et al., 2018).

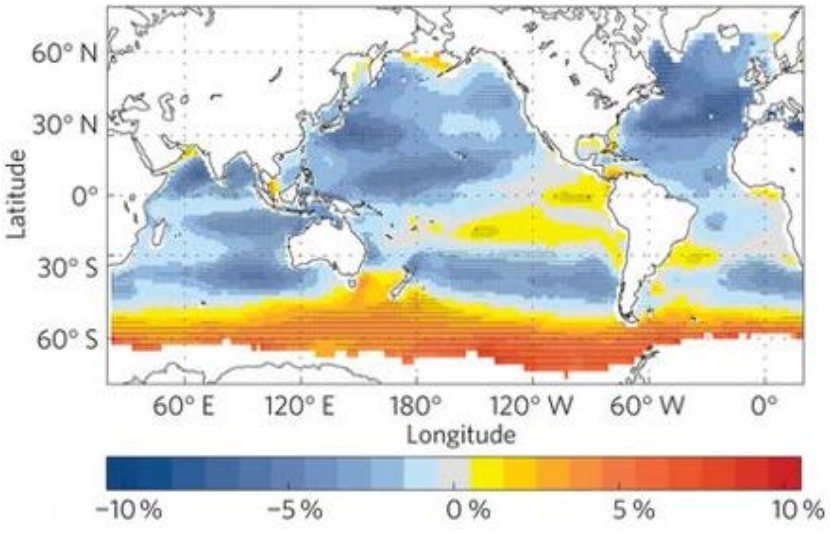

Figure 7: Averaged projected changes in annual mean significant wave height for 2070-2100 compared to 1979-2009 (Hemer et al., 2013).

2.4 Bio-morphodynamic modelling

The feedbacks between morphodynamics, hydrodynamics and vegetation are important to consider when modelling scenarios featuring vegetation. Vegetation affects flow resistance, which affects the morphodynamics, while the morphology affects the inundation regime, which affects the vegetation dynamics. Bio-morphodynamic modelling is a type of numerical modelling which dynamically integrates changes in both hydro-morphology and vegetation, and makes these interact with each other. As opposed to static vegetation, where changes in vegetation are not integrated, dynamic vegetation integration into hydro-morphodynamic modelling allows for more realistic behavior and results, providing results that more closely resemble situations found in the field (Oorschot et al., 2016).

Because bio-morphodynamic modelling with dynamic vegetation provides more realistic results than static vegetation modelling, it is an important tool in providing accurate results in situations where ecological feedbacks are important. Bio-morphodynamic models work through communication between hydrodynamic, morphodynamic and biological parts of the larger model (Figure 8). By having these different parts communicate with each other continuously, realistic feedbacks can be integrated in the model results. Examples of feedbacks integrated within bio-morphodynamic models include reduction of biomass through uprooting by flow and vegetation providing flow resistance in rivers (Perona et al., 2014).

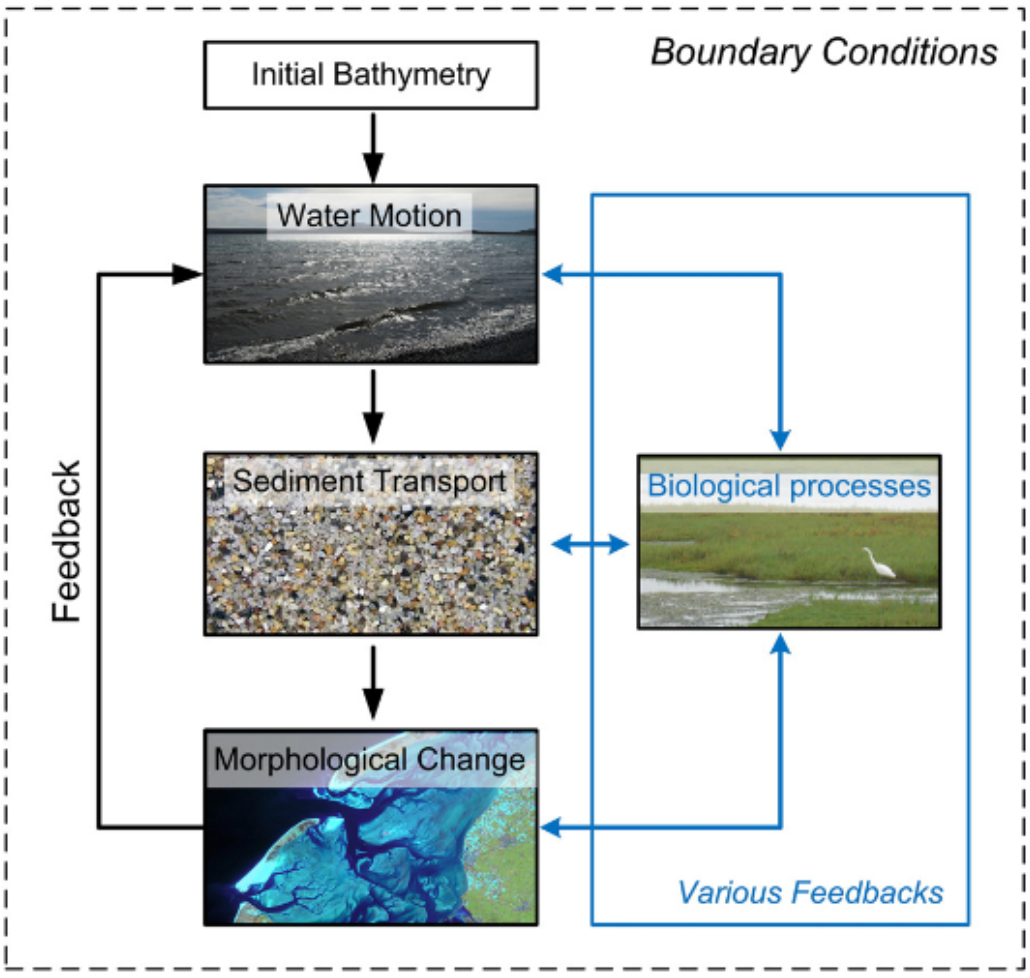

Figure 8: Example of a bio-morphodynamic model with the feedbacks between the different parts (Coco et al., 2013).

Bio-morphodynamic modelling has been applied to a variety of situations, including rivers (Perona et al., 2014; Francalanci et al., 2013; Bärenbold et al., 2016), tidal flats (Zhou et al., 2016), mangroves (van Maanen et al., 2015) and salt marshes (Best, et al., 2018). Development of accurate bio-morphodynamic models for mangroves is still a work in progress, with room for progress in different areas. Among these areas are the hydrodynamics in pneumatophore canopies, where the current models have proven to have significantly deviating turbulence characteristics compared to observations from flume experiments (Horstman et al., 2016). Research on bio-morphodynamic modelling is at a more advanced stage for salt marshes than for mangrove systems, which as such can serve as inspiration for applying bio-morphodynamic modelling to mangrove systems. A salt marsh is a type of ecosystem that is similar to mangroves. Salt marsh systems also occur on coastlines in the intertidal zone, salt marshes are subject to similar threats as mangrove systems and both provide coastal protection. There are three main differences between the two systems. The first is the latitude at which they can be found, with mangroves appearing at tropical and sub-tropical latitudes while salt marshes appear at temperate and high latitudes. The second is the vegetation present in the systems, with salt marshes mostly containing herbaceous or low shrubby vegetation, while mangrove systems contain mostly trees (Chmura, 2009). The third is that mangroves are capable of growing on completely waterlogged soils, which allows them to inhabit lower positions relative to mean high-water level compared to salt marshes (Augustinus, 1995).

Schuerch et al. (2013) studied the effect of changing storm patterns on the ability of salt marshes to keep up with sea level rise, finding that an increase in storm frequency helps salt marshes survive all but the fastest sea level rise scenarios until at least 2100. This is because during storms, deep flooding of the marshes and resuspension of sediment in adjacent areas cause an increased sediment supply to the marshes. Waves are the main driver for lateral retreat of salt marshes, transporting sediment landward and heightening the platform levels, with higher waves causing more lateral retreat (Best et al., 2018). The sediment supply from lateral edge erosion of salt marshes could be essential in helping vertical sediment accretion of salt marshes keep up with sea level rise (Hopkinson et al., 2018). Whether this is the same for mangrove systems cannot be established without further research.

3 Methods

In this study, mangrove behavior and landform evolution through the complex interactions between hydro-morphodynamics and vegetation characteristics are simulated. In this section, an overview of the models used in the study will be given in section 3.1. A mangrove system with waves is modelled by using an open-source hydro-morphodynamic model, Delft3D (Deltares, 2014). It uses the Delft3D-FLOW module for simulating hydrodynamics and morphodynamics with the surf beat/roller model simulating waves (Reniers et al., 2004), described in section 3.2. A dynamic vegetation model that is controlled by a MATLAB script is coupled to Delft3D, which is described in section 3.3. Finally, the set-up of the models used in this study is described in section 3.4.

3.1 Model description

The model consists of a hydro-morphodynamic model in Delft3D-FLOW and a dynamic vegetation model in MATLAB. The dynamic vegetation model, which is used to convey the dynamic mangrove growth, is based on the model described in van Maanen et al. (2015). The model used in this study includes the equations used for mangrove growth, biomass stress, inundation stress and the number of pneumatophores from van Maanen et al. (2015), with the specific parameters changed to resemble the characteristics of *Avicennia germinans*. The complete model takes into account hydrodynamics including externally forced waves and tides, sediment dynamics, morphology and vegetation (Figure 9). With each time step, the hydrodynamics, erosion, deposition and resulting bathymetry are calculated. With every ecological time step of one month, the change in stresses and their effects on the vegetation colonization, growth and mortality are calculated. Subsequently, the changed vegetation parameters are input back into the model, where their effect on the flow regime is considered in the hydrodynamic calculations.

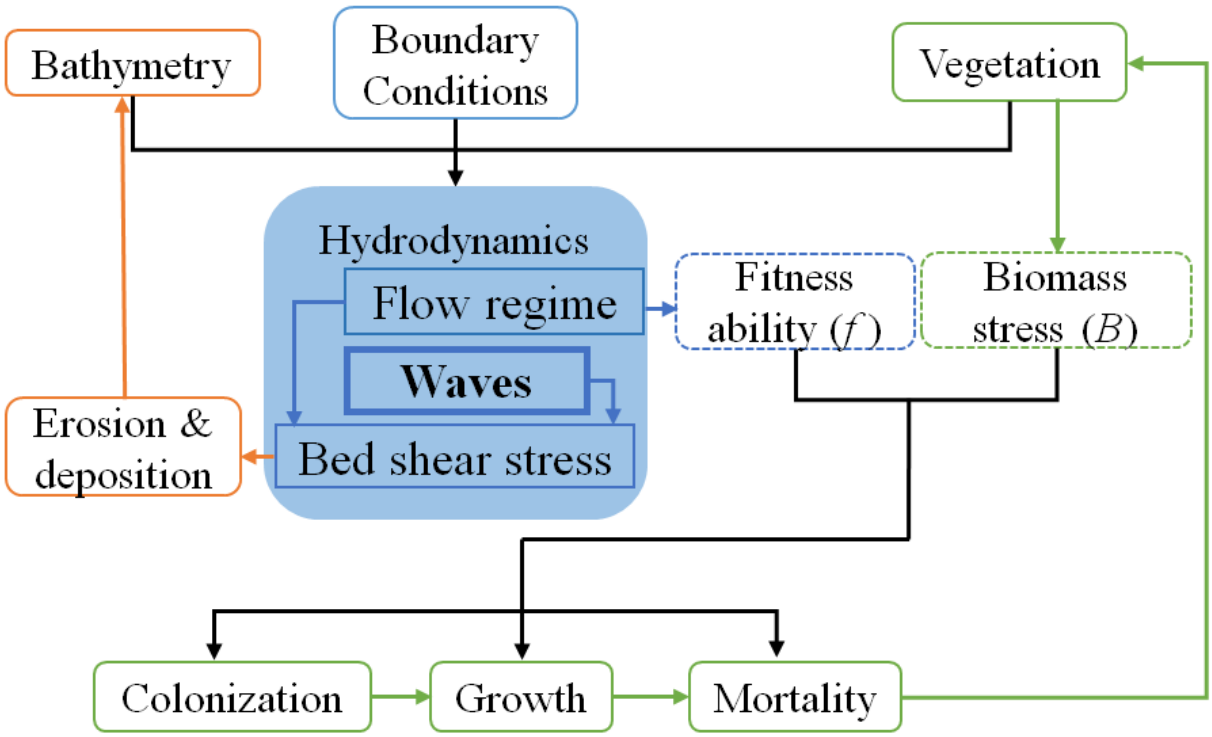

Figure 9: Schematic description of the different parts of the model. Adapted from (Xie, 2018) with added waves.

Tides are simulated through a harmonic boundary condition, while waves are simulated by the roller model. Wave action is an important part of near-shore processes in the model because of a variety of factors (Deltares, 2014). Waves generate turbulence, enhancing vertical mixing processes. Waves also generate a net mass flux through Stokes drift and generate long-shore currents and cross-shore set-up through variations in the wave-induced radiation stress. Finally, wave action enhances the bed shear stress. While waves have shown to be damped by vegetation (Mazda et al., 1997), this process is not included in the roller model (Best et al., 2018).

3.2 Hydro-morphodynamic model

Delft3D-FLOW models the hydrodynamics and morphodynamics of the system. Because it is a one-dimensional model, only x-direction processes are considered. The flow field is obtained through solving the shallow water equations (Zhou et al., 2016):

$$\frac{\partial \eta}{\partial t} + \frac{\partial (hu)}{\partial x} = 0 \tag{1}$$

$$\frac{\partial u}{\partial t} + u\frac{\partial u}{\partial x} = -g\frac{\partial \eta}{\partial x} + v\frac{\partial^2 u}{\partial x^2} - g\frac{u|u|}{C_z^2 h} \tag{2}$$

Where u is the depth-averaged velocity in m/s, t is the time in s, h is the water depth in m, η is the water level in m, v is the horizontal eddy viscosity coefficient in m^2/s, C_z is the Chézy friction coefficient in m$^{1/2}$/s and g is the gravitational constant in m/s^2. The bed shear stress consists of a tide-induced (τ_c) and a wave-induced bed shear stress (τ_w), both in Pa (Deltares, 2014):

$$\tau_{max} = \tau_w + \tau_c \tag{3}$$

In which the wave-induced bed shear stress is calculated as follows:

$$\tau_w = \frac{1}{4}\rho f_w \left(\hat{U}_\delta\right)^2 \tag{4}$$

Where ρ is the density of water in kg/m^3, f_w is the total wave-related friction factor and $\hat{U}_\delta$ is the peak orbital velocity at the bed in m/s, which is defined as follows (Van Rijn L. C., 1993, 2012):

$$\hat{U}_\delta = \frac{\pi H_s}{\mathrm{T}_p \sinh(2\frac{\pi}{L}h)} \tag{5}$$

Where H_{rms} is the root mean square wave height and T_p is the peak wave period in s. Both of these parameters are user-defined as the values shown in Table 4. L is the wave length in m, and h is the water depth in m. The total wave-related friction factor is calculated as follows:

$$f_w = \exp[-6 + 5.2\left(\frac{\hat{A}_\delta}{k_{s,w}}\right)^{-0.19}] \tag{6}$$

Where $k_{s,w}$ is the wave-related roughness in m, which is related to the estimated ripple height. $\hat{A}_\delta$ is the peak orbital excursion at the bed in m, which is calculated as follows:

$$\hat{A}_\delta = \frac{T_p \hat{U}_\delta}{2\pi} \tag{7}$$

The tide-induced bed shear stress is calculated as follows:

$$\tau_c = \frac{\rho g u^2}{C_z^2} \tag{8}$$

The model features cohesive sediment. The transport of this sediment is simulated by the following advection equation:

$$\frac{\partial (ch)}{\partial t} + \frac{\partial (uch)}{\partial x} = Q_{mud,e} - Q_{mud,d} \tag{9}$$

In which c is the depth-averaged sediment concentration in kg/m^3, and $Q_{mud,e}$ and $Q_{mud,d}$ are respectively the erosion and deposition fluxes, given by the Partheniades-Krone formulations:

$$Q_{mud,e} = M_e(\frac{\tau_{max}}{\tau_{cr,e}} - 1) \text{(if } \tau_{max} > \tau_{cr,e}\text{, else } Q_{mud,e} = 0) \tag{10}$$

$$Q_{mud,d} = w_s c(1 - \frac{\tau_{max}}{\tau_{cr,d}}) \text{ (if } \tau_{max} < \tau_{cr,d}\text{, else } Q_{mud,d} = 0) \tag{11}$$

Where M_e is the erosion parameter in kg/m^2/s and w_s is the settling velocity in m/s. Because $\tau_{cr,d}$ is set to a very large value, equation (11) can be simplified to:

$$Q_{mud,d} = w_s c \text{ (if } \tau_{max} < \tau_{cr,d}\text{, else } Q_{mud,d} = 0) \quad (12)$$

Bed level change is computed the following way:

$$(1 - \epsilon_p)\frac{\partial z_b}{\partial t} = \frac{1}{\rho_s}(Q_{mud,d} - Q_{mud,e}) \quad (13)$$

Where ϵ_p is the bed porosity and ρ_s is the density of the sediment in kg/m^3. Bed change is enhanced by the morphological factor, which increases the morphological changes during one simulated tidal cycle by the value of said factor (Deltares, 2014).

The effect of waves is simulated in the model through the surf beat/roller model. This extension of Delft3D-FLOW was developed to simulate the effect of short waves on long bound waves (Tajziehchi, 2006). The roller model uses the peak frequency and wave direction of the short waves and models the forcing of these waves on the bound waves. For this, it uses a short wave spectrum input file containing wave height, period and direction. These settings can be found in Appendix A1. The roller model only models the wave energy on the group scale, proportional to the square of the wave envelope (Reniers et al., 2004). In the current model formulation, the roller model bed friction is not affected by the presence of vegetation (Best et al., 2018). The manner in which the roller model calculates morphological change from wave energy is depicted in Figure 10. Because our model is one-dimensional, we only consider processes in the cross-shore direction.

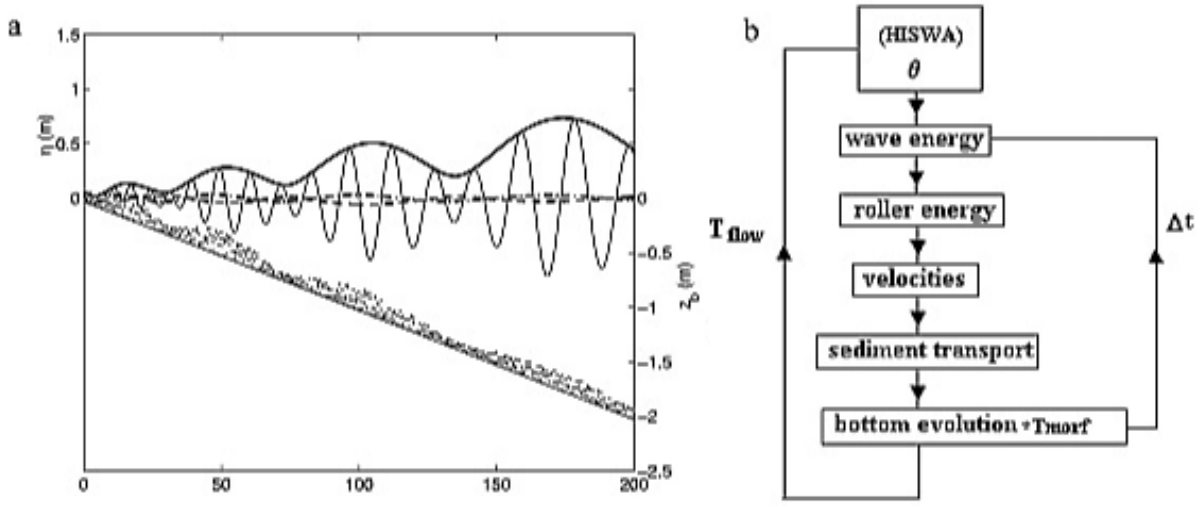

Figure 10: (a) Depiction of wave groups normally incident on a beach with corresponding wave envelope (thick solid line), bound infragravity wave (dashed line), and free returning infragravity wave (dash-dotted line). (b) Flow diagram for morphodynamics computations. Taken from Reniers et al. (2004).

The short-wave energy balance, from which the propagation of the short waves is obtained, is defined as follows (Deltares, 2014):

$$\frac{\partial E}{\partial t} + \frac{\partial}{\partial x}\left(EC_g \cos(\alpha)\right) = -D_w \quad (14)$$

Where E is the short-wave energy, α is the wave direction, C_g is the wave group celerity in m/s and D_w is the dissipation of wave energy. The wave energy E is defined as:

$$E = \frac{1}{8}\rho_0 h H_{rms}^2 \quad (15)$$

Where H_{rms} is the root mean square wave height. D_w is given by the following equation by Roelvink (1993):

$$D_w = 2\alpha f_m \left(1 - \exp\left(-\left(\frac{\sqrt{\frac{8E}{\rho g}}}{\gamma h} \right)^n \right) \right) E \tag{16}$$

Where f_m is the friction coefficient between the bed and the fluid mud layer, γ is an empirical coefficient related to wave breaking and n is Manning's coefficient in $m^{-1/3}s$. Wave breaking causes wave energy to transform into roller energy, which is located in the down-wave region (Deltares, 2014). The change in roller energy is computed through the roller energy balance:

$$\frac{\partial E_r}{\partial t} + \frac{\partial}{\partial x}(2E_r C \cos(\alpha)) = D_w - D_r \tag{17}$$

Where E_r is the roller energy, C is the wave celerity in m/s and D_r is a function of the roller energy E_r. D_r is given by the following equation:

$$D_r = 2\beta g \frac{E_r}{C} \tag{18}$$

Where β is a user-defined coefficient of approximately 0.1. The wave energy and roller energy cause a variation in radiation stresses. Because our model is one-dimensional and the wave direction is perpendicular to the beach, we only consider the radiation stresses in the cross-shore direction:

$$S_{xx} = \left(\frac{C_g}{C}\left(1 + \cos^2(\alpha)\right) - \frac{1}{2}\right) E + 2\cos^2(\alpha)\, E_r \tag{19}$$

The radiation stress consists of two parts: surface stress and depth-uniform stress. The surface stress reads:

$$F_{x.r} = \frac{D_r}{C}\cos(\alpha) \tag{20}$$

The depth-uniform stress, being the total radiation stress minus the surface stress, reads:

$$F_{w,x} = -\frac{\partial S_{xx}}{\partial x} - F_{x,r} \tag{21}$$

The momentum equation, when leaving out most of the terms, can be written as follows:

$$\frac{\partial U}{\partial t} + \cdots + \frac{gU\sqrt{U^2}}{C^2(d+\zeta)} + \cdots = \cdots + F_x \tag{22}$$

Where U is the depth-averaged cross-shore velocity in m/s, d is the water depth in m and ζ is the water level in m. Delft3D also includes the Stokes drift, which horizontally displaces a fluid particle in the direction of wave propagation. The mass flux induced by the Stokes drift is computed as follows:

$$M^S = \int_{-d}^{\bar{\zeta}} \rho_0 u^S dz = \frac{E}{\omega} k \tag{23}$$

Where u^S is the Stokes drift, E is the wave energy, ω is the wave frequency and k is the wave number. The depth-averaged Stokes drift reads:

$$U^S = \frac{M^S}{\rho_0(d+\zeta)} \tag{24}$$

3.3 Vegetation model

For the sake of model simplicity, only one mangrove species is simulated. The specific mangrove species simulated in the model is *Avicennia germinans*, also known as "black mangrove". The vegetation behavior is controlled through a MATLAB script, which will provide updated parameters to Delft3D-FLOW with each time step. Vegetation is included in Delft3D-FLOW as trachytopes (after the Greek word *τραχύτης*, which means roughness), which affect the roughness in a grid cell (Deltares, 2014). The mangroves and their pneumatophores are represented in the model as cylinders with rough surfaces. The roughness formulation used for the vegetation is based on the work by Baptist (2005). The input for this formula includes the vegetation height h_v in m, the vegetation number n in 1/m, the drag coefficient C_D and the roughness of the bed itself without vegetation C_b in $m^{1/2}/s$. There are two different situations for the bed roughness and flow resistance calculations (Deltares, 2014). The first situation, with non-submerged vegetation $h \leq h_v$ gives the equations:

$$C = C_b \tag{25}$$

and

$$\lambda = C_D n \tag{26}$$

Where C is the net bed roughness and λ is the flow resistance. These parameters influence the flow equations as shown in section 3.2, which in turn influence the morphodynamics. In the case of submerged vegetation $h > h_v$ another requirement is needed, namely that the bed shear stress and net bed roughness are related through the depth averaged velocity u and the velocity within the vegetation layer u_v in the following way:

$$\frac{u^2}{C^2} = \frac{u_v^2}{C_b^2} \tag{27}$$

This results in the formula for the net bed roughness:

$$C = C_b + \frac{\sqrt{g}}{\kappa} \ln\left(\frac{h}{h_v}\right) \sqrt{1 + \frac{C_D n h_v C_b^2}{2g}} \tag{28}$$

Where κ is the Von Kármán constant which approximately equals 0.41. The formula for the flow resistance reads:

$$\lambda = C_D n \frac{h_v}{h} \frac{C_b^2}{C^2} \tag{29}$$

The vegetation in the model is dynamic, which means that it calculates mangrove growth and mortality (van Maanen et al., 2015). The equations used in this model use specific vegetation parameters, all of which are described in Appendix B. The vegetation parameters for maximum age, maximum stem diameter, maximum shoot height and the growth constants are taken from Chen & Twilley (1998).

The growth of the vegetation is influenced by the fitness ability, biomass stress and current mangrove size through the following equations (Shugart, 1984):

$$\frac{dD}{dt} = \frac{GD(1 - DH/D_{max}H_{max})}{(274 + 3b_2D - 4b_3D^2)} \cdot f \cdot B \tag{30}$$

$$H = 137 + b_2D - b_3D^2 \tag{31}$$

Where D is the stem diameter in cm, H is the tree height in cm, D_{max} is the maximum stem diameter in cm, H_{max} is the maximum tree height in cm, G, b_2 and b_3 are growth constants, f is the fitness ability and B is the biomass stress. The fitness ability and biomass stress affect the colonization, growth and mortality of vegetation. High values of f and B are beneficial for vegetation growth, while low values promote vegetation mortality. If the vegetation has a long period of suppressed growth, it dies. This is calculated at the end of each ecological year through the average of $f * B$. If this is lower than the critical value for mortality (set to 0.5) for 5 consecutive years, the vegetation dies. If the vegetation in a specific grid cell consists of trees of different sizes, the younger trees die first, until $f * B$ rises above the critical value again. These younger trees are smaller and more vulnerable than the older trees.

The fitness ability f is defined as follows:

$$f = aP^2 + bP + c \tag{32}$$

Where P is the relative hydroperiod, which is the ratio between the amount of time a grid cell is inundated and the total ecological timestep. a, b and c are species-specific constants. For *Avicennia germinans,* this gives the curve shown in Figure 11a. This curve shows that the optimal relative hydroperiod for *Avicennia germinans* is 0.5, and that it is able to survive as long as the relative hydroperiod is between 0.25 and 0.75. The optimal relative hydroperiod is based on literature, which shows that *Avicennia germinans* survives best around mean water level (Ellison & Farnsworth, 1993). Fitness ability controls the growth and mortality of vegetation. Fitness ability also controls the colonization of grid cells. If a cell contains no vegetation, it will colonised if $f > 0$. Then, if vegetation is already present, it will only receive more colonisation if $f * B$ exceeds the critical value of 0.5.

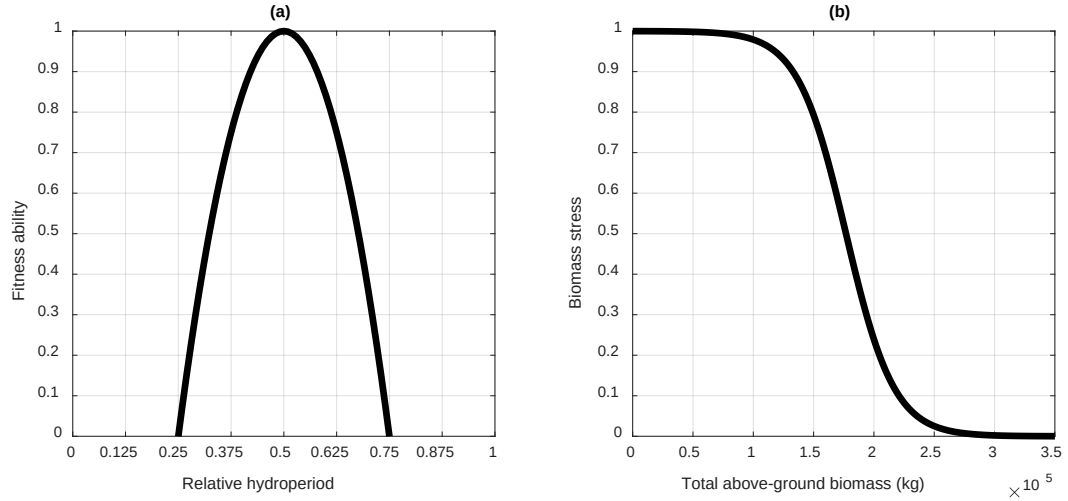

Figure 11: The curves of fitness ability and biomass stress of the species Avicennia germinans, based on its characteristics described in Appendix B.

The biomass stress, which describes that mangroves compete for limited resources in a specific area, is calculated through the following equation:

$$B = \frac{1}{1 + \exp[d(W_{0.5} - W)]} \tag{33}$$

In which d is a constant which controls the decreasing rate of biomass stress, $W_{0.5}$ is the characteristic biomass, described as the value of W for which B equals the critical value $B = 0.5$, and W is the total aboveground biomass in a grid cell in kg. W for an individual tree is calculated through the following equation (Komiyama et al., 2008):

$$W = \alpha \cdot \mathrm{DBH}^{\beta} \tag{34}$$

In which α and β are biomass growth constants and DBH is the diameter of the tree at breast height in cm. The characteristic biomass $W_{0.5}$ is calculated through the use of the "zone of influence" described in Berger & Hildenbrandt (2000). The radius of this zone is calculated by the following equation:

$$R = 10\sqrt{\frac{0.5 * DBH}{100}} \tag{35}$$

In which R is the radius of the zone of influence in m. The ideal biomass is calculated using the following equation:

$$W_{0.5} = \left(\frac{A_{cell}}{(2 * R)^2}\right) * W_{max} \tag{36}$$

Where A_{cell} is the surface area of a grid cell, which in this study equals 2500 m^2, and W_{max} equals the maximum vegetation biomass. Calculating these for *Avicennia germinans* gives a $W_{0.5}$ of 1.79. Putting these equations together gives the curve shown in Figure 11b.

The pneumatophores are all modelled to be the same size, but the number of pneumatophores is calculated through the following equation:

$$N_{root} = m \cdot \frac{1}{1 + exp[f_i(D_{max}/2 - D)]} \tag{37}$$

Where m is the maximum number of pneumatophores, the value of which is obtained from Hogarth (2007), and f_i is a constant which describes the increasing rate of the amount of pneumatophores.

3.4 Model set-up

The grid of the model used in this study consists of 240 grid cells in a line, which results in a 1-dimensional model, based on the model by Xie (2018). The model domain is 12 km long with each of the 240 grid cells having an area of 50 by 50 m. The model has cross-shore variability and long-shore uniformity.

The detailed settings of the hydrodynamic model can be found in Appendix A. The duration of the model is 10 hydrodynamic years with a time step of 0.5 minutes and a morphological acceleration factor of 30 based on sensitivity tests, amounting for 300 morphological years. The eventual morphological change in one time step derives from multiplying the amount of morphological change happening in each hydrodynamic time step by the morphological acceleration factor. This allows for noticeable morphological change, while keeping the model run time at a reasonable level.

Featuring changing wave height, vegetation and sea level rise conditions between scenarios, forty different models are run. The changing conditions between the scenarios are shown in Table 2. The wave height changes in order to study the variation between no waves, small waves, medium-sized waves and large waves. The presence of vegetation changes in order to study the effect of the vegetation. The different sea level rise scenarios are used to study how the system responds to both different rates of sea level rise and whether this rate is constant or accelerates through time. The results of these model runs are analyzed for hydrodynamic characteristics, for bed morphology, for the amount of mangrove trees, for the vegetation biomass and for residual sediment fluxes.

The tide is an S2 tide with an amplitude of 2.5 m, and it is defined through a harmonic boundary condition. This boundary condition is also used to simulate sea level rise using tides with a period many factors larger than that of the tide. Because the tides act as a cosine wave, the exponential sea level rise causes an initial drop in sea level equal to the amplitude of the cosine wave. This initial drop in sea level needs to be counteracted by another tide with a phase of zero and a period that makes it act as a static sea level. An illustration of these tides is given in Figure 12, with a cosine wave in blue and the parts used for sea level rise in red.

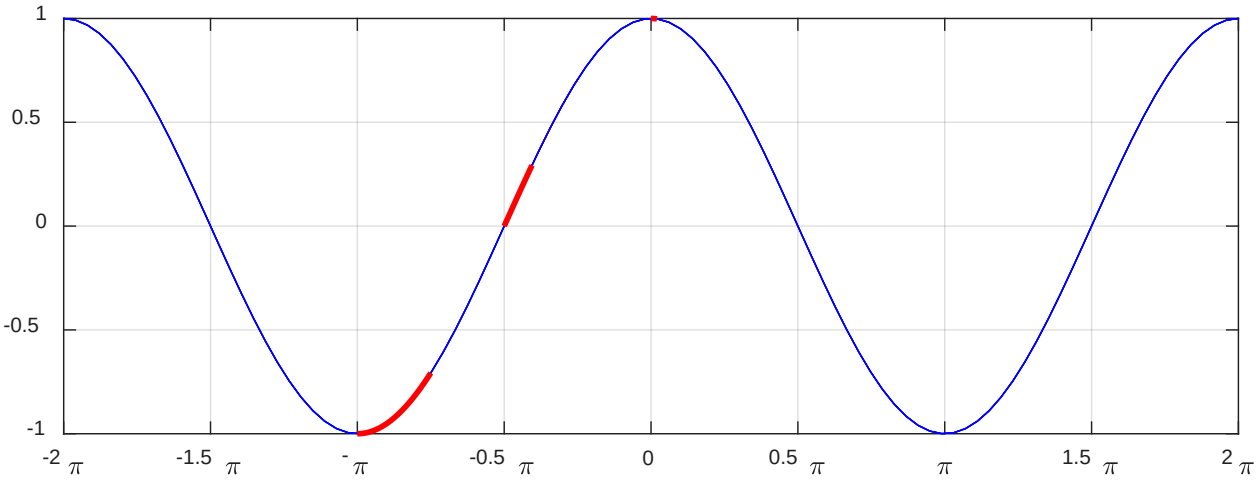

Figure 12: Graphical representation of the parts of the cosine wave used for the simulation of sea level rise.

Table 2: The different model scenarios.

Case	Wave height (m)	With vegetation	Sea level rise rate	Sea level rise pattern
A: Waves				
A1	0.0	No	None	None
A2	0.3	No	None	None
A3	0.5	No	None	None
A4	1.0	No	None	None
B: Vegetation				
B1	0.0	Yes	None	None
B2	0.3	Yes	None	None
B3	0.5	Yes	None	None
B4	1.0	Yes	None	None
C: Slow linear sea level rise				
C1	0.0	No	Slow	Linear
C2	0.3	No	Slow	Linear
C3	0.5	No	Slow	Linear
C4	1.0	No	Slow	Linear
C5	0.0	Yes	Slow	Linear
C6	0.3	Yes	Slow	Linear
C7	0.5	Yes	Slow	Linear
C8	1.0	Yes	Slow	Linear
D: Fast linear sea level rise				
D1	0.0	No	Fast	Linear
D2	0.3	No	Fast	Linear
D3	0.5	No	Fast	Linear
D4	1.0	No	Fast	Linear
D5	0.0	Yes	Fast	Linear
D6	0.3	Yes	Fast	Linear
D7	0.5	Yes	Fast	Linear
D8	1.0	Yes	Fast	Linear
E: Slow exponential sea level rise				
E1	0.0	No	Slow	Exponential
E2	0.3	No	Slow	Exponential
E3	0.5	No	Slow	Exponential
E4	1.0	No	Slow	Exponential
E5	0.0	Yes	Slow	Exponential
E6	0.3	Yes	Slow	Exponential
E7	0.5	Yes	Slow	Exponential
E8	1.0	Yes	Slow	Exponential
F: Fast exponential sea level rise				
F1	0.0	No	Fast	Exponential
F2	0.3	No	Fast	Exponential
F3	0.5	No	Fast	Exponential
F4	1.0	No	Fast	Exponential
F5	0.0	Yes	Fast	Exponential
F6	0.3	Yes	Fast	Exponential
F7	0.5	Yes	Fast	Exponential
F8	1.0	Yes	Fast	Exponential

The wave formulas of all tides present in the models, in the form of $z(x,t) = A\ \cos(kx - \omega t + \varphi)$, are given in Table 3.

Table 3: Tides at the seaward boundary and their wave formulas

Tide	**Formula**
S2	$z(x,t) = 2.5\ \cos(x - 0.000145444t)$
Slow linear sea level rise	$z(x,t) = 4.506657562\cos(x - 9.42600696342761 * 10^{-10}t + \frac{1}{2}\pi)$
Fast linear sea level rise	$z(x,t) = 7.579378628\cos(x - 9.42600696342761 * 10^{-10}t + \frac{1}{2}\pi)$
Slow exponential sea level rise	$z(x,t) = 4.506657562\cos(x - 2.488829720 * 10^{-9}t + \pi)$
Fast exponential sea level rise	$z(x,t) = 7.579378628\cos(x - 2.488829720 * 10^{-9}t + \pi)$
Slow exponential sea level rise counteraction	$z(x,t) = 4.506657562\cos(x - 4.8481 * 10^{-17}t)$
Fast exponential sea level rise counteraction	$z(x,t) = 7.579378628\cos(x - 4.8481 * 10^{-17}t)$

The slow and fast sea level rise scenarios are based on the mean of the IPCC RCP2.6 and RCP8.5 scenarios respectively. These scenarios provide a mean of 0.44 m and 0.74 m over the 21st century, amounting to 1.32 m and 2.22 m over three centuries (Figure 13).

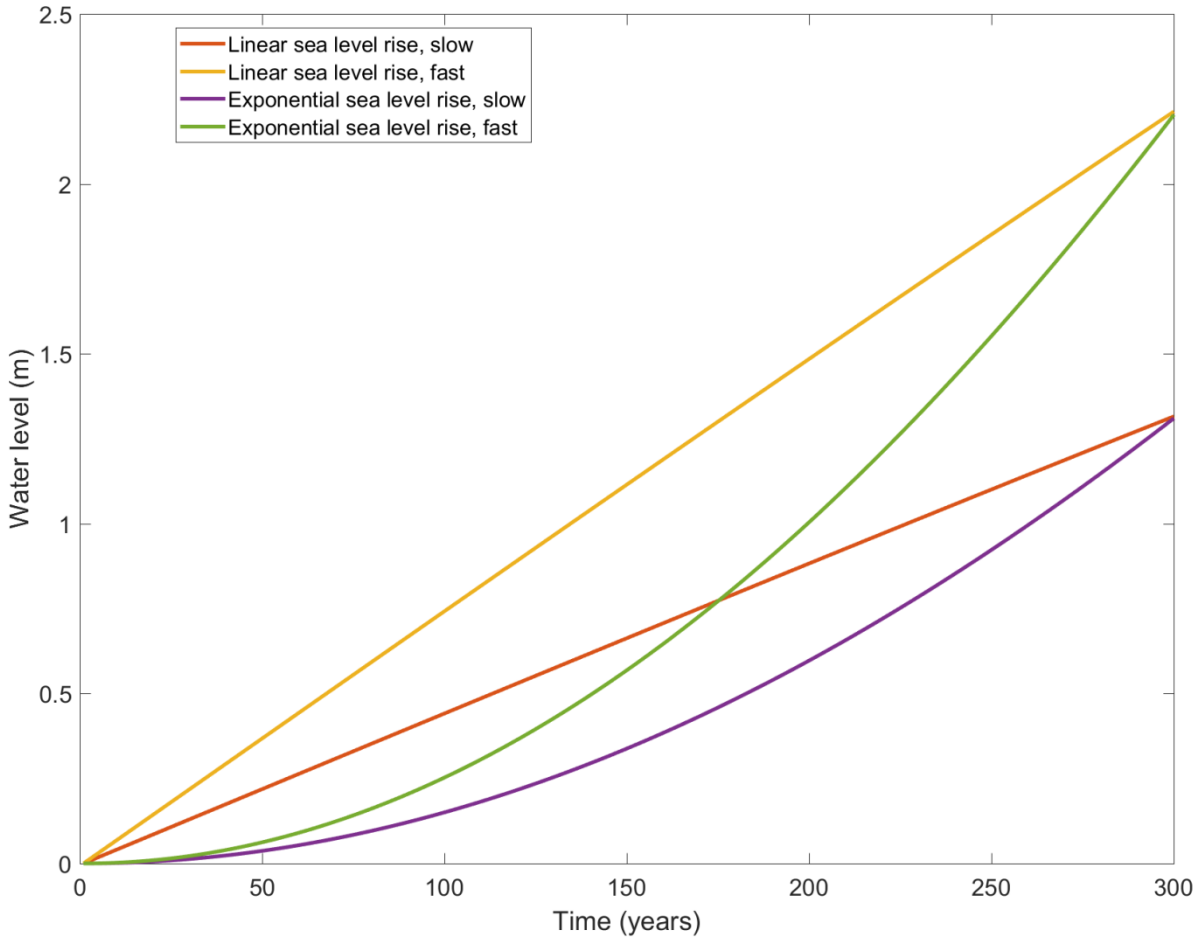

Figure 13: The different sea level rise scenarios

For the roller model, in order to define a corresponding peak wave period for each significant wave height, the usage instructions for the JONSWAP spectrum model by Det Norske Veritas (2011) are used. This recommends that a reasonable spectrum can be constructed as long as $3.6 < \frac{Tp}{\sqrt{H_s}} < 5$ holds true, where T_p is the peak wave period and H_s is the significant wave height. Using the mean of this range, which equals 4.3, the peak wave period can be calculated using $T_p = 4.3 * \sqrt{H_s}$. The results of applying this equation to our proposed wave heights can be found in Table 4.

Table 4: The wave heights and corresponding wave periods simulated in the different model scenarios

Significant wave height Hs (m)	**Peak wave period (s)**
0.3	2.4
0.5	3.0
1.0	4.3

4 Results

In this section, the model results are analyzed. First, the short-term hydrodynamics are explored. This is done first in the scenario without waves or vegetation, then by comparison of the scenarios with and without vegetation and finally by comparing the effects of different wave heights. These analyses give insight into the effect these factors might have on the long-term development of the system. The long-term development is then explored by looking at the changes in hydrodynamics, bed morphology and vegetation over the entire 300 years. Finally, the effects of the different sea level rise scenarios on the entire system are explored.

4.1 Short-term developments

4.1.1 No waves

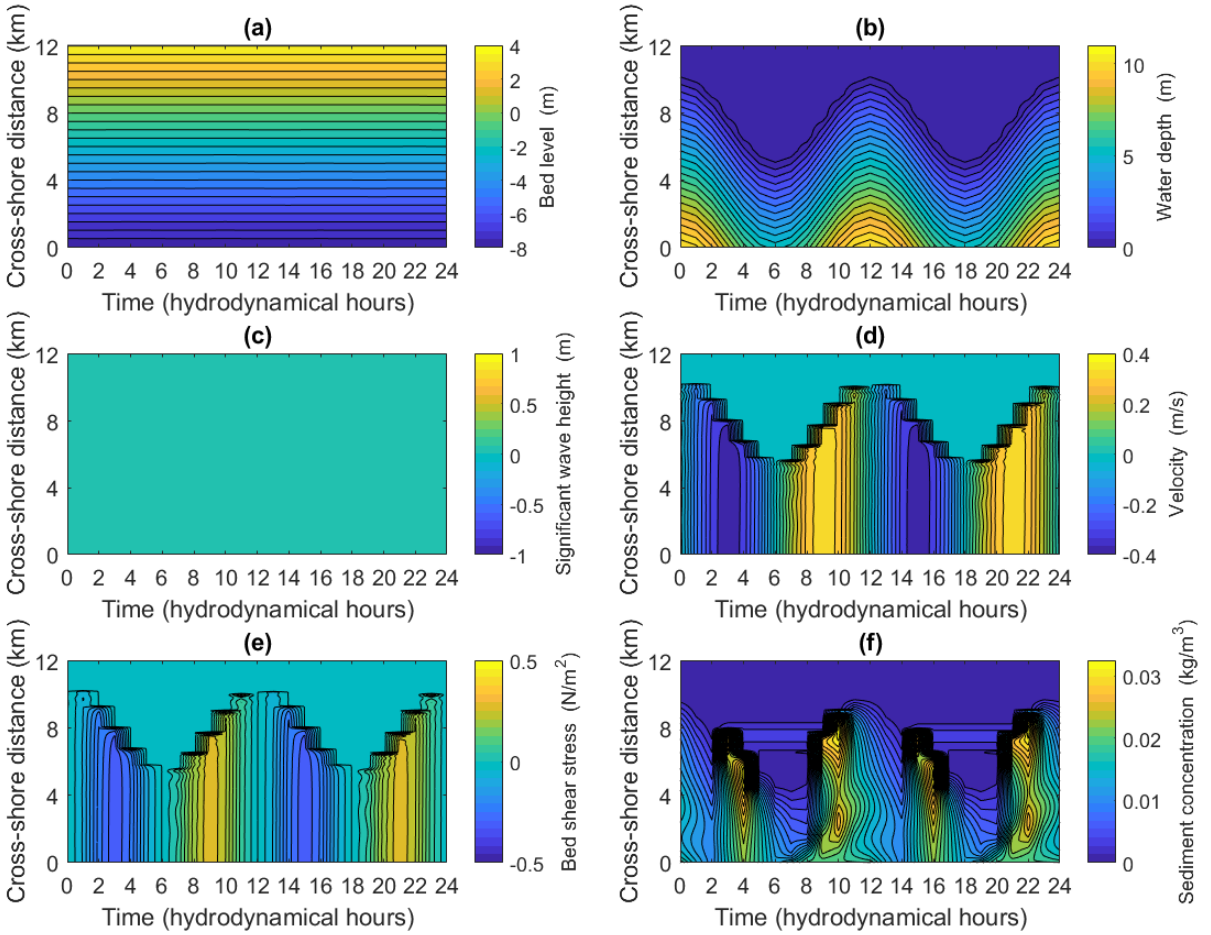

Figure 14: Hydrodynamics of the first two tidal cycles of the scenario without waves, with vegetation and without sea level rise.(a) Bed level, (b) Water depth, (c) Significant wave height, (d) Flow velocity, (e) Bed shear stress, (f) Suspended sediment concentration.

Without waves, the hydrodynamics of the system are dominated by the tide (Figure 14). The bed shear stress (Figure 14e) and flow velocity (Figure 14d) both show their highest values during ebb and flood. The absolute velocity values are slightly higher during ebb than during flood closer to the sea boundary, with a velocity of 0.36 during flood and -0.37 during ebb, while the reverse is true closer to the coast with a velocity of 0.41 m/s during flood and -0.23 m/s during ebb. A similar trend is seen for the bed shear stress. The sediment concentration (Figure 14f) reaches peak values during flood, when sediment is brought into the system from the seaward boundary. Note that the sediment concentration does not increase to values above 0.04 kg/m^3.

4.1.2 Effect of vegetation

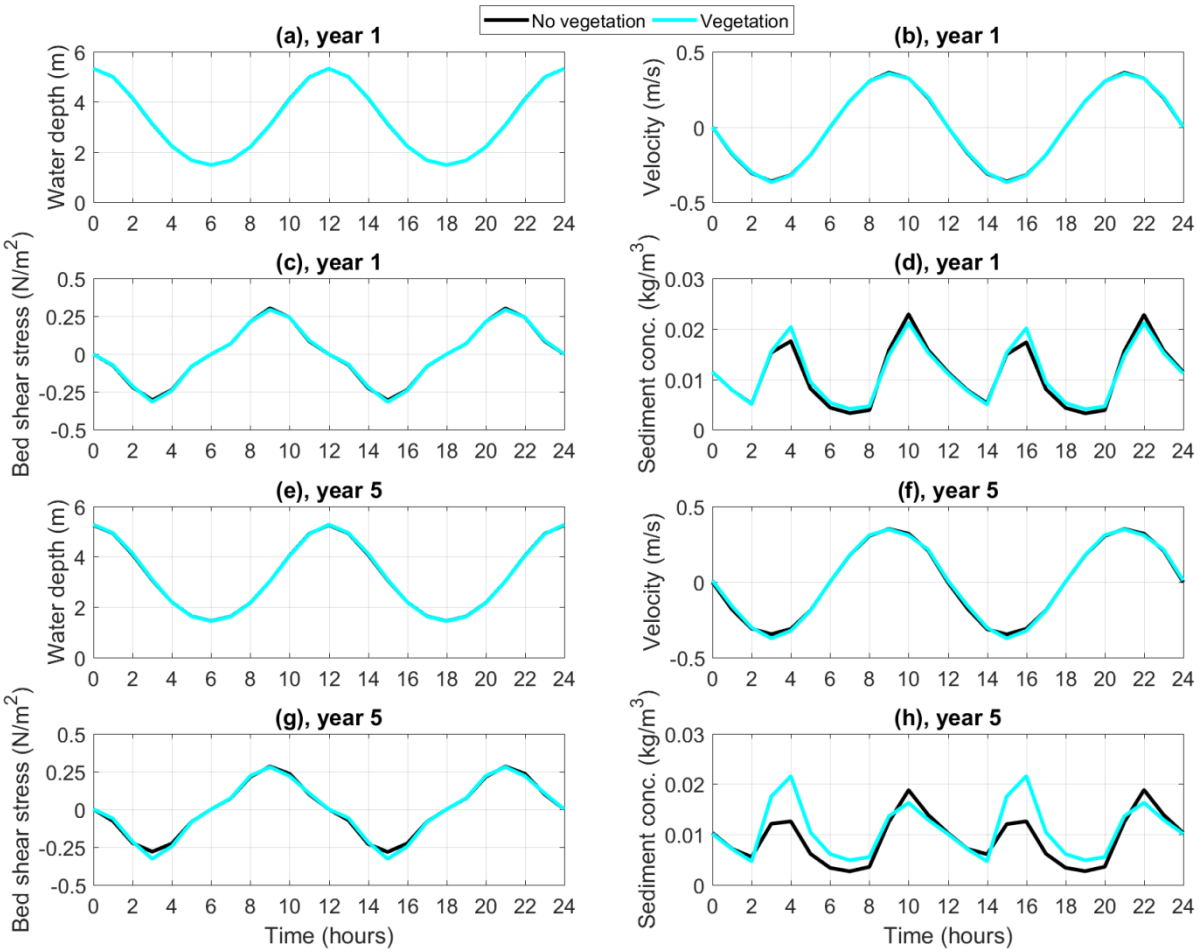

Figure 15: Mean water depth, flow velocity, bed shear stress and suspended sediment concentration for the first two tidal cycles of the first year and the fifth year. Both scenarios are without sea level rise or waves.

The effect of vegetation on the hydrodynamics of the system can be observed even in the beginning of the model simulation, when the vegetation is still very young, both through the tidal cycle and throughout the entire profile (Figure 15 and Figure 16). The added roughness of the vegetation causes the velocity and the bed shear stress to be enhanced during ebb, while they are inhibited during flood (Figure 15b, c, f and g, Figure 16e through l). This matches observations of enhanced ebb velocities in the presence of mangroves, although those observations were made in mangrove creek systems, which are not present in our model set-up (Horstman et al., 2019). This tidal asymmetry causes the sediment concentration to increase during ebb and to decrease during flood relative to the scenario without vegetation (Figure 15d and h, Figure 16n and p). This tidal asymmetry, which causes the difference in suspended sediment concentration and bed shear stress, increases as the vegetation matures (Figure 15f through h).

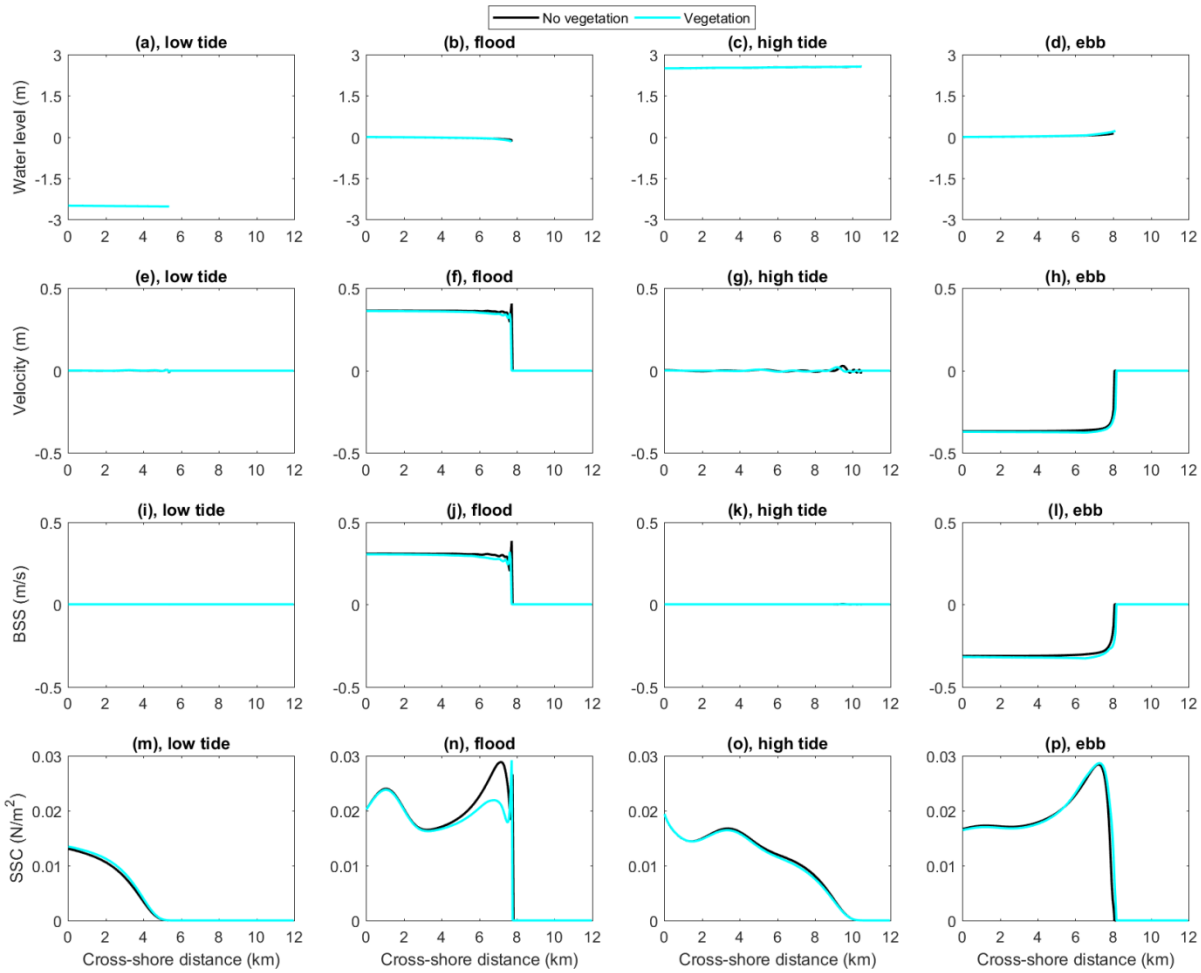

Figure 16: Water level, flow velocity, bed shear stress and suspended sediment concentration through the first tidal cycle for the scenarios with and without vegetation. Both scenarios are without sea level rise or waves.

4.1.3 Effect of waves

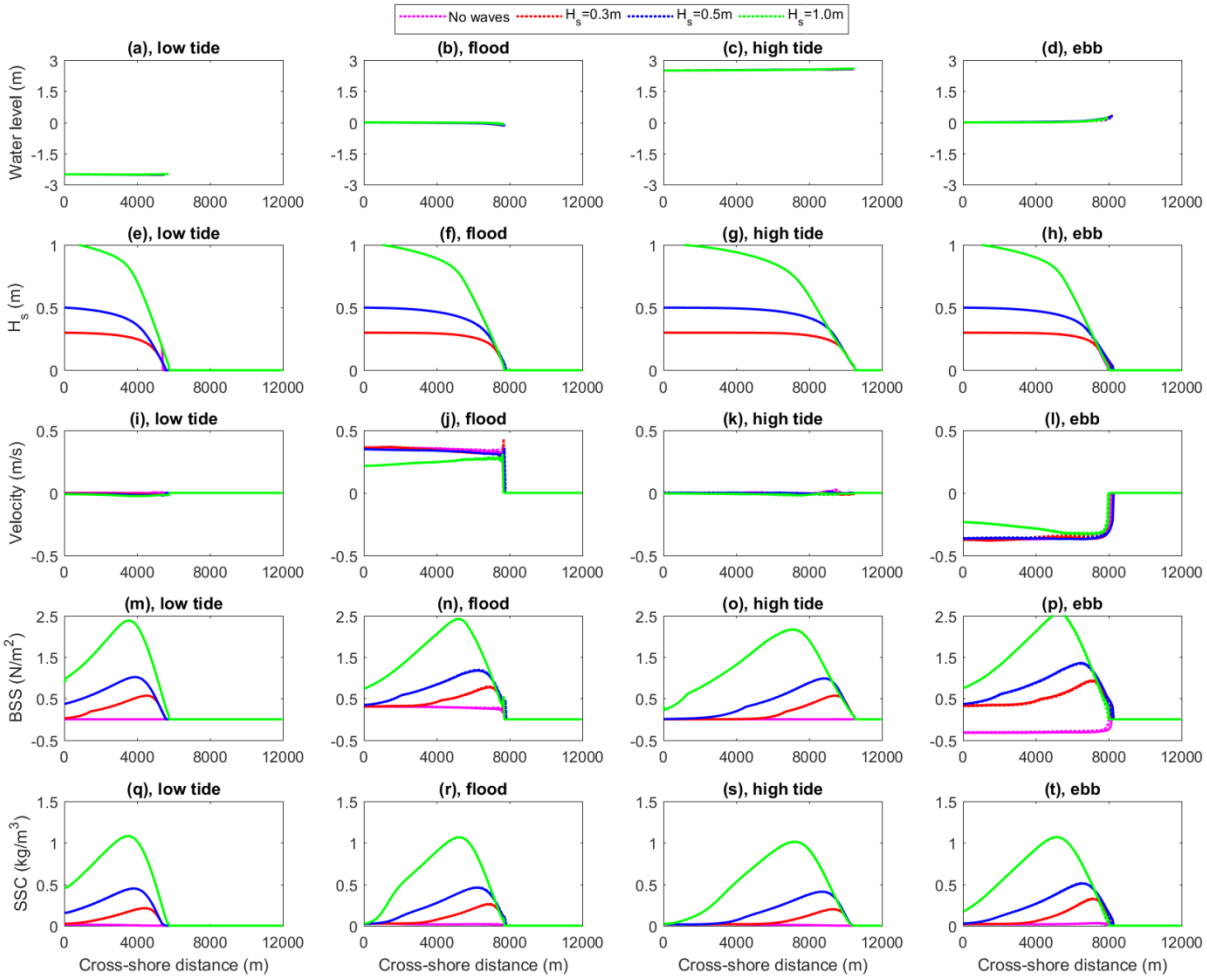

Figure 17: Water level, significant wave height, flow velocity, bed shear stress and suspended sediment concentration through a tidal cycle for different wave heights. Dashed lines indicate scenarios without vegetation, while solid lines indicate scenarios with vegetation.

Figure 17 shows how the hydrodynamics change through space at different points in a tidal cycle. It shows the effect of waves on the hydrodynamics of the system. The main effect of waves can be seen in the bed shear stress (Figure 17m through p) and sediment concentration (Figure 17q through t). The bed shear stress increases with increasing wave height, causing more erosion. While the direction of the bed shear stress depended on the direction of the tidal wave without waves, waves cause the bed shear stress to always be positive. Without waves, there was already a slightly higher bed shear stress during ebb than during flood (Figure 17n and p), and this difference increases in the presence of waves. The presence of waves enhances the suspended sediment concentration, but does not significantly affect the variation of the suspended sediment concentration throughout the tidal cycle. Waves cause the velocity to become more asymmetric, enhancing it during ebb and reducing it during flood. The significant wave height is unaffected by the presence of vegetation because the roller model does not account for wave damping by vegetation, as discussed in the Methods section. However, it is affected by the tide, with larger wave heights showing more temporal variation through the tidal cycle.

In the breaking zone, where the significant wave height reduces the fastest (Figure 17e through h), the sediment concentration increases to more than 0.3 kg/m^3 for a significant wave height of 0.3 m. This increases to 0.5 kg/m^3 for a significant wave height of 0.5 m and 1 kg/m^3 for a significant wave

height of 1 m. Not only does the maximum suspended sediment concentration show a large difference between the different wave heights, the position of the peak suspended sediment concentration on the profile change as well. This is likely a result of the location of wave breaking. The peak suspended sediment concentration is linked to the breaking of waves, and for the scenario with 1 m significant wave height, the waves start to break very close to the seaward boundary. This can be seen in the sharp reduction in wave height occurring closer to the seaward boundary, which causes a shift of the peak suspended sediment concentration towards the seaward boundary (Figure 17e through h).

The behavior of the bed shear stress through the tidal cycle also shows to be affected by the wave height. During low and high tide (Figure 17m and o), when there is no tidal current, there is also no current-related bed shear stress. As a result, the total bed shear stress consists solely out of the wave-related bed shear stress, which is always positive. During flood and ebb, the bed shear stress is significantly higher in situations with waves, showing waves' effect on the bed shear stress in the nearshore zone. Not only do waves cause a wave-related bed shear stress by themselves, the effects of breaking waves on the near-shore hydrodynamics also enhance the current-related bed shear stress.

4.2 Long-term developments

4.2.1 Hydro-morphodynamics

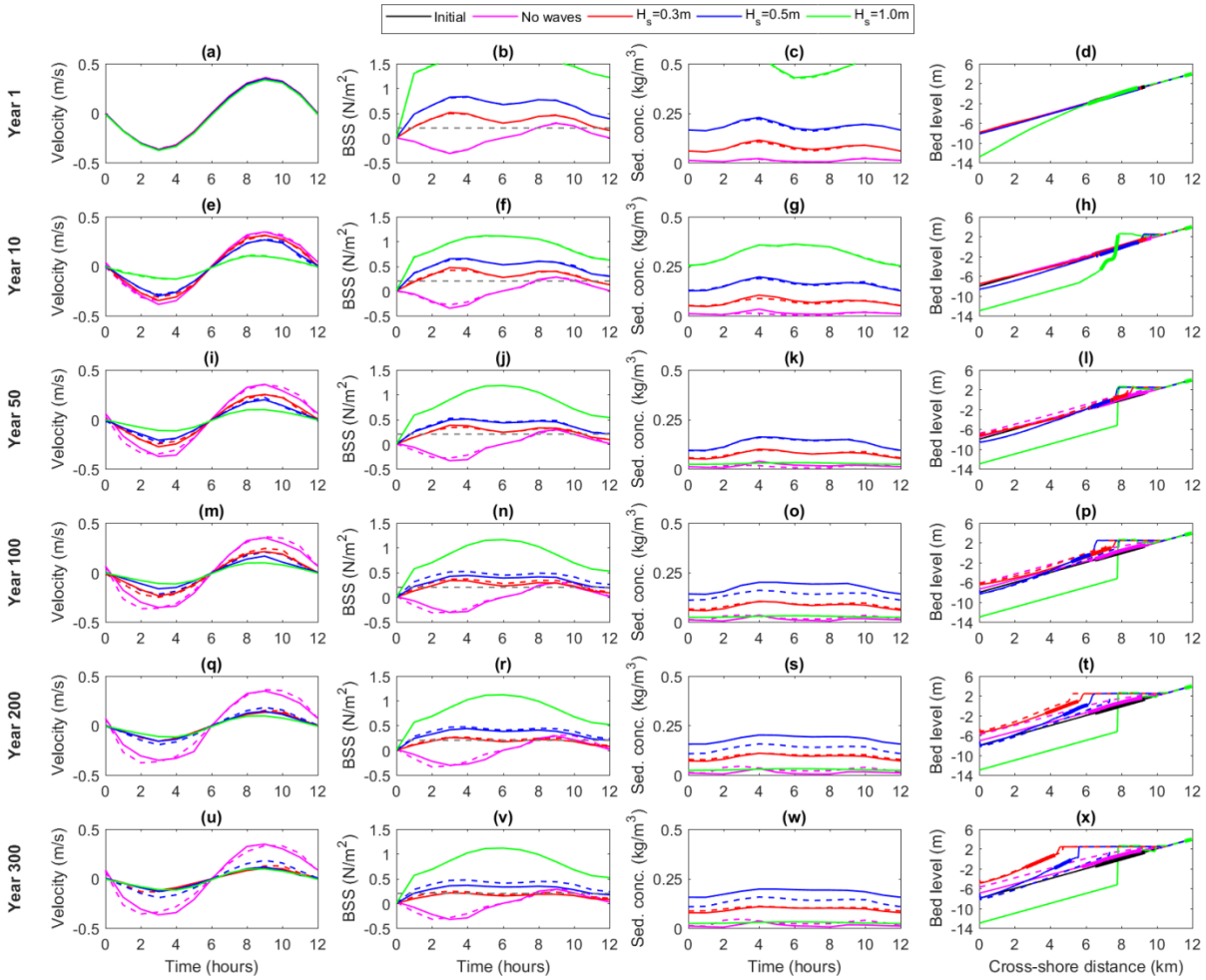

Figure 18: Change of mean velocity, bed shear stress, suspended sediment concentration and bed profile through time for different wave heights. Solid lines are with vegetation, dotted lines without.

The hydrodynamics of the system change over the years, influencing the morphology and vice versa (Figure 18). The magnitude of the flow velocity decreases for all wave scenarios, with the rate of change of flow velocity depending on the significant wave height (Figure 18a, e, i, m, q and u). The decrease in flow velocity can be attributed to coastal accretion, which decreases the water depth and thus decreases the flow velocity (Equation (2)). The reason why the velocity also decreases for the H_s = 1.0 m scenarios, where coastal erosion is dominant, can be explained by the cliff forming. This sharp gradient causes the $\frac{\partial^2 u}{\partial x^2}$ term to become negative, with a relatively large magnitude, causing a decrease in the flow velocity. The flow velocity decreases more for scenarios with vegetation than for scenarios without vegetation, which can be attributed to the increased drag force due to the vegetation. The change in velocity directly influences the bed shear stress, which shows the same trends (Figure 18b, f, j, m, r and v). For the scenario without waves, the flow velocity and bed shear stress change the least, while they change the most and the fastest for the H_s = 1.0 m scenario. The difference between the H_s = 0.3 m scenario and the H_s = 0.5 m scenario is less linear. For the scenarios with vegetation, they decrease through time, with the H_s = 0.5 m scenario changing faster at first and slower later on. As shown in Figure 17, the tidal current is the main driver for bed shear stress. The bed shear stress is largest in the nearshore zone, where the tidal current is in close

contact with the bed. As the morphology becomes steeper, the flow velocity and bed shear stress decrease.

The connection between the morphology and the hydrodynamics can be seen in that rate of change of the velocity corresponds with the change in morphology (Figure 18d, h, l, p, t and x), with the scenario without waves changing very slowly and the H_s = 1.0 m scenario changing very quickly. The decelerating rate of change of the H_s = 0.5 m scenario can also be seen in the morphology, with the progradation of the H_s = 0.5 m scenario being faster at first but being overtaken by the H_s = 0.3 m scenario between the 200th and the 300th year. This overtaking is affected by the sediment concentration, which becomes constant through time around year 100 for H_s = 0.3 m and between year 200 and 300 for H_s = 0.5 m (Figure 18 c, g, k, o, s and w). This stabilization of the sediment concentration through the tidal cycle does not happen for the scenarios without vegetation. The effect of vegetation is very apparent in the scenario without waves, causing the effect of the tide on the velocity and the bed shear stress to become more asymmetric when vegetation is not being taken into account. This asymmetry is shown in the moments of maximum flow velocity and bed shear stress deviating from the moments of peak flood and ebb. The amount of time it deviates increases through time.

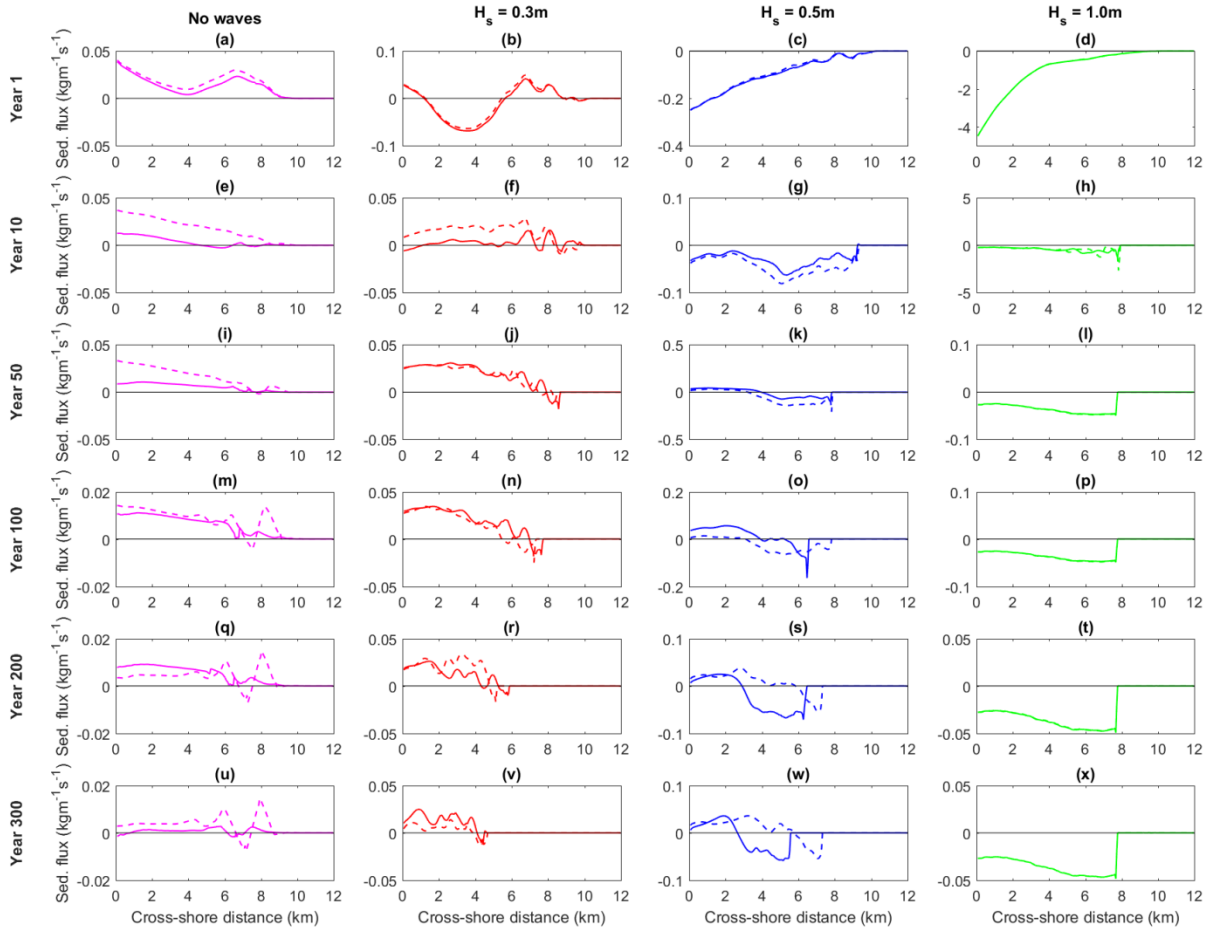

Figure 19: Net sediment fluxes over one tidal cycle at different years over the profile for different wave heights. Dashed lines indicate scenarios without vegetation, while solid lines indicate scenarios with vegetation.

The net sediment flux, at first glance, shows contradictory results to the morphological evolution (Figure 19). These sediment fluxes are computed through multiplying the flow velocity, sediment

concentration and water depth by each other in every grid cell for each time step during one tidal cycle. Only grid cells with a water depth of at least 10 cm are considered, since this is the threshold depth set in Delft3D. Then, during the tidal cycle, all values with a negative velocity are added together to form the ebb flux. The same is done with positive velocities for the flood flux, and finally these are added together to form the net flux. They show that during times of coastal progradation, the net flux in the near-shore part of the profile is negative for scenarios with waves. A negative net flux means that more sediment is transported from a grid cell in a seaward direction than in a landward direction. This discrepancy can be explained through the computation of the net sediment flux. This computation takes into consideration the flow velocities, water depth and suspended sediment concentration, but fails to take into consideration the Stokes drift and other wave-induced processes. If the flow-related sediment flux indicates erosion, but the bed level change indicates accretion, the accretion can be accredited to wave action.

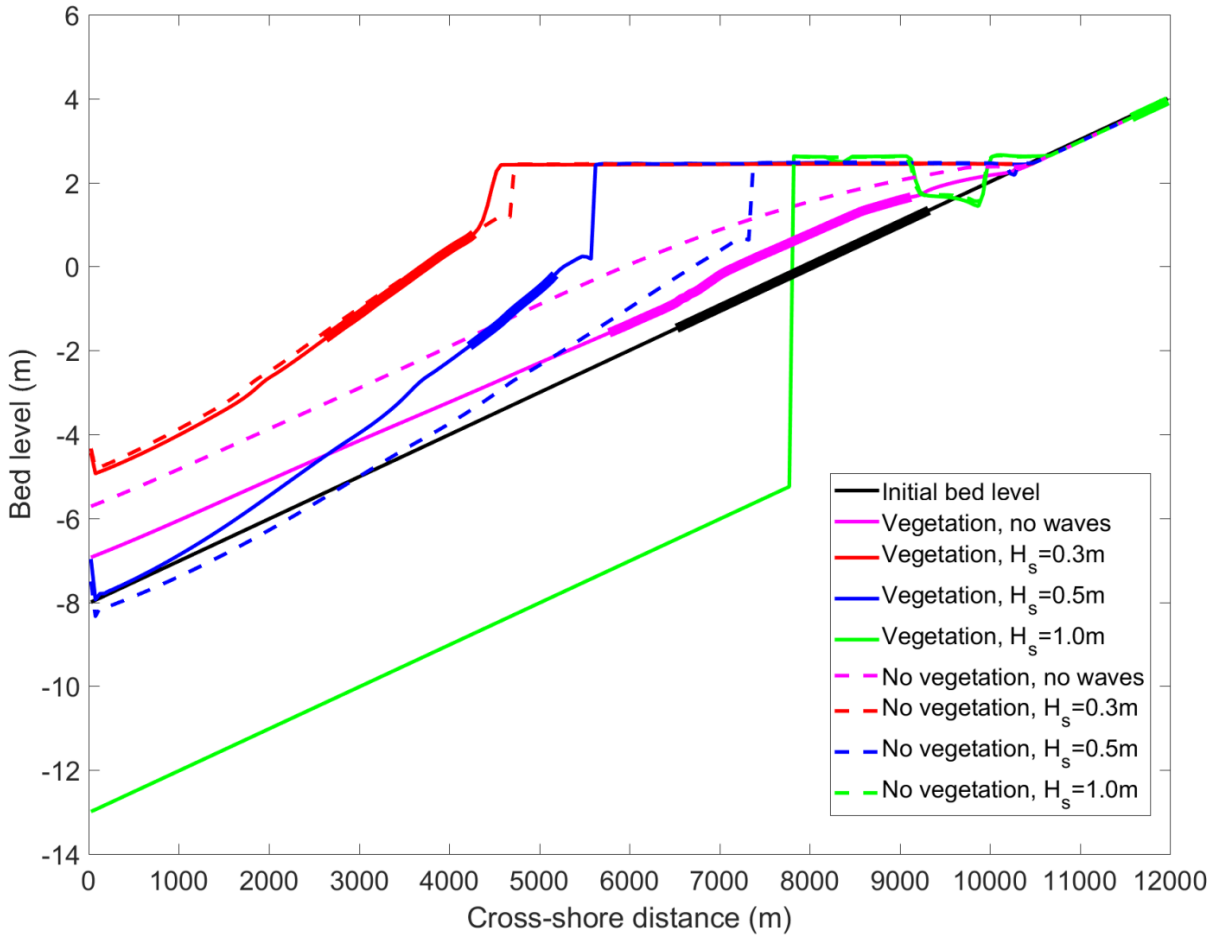

Figure 20: Final bed profiles for all scenarios without sea level rise. The bold parts show locations where vegetation is present.

After 300 years of morphological change (Figure 20), the effect of waves shows in the bed profile development. While the profile does not change very much without waves, waves cause major changes to the morphodynamics of the system. As shown in the previous section, waves have a significant effect on the hydrodynamics of the system, which promotes morphological change. The waves stir up sediment (Figure 17), and through Stokes drift transport sediment towards the coast where it is deposited, causing coastal progradation.

For the scenarios with a significant wave height of 0.3 m and 0.5 m, this causes coastal progradation due to the higher rate of sediment deposition during high tide. For the scenario with a significant wave height of 1.0 m, the breaking of the waves close to the sea boundary causes sediment to be transported away from the coast, causing a large cliff.

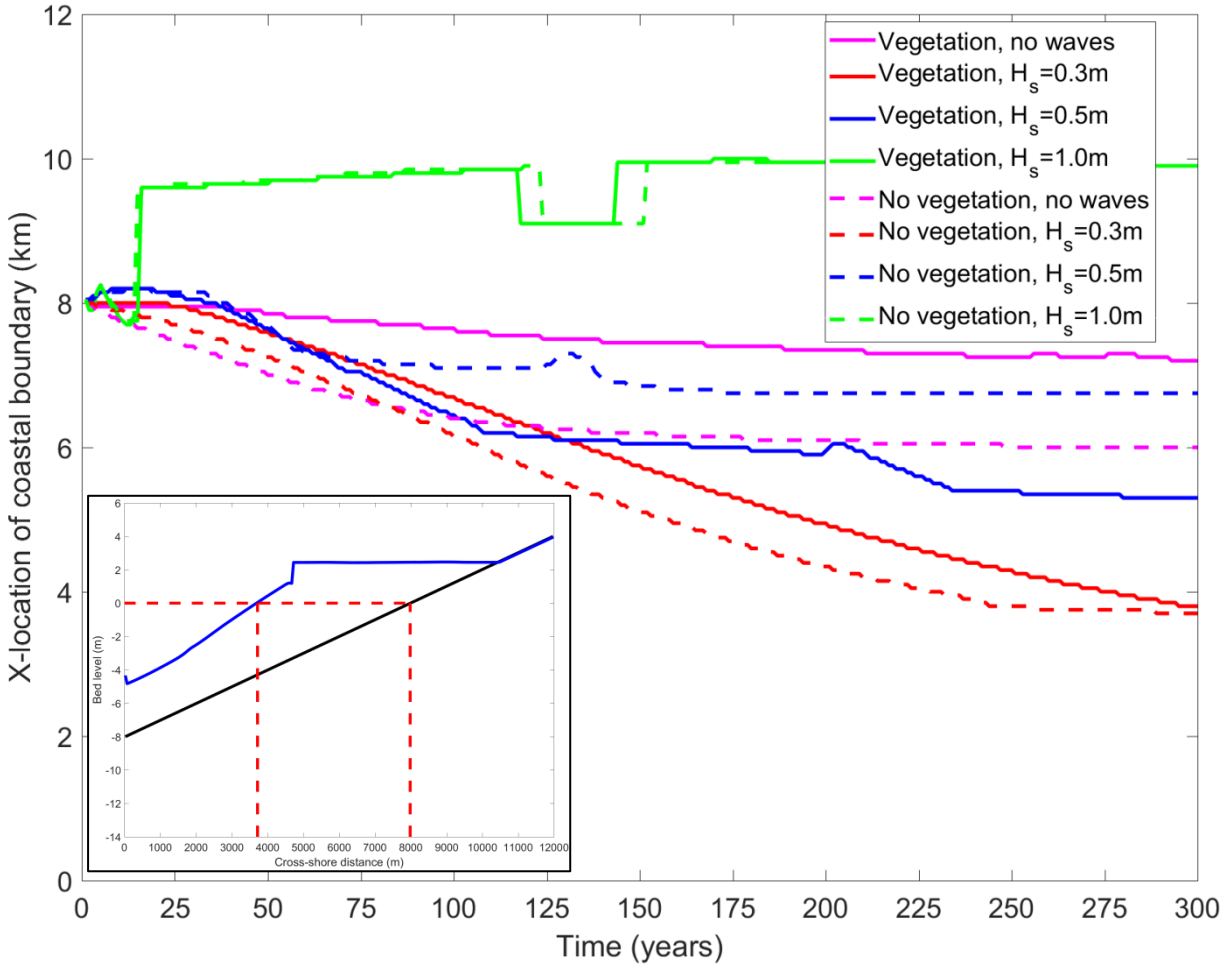

Figure 21: The change in the coastal boundary location over time. The figure in the bottom-left corner shows how the boundary is defined as the first grid cell from the seaward boundary where the bed level is closest to mean water level (0m).

Coastal progradation and regression can be analyzed by tracking the coastal boundary (Figure 21). For all scenarios, the coastal boundary initially moves seaward. For the H_s = 1.0 m scenario, the boundary starts moving inland within 20 years due to wave erosion. For all other scenarios, the coast keeps prograding through time. For the scenario without waves, vegetation causes the coast to prograde less. For the H_s = 0.3 m scenario the difference between vegetation and no vegetation is less apparent, with the scenario without vegetation still having a slightly more seaward boundary at first but eventually ending up at the same point. For the H_s = 0.5 m scenario this relation is reversed, with vegetation causing more progradation. At approximately t = 100 years, the H_s = 0.5 m scenario reaches a stable state without coastal progradation or degradation for about a hundred years, after which it progrades again for about 25 years before becoming stable again. Because of this, the H_s = 0.5 m scenario ends up with less total coastal progradation than the H_s = 0.3 m scenario despite the faster progradation in the first 100 years.

Stokes drift, which causes sediment transport towards the coast, and bed shear stress, which causes erosion, are both driven by waves. While both the Stokes drift and the wave-related bed shear stress are related to the wave energy and thus the wave height, the relations are not the same. Since a linear increase in wave height will not cause a linear increase in Stokes drift and bed shear stress, the net balance between these processes will shift with an increasing wave height. Small waves (H_s = 0.3 m) overwhelmingly transport sediment towards the coast, causing coastal progradation. On the other hand, for medium-sized waves (H_s = 0.5 m), the balance shifts towards erosion. This is seen in the larger negative sediment fluxes (Figure 19). This causes the amount of coastal progradation to decrease compared to the small waves. For large waves (H_s = 1.0 m), the balance shifts even further towards erosion.

That vegetation causes the scenario without waves to prograde less while causing the scenario with waves to prograde more, leads to the conclusion that it is a combination of wave height and vegetation presence that dictates the balance mentioned above and thus the amount of coastal progradation in mangrove systems. This is evident from the model results as seen in Figure 22, which shows results for year 75, where vegetation has an opposite effect on bed shear stress and velocity when comparing the scenario without waves with the scenario with H_s = 0.5 m. While these factors get increased by vegetation without waves, they get decreased with H_s = 0.5 m. This results in the behaviour seen in Figure 21, where the presence vegetation has different effects on the coastal progradation for the H_s = 0.5 m scenario compared to the H_s = 0.3 m scenario.

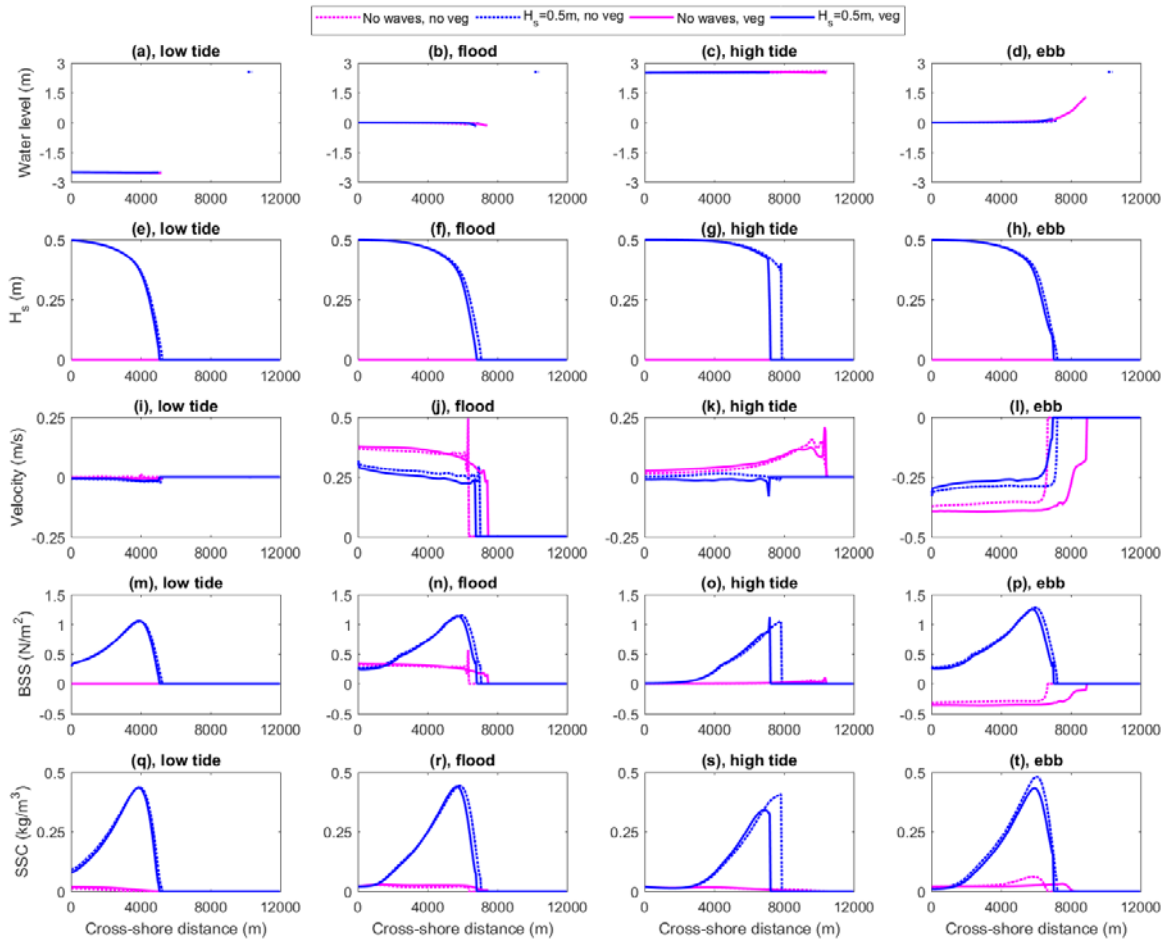

Figure 22: Water level, significant wave height, flow velocity, bed shear stress and suspended sediment concentration comparison between the scenarios without waves and with a significant wave height of 0.5 m during a tidal cycle in year 75.

4.2.2 Vegetation

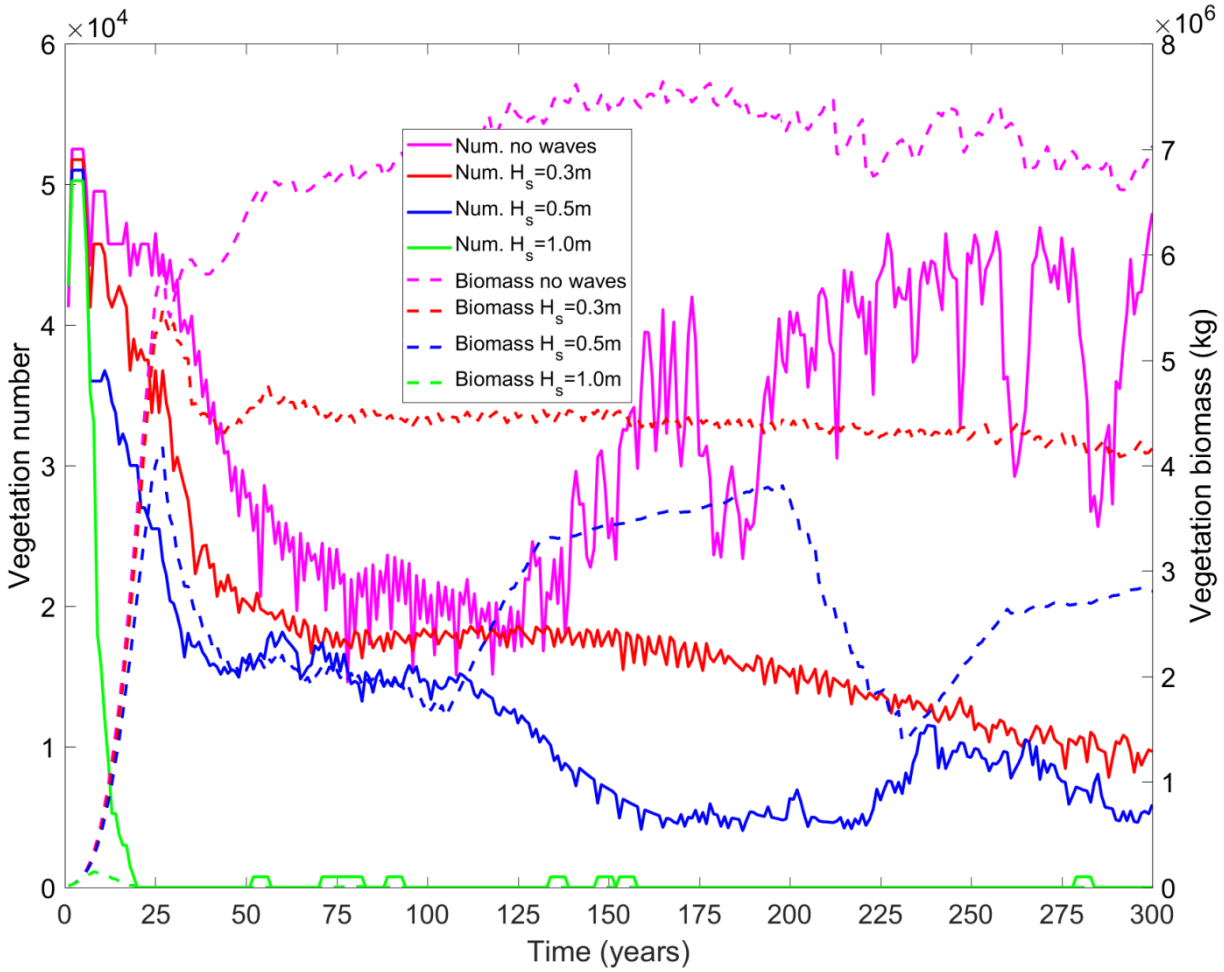

Figure 23: The change in vegetation number (solid lines) and vegetation biomass (dotted lines) over 300 years for all scenarios without sea level rise.

The development of vegetation through time, shown in Figure 23, shows the difference in number of plants and total vegetation biomass between the different wave height scenarios. The vegetation number is the number of individual trees regardless of size. Both vegetation number and biomass are influenced by the wave height. At almost all points in time, a higher wave height results in lower vegetation number and biomass.

The vegetation, measured through vegetation number and biomass, has different phases of development. Very high vegetation number combined with very low biomass means the vegetation is still very young and small. High biomass and low number means that there are few trees, but that those trees are very large. When looking at these parameters individually, this information gets lost. Therefore, it is important to view these two parameters relative to each other. In Figure 24, the ratio between these parameters is shown. It shows that while the separate vegetation number and total biomass may show a succession from low to high with decreasing wave height, this is not the case when looking at the average tree biomass. The average tree biomass shows a more complicated relation with wave height, changing significantly through time.

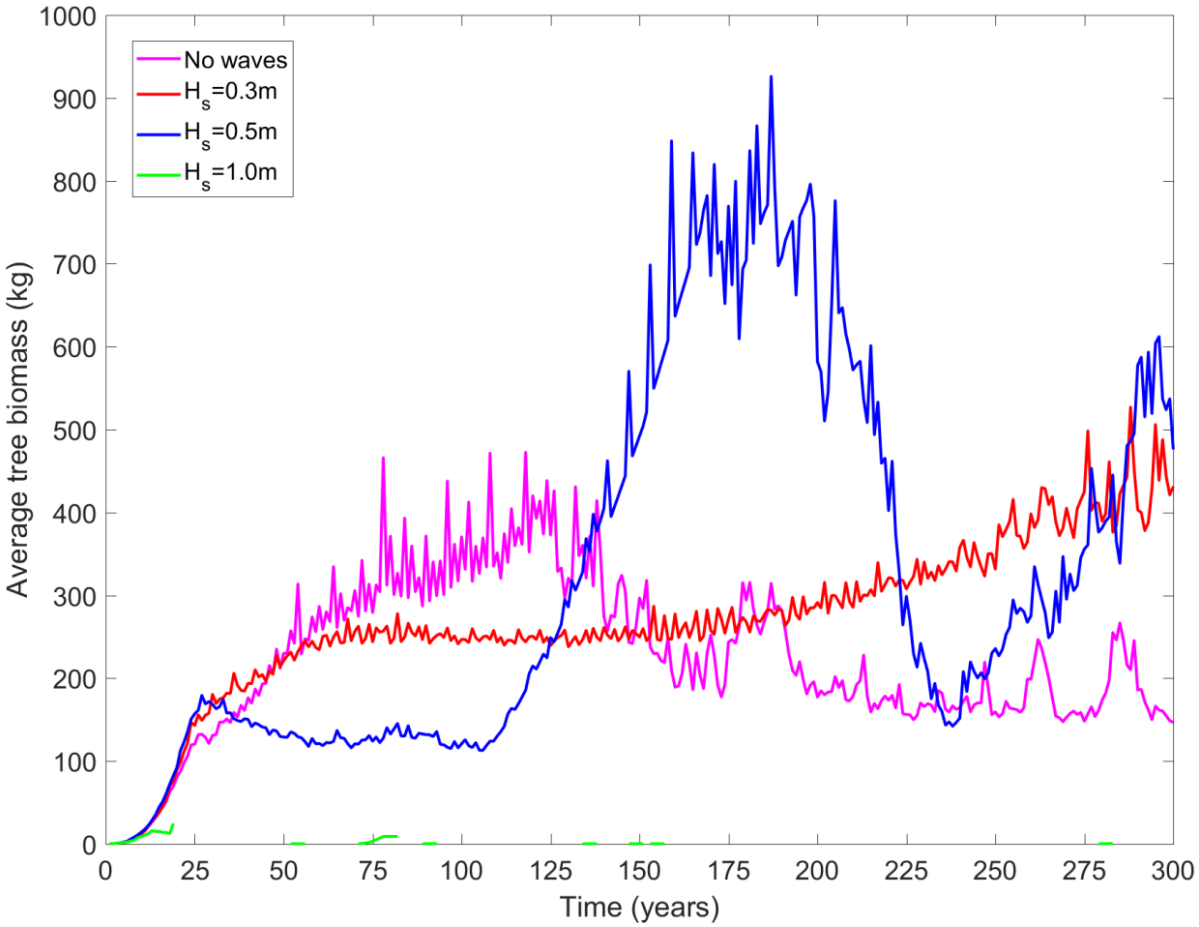

Figure 24: The change in average tree biomass over 300 years for all scenarios without sea level rise.

Knowing this, we can use these parameters to take a closer look at the development of the mangrove forest through time. Without waves (Figure 25), the total vegetation biomass stays relatively stable after the initial growth of the forest. The composition of the forest does change over time. At first, the trees in the center of the mangrove forest, located where the hydroperiod is ideal for *Avicennia germinans*, mature. This is shown in the average tree biomass increasing while the vegetation number does not. After the forest has matured, it transitions to relatively many small trees. This is shown in the vegetation number increasing while the biomass stays the same. After this transition, the vegetation number fluctuates significantly. This signifies a change to a more dynamic forest, where large numbers of small trees die and colonize in relatively short time periods, in the order of 10^4 trees dying or colonizing in less than 10 years. This die-off and colonization is related to the boundary movement, with the trees dying off and colonizing at the edges of the forest as the boundary, and with it the ideal hydroperiod, move seaward.

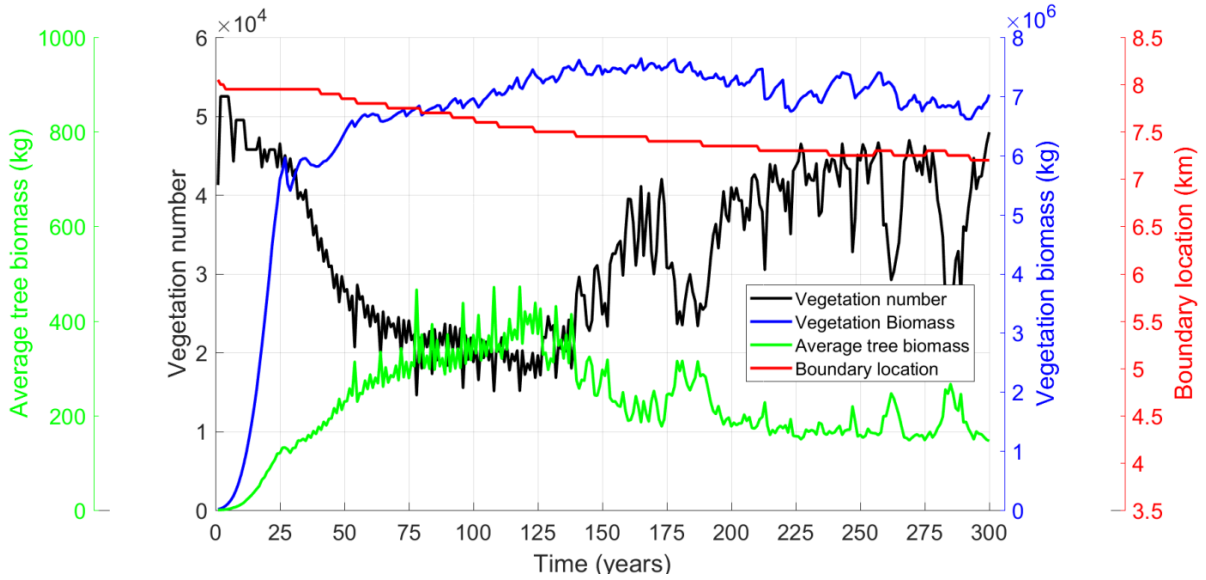

Figure 25: The change in vegetation and the location of the coastal boundary over 300 years for the scenario without sea level rise and no waves.

Introducing waves to the system changes the vegetation development (Figure 26). With H_s = 0.3 m, instead of changing to include more small vegetation, the average tree biomass keeps increasing with the years. The vegetation number decreases to circa 10.000 individuals around the 300th year, which is lower than the lowest vegetation number found in the scenario without waves. The most likely explanation for this is the increased steepness of the shore face upon which the vegetation is located (Figure 20). The increased coastal progradation in the surf zone caused by these waves causes a steeper shore face slope, which leads to a smaller, steeper intertidal area. This results in fewer habitable grid cells for the vegetation, because the mangroves only survive in a specific hydroperiod. This leaves little space for saplings to establish themselves, causing the lower vegetation number. Moreover, the growing mangroves force more biomass stress upon each other, since the biomass stress is related to the total biomass, causing the smaller mangroves to die.

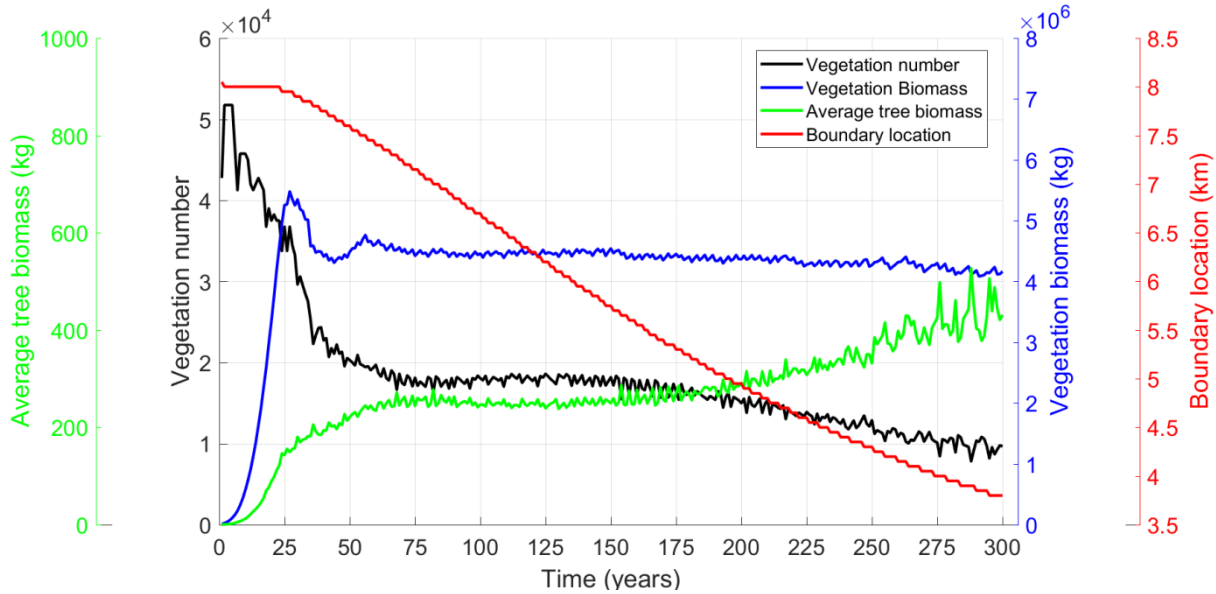

Figure 26: The change in vegetation and the location of the coastal boundary over 300 years for the scenario without sea level rise and a significant wave height of 0.3 m.

With larger waves (H_s = 0.5 m) the development is different (Figure 27), showing more change through time, especially between the 125th and the 225th year (Figure 28). For the first 75 years after the initial growth period, it can already be seen that both the total vegetation biomass and the average tree biomass are significantly smaller than for H_s = 0.3 m, while the vegetation number remains similar. This leads to the conclusion that this difference in wave height inhibits the establishment of saplings less than it inhibits mangrove growth. This is due to the increased morphological change facilitated by waves, which influence the relative hydroperiod in a cell and thus the fitness ability. The fitness ability controls the growth of mangroves to a larger degree than to which it controls the colonization, since the only requirement for colonization is $f > 0$.

Between year 50 and year 100, the coastal development is overwhelmingly in the horizontal direction. The vegetation responds to this change by planting new saplings on the seaward side and killing off mature trees on the landward side of the slope. Between year 100 and year 110, the coastal development is in the vertical direction, moving the coastal boundary over 200 meters, while the vegetation changes very little. After this vertical movement, the morphology of the system changes relatively little for the next 90 years, during which the coastal boundary moves less than 300 meters seaward. This stabilizing morphology corresponds with a change in the vegetation parameters, with a drop in the vegetation number and an increase in the total vegetation biomass, with the average tree biomass increasing to more than 900 kg. This is due to the vegetation maturing, exerting more biomass stress on the younger, smaller trees, causing them to die off.

The trend of slower coastal progradation continues until year 200. Between year 200 and year 210, the coastal slope changes back to its shape in year 100, albeit slightly steeper. This causes the mature vegetation at the landward side of the mangrove forest to die off, while saplings colonize the seaward edge of the mangrove forest as the location of ideal hydroperiod shifts seaward. After this short regression the coast progrades again, while the change in vegetation continues. Both the total and the average vegetation biomass keep decreasing as the coastal boundary moves seaward until year 232, when they start increasing again.

This behavior teaches us two things. Firstly, that the vegetation follows the morphology. Secondly, that horizontal coastal development promotes a constant dynamic of establishing saplings and dying mature trees, while vertical coastal development promotes the growth of established trees with little sapling establishment. This can be explained through the fitness ability of the mangroves. Horizontal coastal development has a larger effect on the relative hydroperiod of a specific grid cell, which ultimately decides the fitness ability, which dictates the colonization, growth and mortality of mangroves.

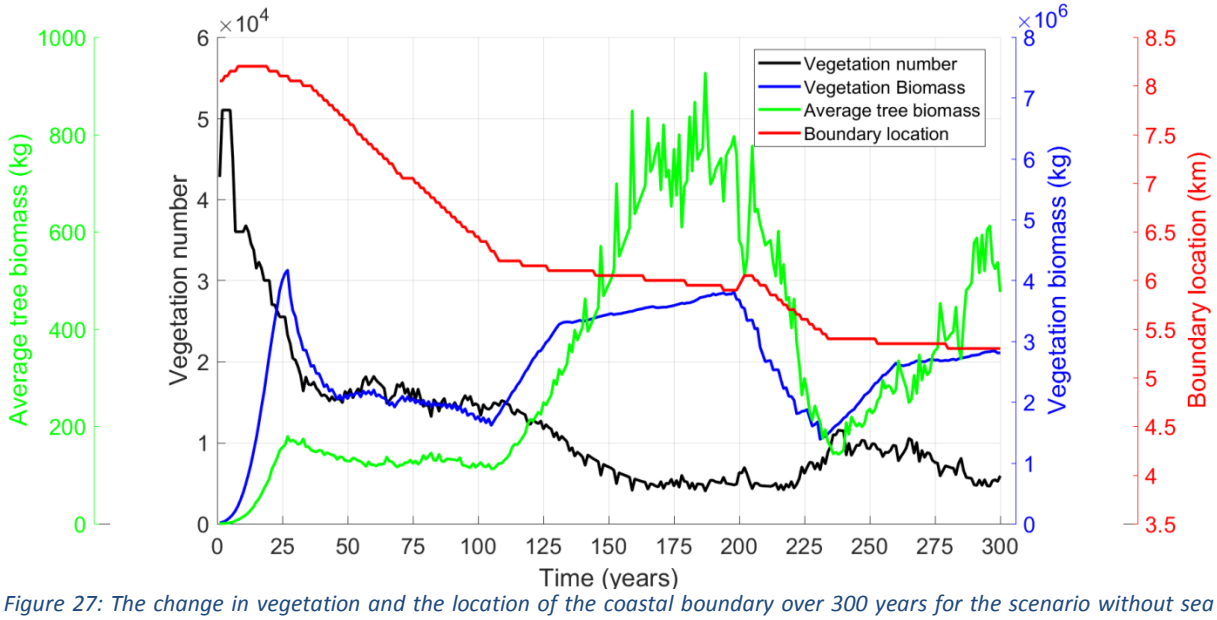

Figure 27: The change in vegetation and the location of the coastal boundary over 300 years for the scenario without sea level rise and a significant wave height of 0.5 m.

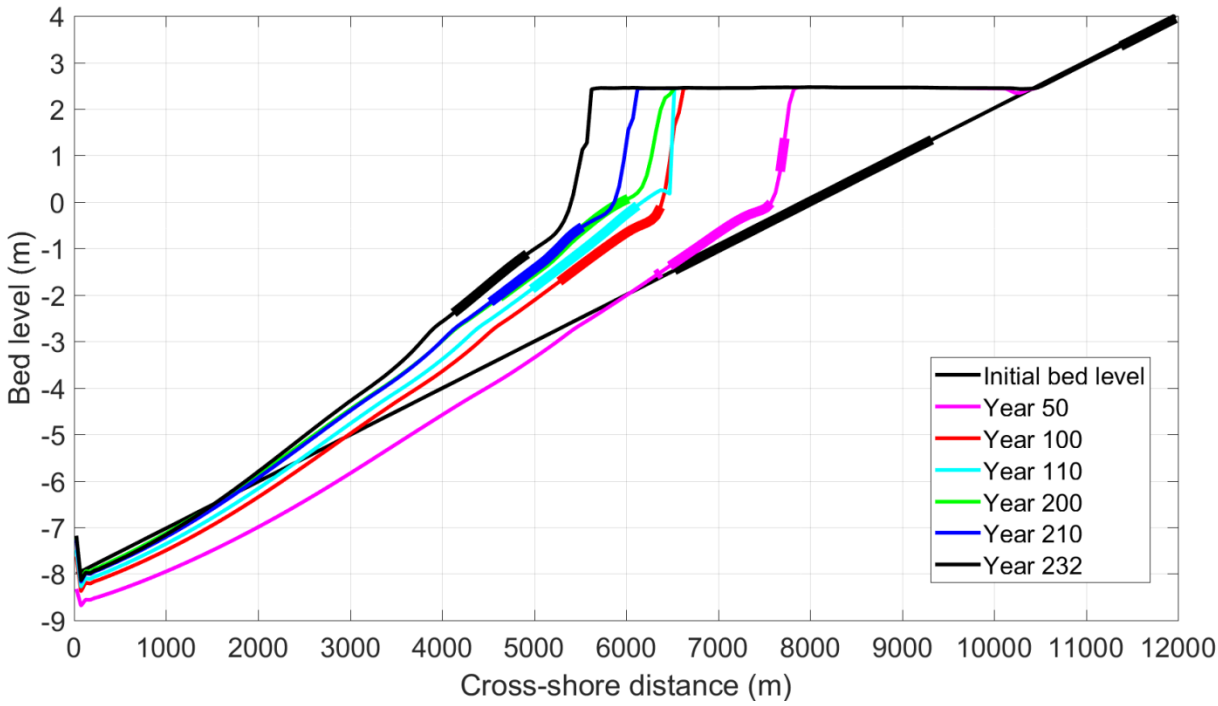

Figure 28: Bed profiles at different times for the scenario without sea level rise and a significant wave height of 0.5 m.

This behavior, in which the coastal boundary movement stagnates for a period of time while the forest matures before moving again, only takes place with H_s = 0.5 m. This can be attributed to the aforementioned balance between wave-induced sediment transport and erosion. This balance is affected by the wave height. The observation that this behavior occurs only for this specific wave height scenario, with all other parameters being equal, leads to the conclusion that the threshold for this kind of behavior to occur in this system lies somewhere between H_s = 0.3 m and H_s = 0.5 m.

With H_s = 1.0 m, the slope becomes so steep there is no area in which the hydroperiod is most favorable for the vegetation to establish itself. Thus, no vegetation is present beyond the first few years in this scenario.

4.3 Sea level rise

4.3.1 Morphodynamics

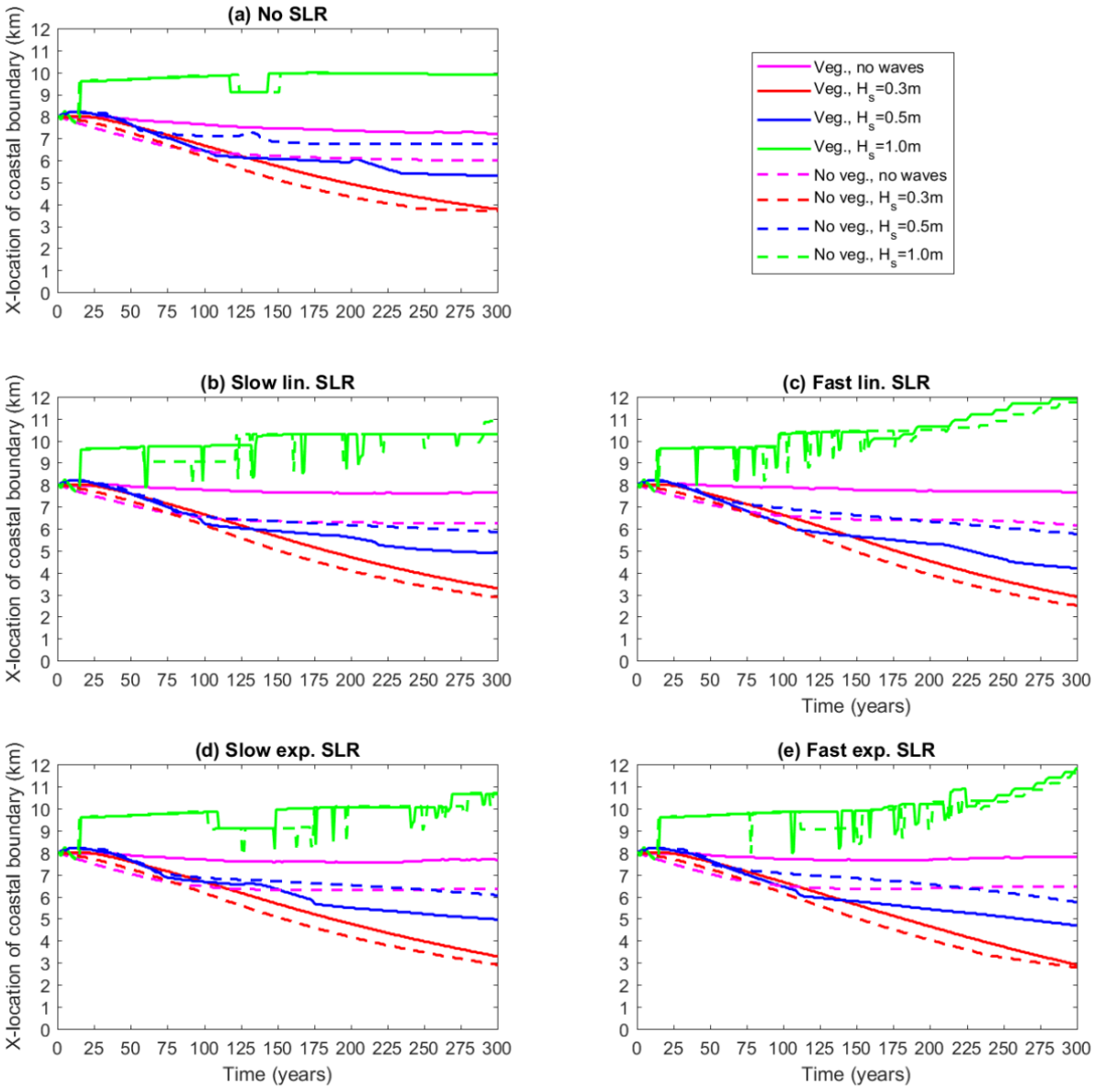

Figure 29: The boundary movement over time for the different sea level rise scenarios.(a) No sea level rise, (b) slow linear sea level rise, (c) fast linear sea level rise, (d) slow exponential sea level rise, (e) fast exponential sea level rise.

Sea level rise increases the water depth, which affects the flow velocity, the current-related and the wave-related bed shear stresses and the Stokes drift. The effect of sea level rise can be seen in the boundary movement for all wave heights (Figure 29). For all scenarios without waves, sea level rise limits the progradation of the coastline by less than 1 km both with and without vegetation. For the scenarios with waves, sea level rise enhances the coastal progradation. This difference can be explained by the effect of the increased water depth on wave action. While without waves, the increased flow velocity causes less progradation, sea level rise decreases the wave-related bed shear stress so that less erosion occurs, causing more progradation.

For the H_s = 0.3 m scenario, sea level rise enhances the coastal progradation with approximately the same amount for all sea level rise scenarios, around 1 km. For the H_s = 0.5 m scenario, the slow sea level rise scenarios (Figure 29b and d) affect the point in time during which the coast transitions from

stable to prograding to stable again. This shows that the sea level rise affects the balance between coastal erosion and sedimentation, which controls the rate of coastal progradation. The fast sea level rise scenarios (Figure 29c and e) also affect the total coastal progradation, increasing it by a kilometer for the fast linear sea level rise scenario. For the H_s = 1.0 m scenario, sea level rise seems to affect the stability of the coastline. In the scenario without sea level rise (Figure 29a), it becomes stable very quickly, only prograding once for a period of 25 years before regressing back. However, with sea level rise, it is prograding and regressing much more frequently.

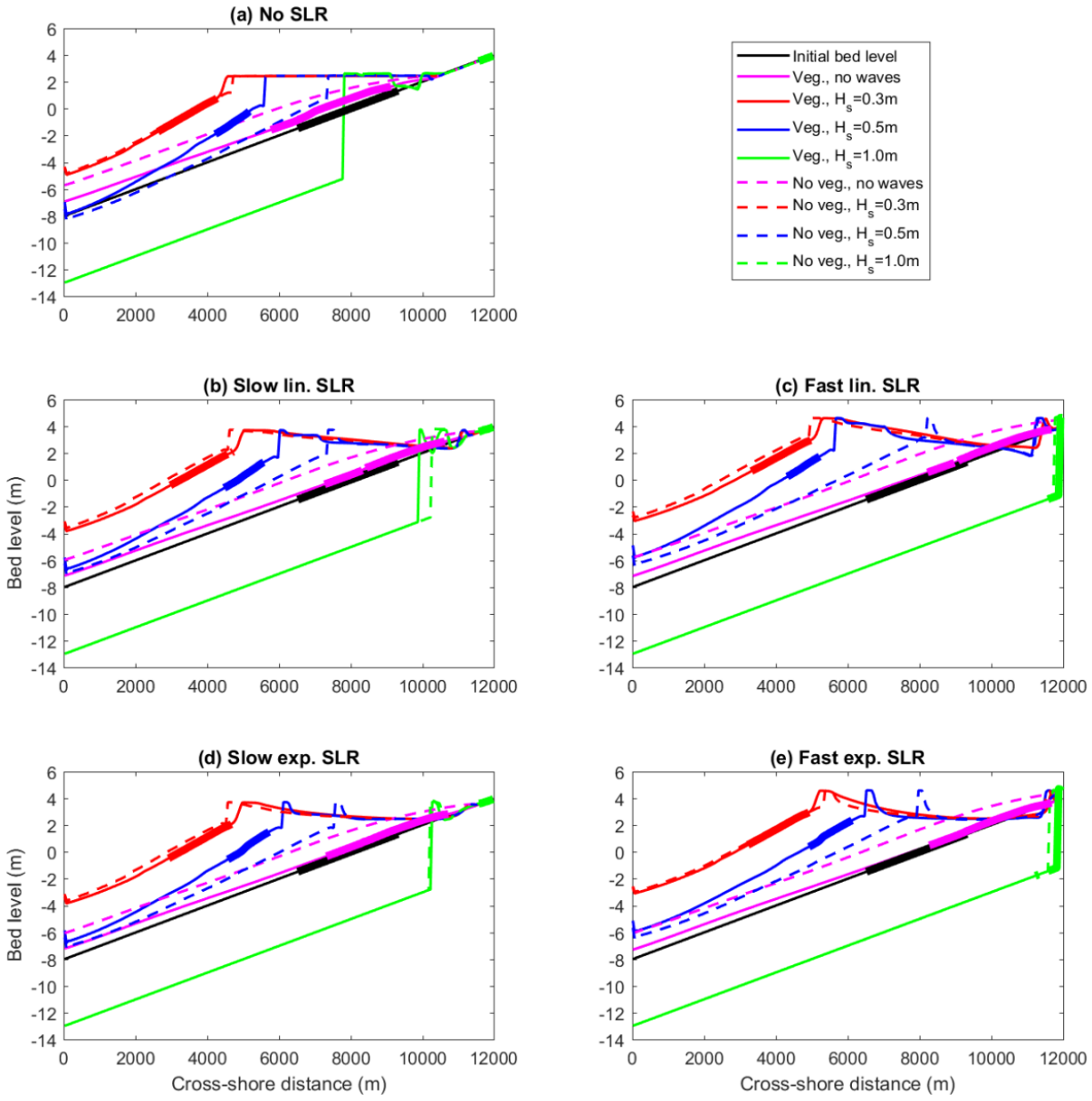

Figure 30: The final bed profiles for the different sea level rise scenarios. (a) No sea level rise, (b) slow linear sea level rise, (c) fast linear sea level rise, (d) slow exponential sea level rise, (e) fast exponential sea level rise.

The influence of sea level rise can clearly be seen on the final coastal profiles, especially in the H_s = 0.3 m and H_s = 0.5 m scenarios (Figure 30). The prograding coastline combined with the sea level rise causes the peak level of the profile to increase. The curvature of the coastal slope on the landward side of the peak, which was a plateau in the scenario without sea level rise, shows a different shape for the linear and the exponential scenarios. This difference is more pronounced for H_s = 0.5 m than for H_s = 0.3 m, especially for the scenarios with slow sea level rise (Figure 30b and d). For the scenario

with H_s = 0.3 m, the slow exponential sea level rise (Figure 30d) gives nearly the same final profile as the linear sea level rise (Figure 30b). For the H_s = 1.0 m scenario, sea level rise causes the cliff formed at the end of the morphological change to be located further landward. The slope of the coast does not change, but the point at which the vertical cliff is located is related to the mean water level. Because the high water level combined with the fast sea level rise is larger than 4 m, which is the highest point of the profile, this causes the vertical cliff to move towards the landward boundary in these scenarios (Figure 30c and e).

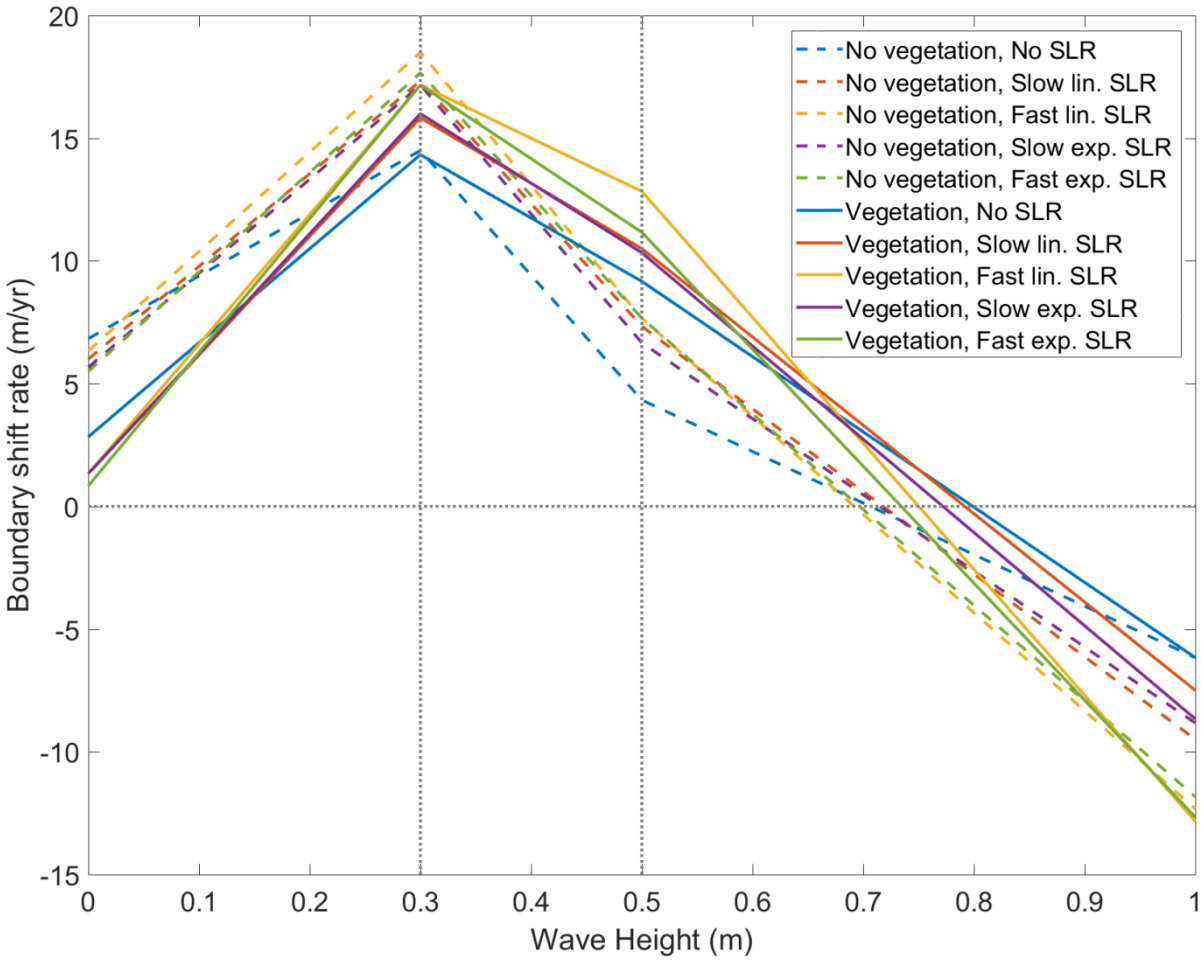

Figure 31: The average boundary shift rate for the different sea level rise scenarios and wave heights.

A few clear trends can be seen in the average boundary shift rate for the different sea level rise scenarios (Figure 31). The average boundary shift rate is defined as the total change in boundary position, as defined in section 4.2.2, divided by the amount of years. A positive average boundary shift rate indicates net progradation, while a negative average boundary shift rate indicates net regression. All sea level rise and vegetation scenarios show their peak boundary shift rate at H_s = 0.3 m, and show a positive boundary shift rate for all wave height scenarios except for those with H_s = 1.0 m.

Without waves, all scenarios show a higher boundary shift rate without than with vegetation. For H_s = 0.3 m, this difference is still present for all scenarios with sea level rise, but it has significantly decreased. For the scenario without sea level rise, this difference has disappeared. For H_s = 0.5 m, it has turned around, showing a higher boundary shift rate with than without than with vegetation. This fits the observations discussed in section 4.2.2 concerning the balance between vegetation,

wave height and coastal progradation, and adds that it is also affected by sea level rise. This matches expectations, since sea level rise affects the water depth and thus the bed shear stress, which is an important part of the coastal progradation balance.

For the scenarios without waves, with H_s = 0.3 m and with H_s = 0.5 m, faster sea level rise means a higher boundary shift rate, with linear sea level rise resulting in a slightly higher boundary shift rate than exponential sea level rise. For the scenarios with H_s = 1.0 m, a faster sea level rise means a more negative boundary shift rate. This shows that the sea level rise enhances the effects of waves on the hydrodynamics through increasing the water depth. This affects the balance between coastal erosion and accretion, which controls the boundary shift rate.

4.3.2 Vegetation

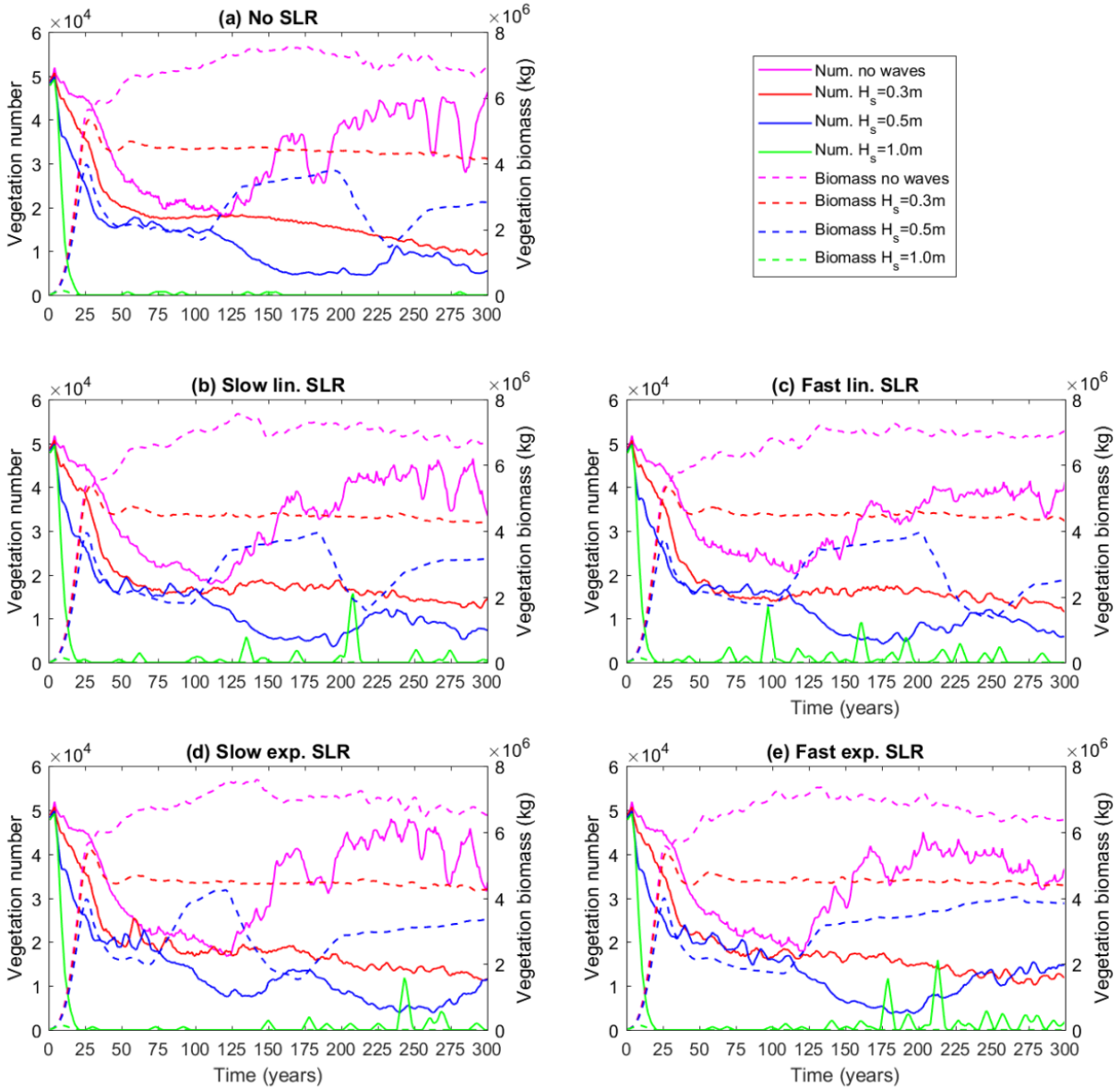

Figure 32: The change in vegetation number (solid lines) and vegetation biomass (dotted lines) over 300 years for the different sea level rise scenarios. (a) No sea level rise, (b) slow linear sea level rise, (c) fast linear sea level rise, (d) slow exponential sea level rise, (e) fast exponential sea level rise.

All sea level rise scenarios show roughly the same trends when it comes to vegetation development for each wave height (Figure 32). For the scenarios without waves, the sea level rise scenarios do not show significant differences from the scenario without sea level rise. When it comes to the H_s = 0.3 m scenarios, there is little change in the vegetation development due to sea level rise. For the H_s = 0.5 m scenarios, there is a significant change in the vegetation development. The slow linear sea level rise scenario (Figure 32b) goes through the cycle of maturing vegetation, die-off and maturing again around 20 years faster than the scenario without sea level rise (Figure 32a). The fast linear sea level rise (Figure 32c) takes remains in the situation with young vegetation at the end of this cycle for approximately 25 years, before maturing again. The slow exponential sea level rise scenario (Figure 32d) goes through this cycle much sooner and faster than the other scenarios. Around the 275th year, the vegetation number increases again. In the fast exponential sea level rise scenario (Figure 32e), the total vegetation biomass never decreases again after maturing. This matches the difference in

the coastal progradation (Figure 31), which shows that the effect of sea level rise on the hydrodynamics affects the balance between sedimentation and erosion, which affects the vegetation dynamics.

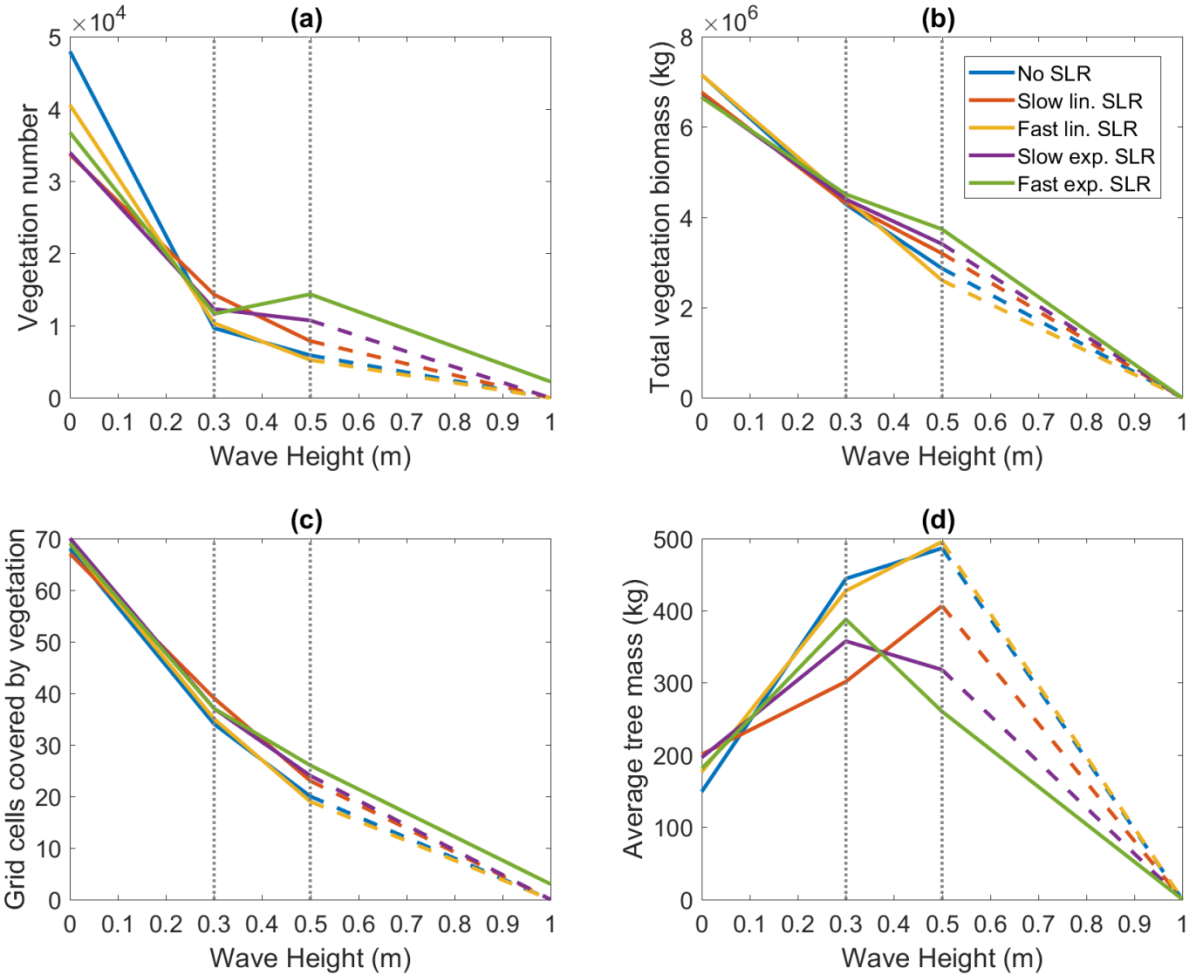

Figure 33: The final (a) vegetation number, (b) total biomass, (c) grid cells covered by vegetation and (d) average tree biomass for the different sea level rise scenarios and wave heights. The dashed lines show values that go to zero for a significant wave height of 1.0 m.

The values of the different vegetation parameters after 300 years show the differences between the different wave height and sea level rise scenarios (Figure 33). The vegetation shows the same trends as the morphology. While there are differences between the different sea level rise scenarios, these are not as large as the differences between the different wave height scenarios. Especially the total vegetation biomass (Figure 33b) and the amount of grid cells covered by vegetation (Figure 33c) show little variation between the different sea level rise scenarios. This shows that wave height has a more significant effect on vegetation dynamics than sea level rise. The vegetation number (Figure 33a) shows more variation between the different sea level rise scenarios, which in turn affects the average vegetation biomass (Figure 33d).

All sea level rise scenarios show a similar relation between vegetation biomass and wave height, with higher wave height resulting in lower vegetation biomass after 300 years (Figure 33b). While there is little variation between the different sea level rise scenarios, some differences do exist. The scenarios with no sea level rise and fast linear sea level rise have the highest biomass without waves, but they drop to the lowest biomass as waves are introduced to the system. The difference between the sea

level rise scenarios can be seen most clearly with a significant wave height of 0.5 m. This difference corresponds with the cycle shown in Figure 32, with the scenarios which reach the final maturation stage of that cycle the soonest having a larger final biomass.

The vegetation number shows a similar trend between scenarios as the vegetation biomass, with decreasing number with increasing wave height (Figure 33a). However, for the fast exponential sea level rise scenario, the vegetation number actually increases between H_s = 0.3 m and H_s = 0.5 m. This is also the only scenario for which the vegetation number does not equal zero with H_s = 1.0 m. The vegetation cover change only increases for the scenarios without waves, while it decreases significantly for all sea level rise scenarios as soon as waves are introduced. It follows the same general trends as the vegetation biomass and vegetation number.

The average tree mass after 300 years increases for all sea level rise scenarios from the scenarios without waves to the H_s = 0.3 scenarios (Figure 33d). Between H_s = 0.3 m and H_s = 0.5 m, it decreases for the exponential sea level rise scenarios, while it continues to increase for all other scenarios. For H_s = 1.0 m, the only scenario for which vegetation is still present is the fast exponential sea level rise. However, this vegetation only consists of very small trees.

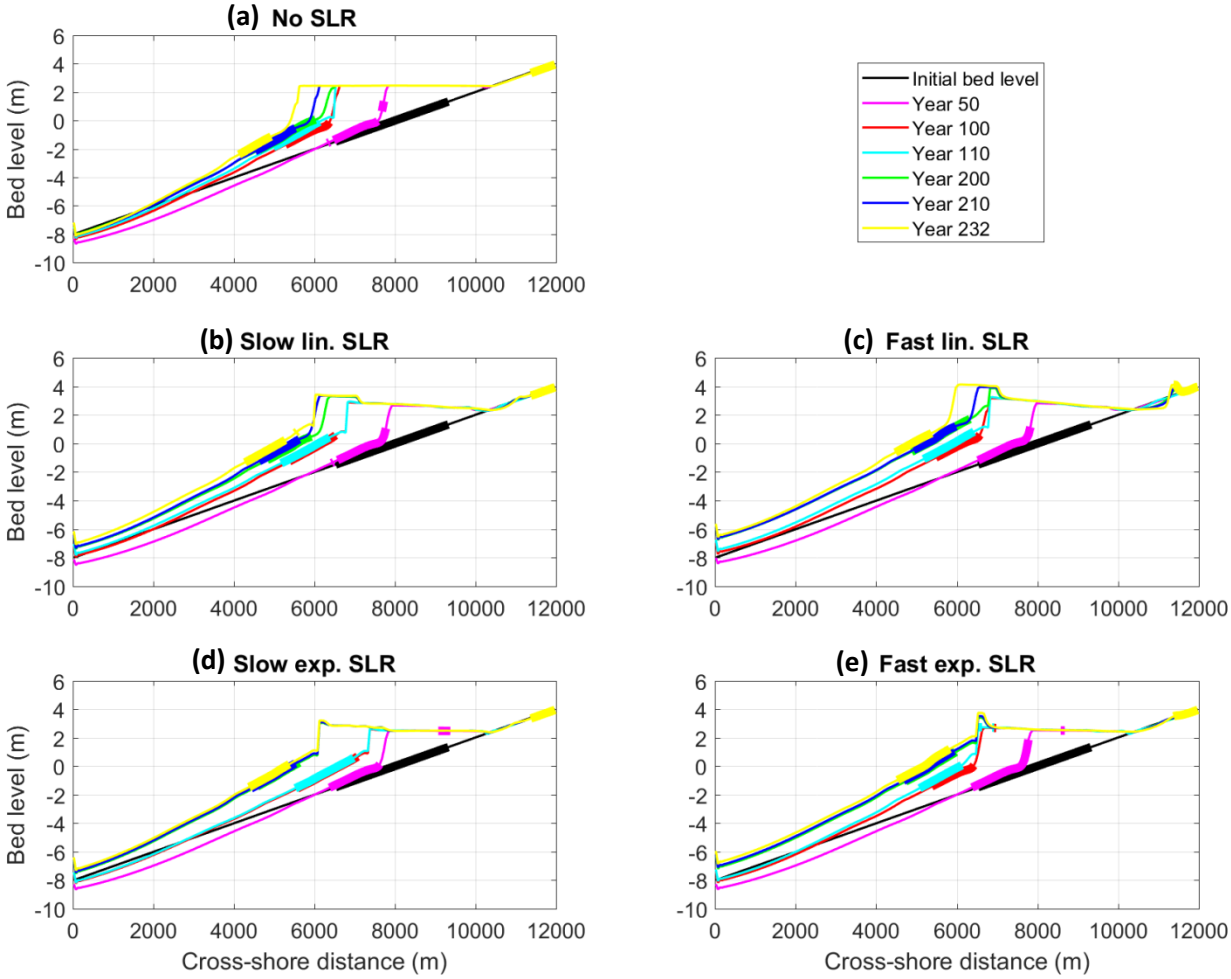

Figure 34: Bed profiles at different times for the different sea level rise scenarios with a significant wave height of 0.5 m. (a) No sea level rise, (b) slow linear sea level rise, (c) fast linear sea level rise, (d) slow exponential sea level rise, (e) fast exponential sea level rise.

In section 4.2.3, special attention was given to the vegetation development under a significant wave height of H_s = 0.5 m. With sea level rise, this vegetation development changes in certain ways. While

the development is mostly the same for both linear sea level rise scenarios, the largest difference lays within the exponential sea level rise scenarios (Figure 32). Comparing the bed profile change highlighted in Figure 28 with the same period in the other sea level rise scenarios, this is also apparent (Figure 34). While both linear sea level rise scenarios (Figure 34b and c) show a similar coastal progression as the scenario without sea level (Figure 34a), the exponential sea level rise scenarios differ from those and from each other. The slow exponential sea level rise scenario (Figure 34d) differs in that the change between year 110 and year 200 is less gradual, and that there is significantly less change between both year 100 and year 110 and between year 200 and year 232. The fast exponential sea level (Figure 34e), on the other hand, shows very similar change between year 50 and year 100 as the other scenarios, but very little horizontal progradation between year 100 and year 232.

This leads to the conclusion that the change in water depth affects the balance between erosion and sedimentation, which controls the coastal progradation. That this behavior is most affected by the type of sea level rise shows that the rate at which the sea level rise changes affects the balance between erosion and sedimentation more than the amount of sea level rise. This morphological difference also affects the vegetation (Figure 32). This supports the observation that the vegetation dynamics follow the morphodynamics.

An explanation for the difference in morphological development can be found in the change in the bed shear stress and in the suspended sediment concentration over time (Figure 35). For the scenario with fast exponential sea level rise, the suspended sediment concentration changes significantly between year 50 and year 100 (Figure 35b and e), while changing a negligible amount between year 100 and year 300 (Figure 35b, h, k, n and q). Both the bed shear stress and the suspended sediment concentration for the scenario with slow exponential sea level rise show a unique situation at year 100 (Figure 35d and e) and year 110 (Figure 35g and h), before showing comparable results as the other scenarios with sea level rise. The reason these scenarios behave this way is the changing nature of the sea level. Because the change in sea level is non-linear for these scenarios, the change in the hydrodynamics will also be non-linear. This is in contrast with the other scenarios, where the sea level rise is linear or nonexistent, and as such, the reaction of the morphodynamic system to the change in sea level will be linear as well.

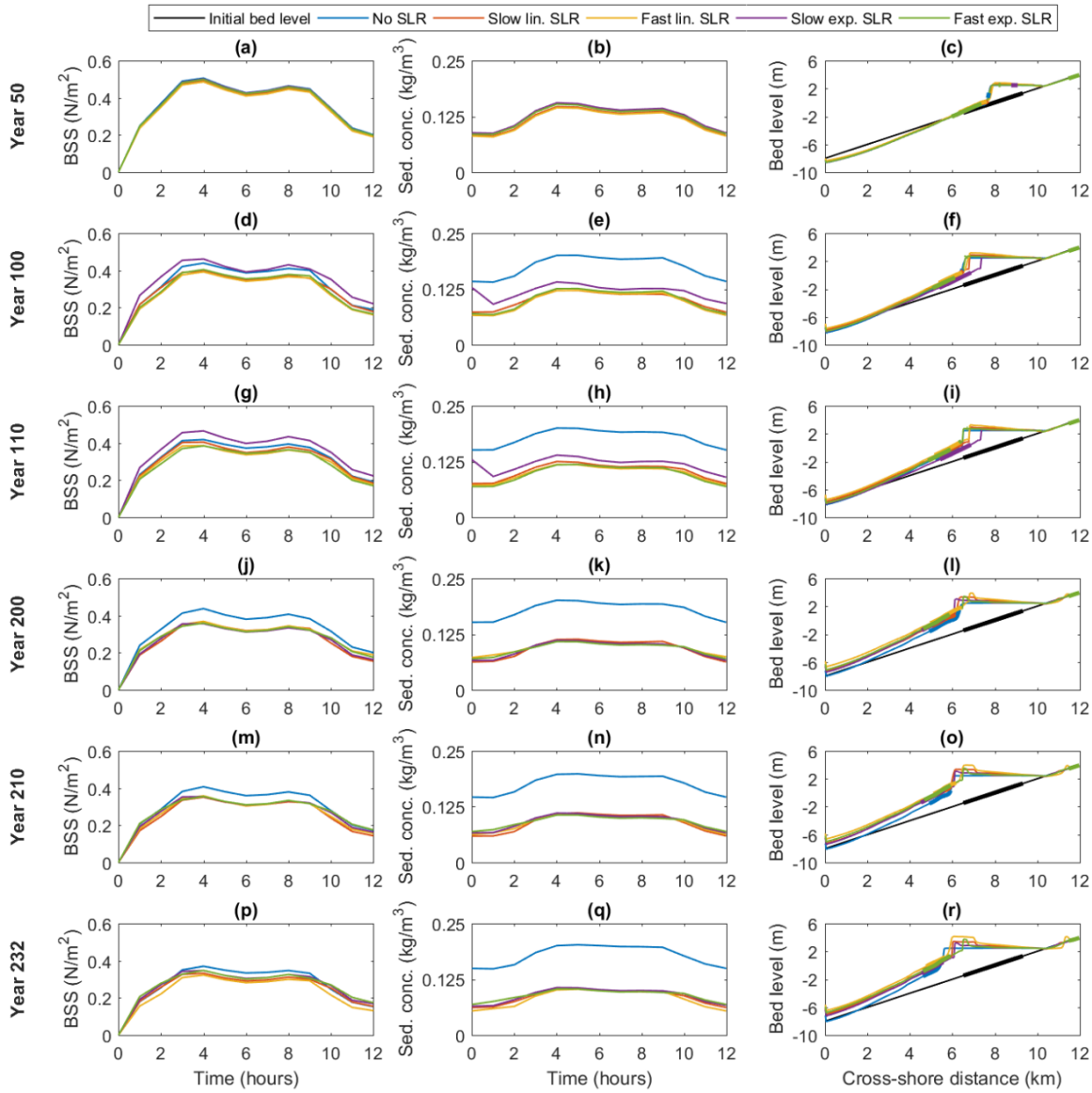

Figure 35: Mean bed shear stress, suspended sediment concentration and the bed profile at different years for the different sea level rise scenarios.

5 Discussion

In this section, the results will be discussed. This will be done through the use of the research questions described in section 1.3 as a guiding line. These research questions will be answered through analysis of the model results and comparison to literature.

5.1 Hydro-morphodynamics

The results show that waves have a significant impact on the development of the mangrove system. The sediment dynamics, morphology and vegetation are all influenced by the presence of waves. The complex relations between these different factors have an impact on the hydrodynamic processes, sediment dynamics and morphological change.

Research question 1a concerned the effect of wave height on the hydrodynamic processes in the system. The presence of waves causes noticeably higher bed shear stresses and sediment concentrations over the profile. Large waves with H_s = 1.0 m cause a significant amount of erosion, leading to sediment concentrations up to thirty times as large as without waves. This corresponds with the findings by Phuoc & Massel (2006), who found that wave intensity drives suspended sediment concentrations. While the presence of waves enhances the bed shear stress during both ebb and flood, this is not true with the flow velocities. While waves are present, the flow velocities are enhanced during ebb, but inhibited during flood. Because of the higher sediment concentrations, wave action causes increased sediment fluxes. A significant contribution to the increased sediment fluxes comes from breaking waves, which release energy on the bed and cause turbulence, stirring up the sediment. The sediment dynamics are affected by Stokes drift, which transports sediment from the seaward boundary towards the coast (Stokes, 1847; van den Bremer & Breivik, 2017). Even though the Stokes drift itself is not shown in the net sediment fluxes, its effect on the near-coastal morphodynamics is apparent.

To answer research question 1a, higher wave heights cause higher bed shear stress and sediment concentrations, and a larger ebb-flood flow velocity asymmetry. This causes larger sediment transport fluxes (Figure 19). This allows for more significant, faster morphological change than without waves.

Research question 1b concerned the impact of wave height on sediment transport in mangrove systems. Sediment transport is affected by the tidal asymmetry, by wave-related processes such as Stokes drift and by vegetation. Small and medium-sized waves cause more sediment to be transported towards the coast, while large waves cause more sediment to be transported away from the coast (Figure 36a). This matches behaviour found in literature, which shows that calm conditions cause coastal accretion while high wave intensity causes coastal regression (Christie et al., 1999). This behaviour is shown in the overwhelmingly negative net sediment fluxes for H_s = 1.0 m, while H_s = 0.3 m has overwhelmingly positive net sediment fluxes (Figure 19). However, the net sediment fluxes are only part of the complete story of sediment transport. The net sediment flux does not capture the wave-related processes such as Stokes drift, which also impact the direction of sediment transport. For example, medium-sized waves show net negative sediment fluxes, which indicate sediment moving away from the coast and thus coastal regression. Meanwhile, the evolution of the cross-shore profile shows coastal progradation. From this, it can be deduced that for medium-sized waves with H_s = 0.5 m, wave action causes sediment to move towards the coast. For large waves with H_s = 1.0 m, the Stokes drift is not sufficient for compensation of the negative sediment flux.

The balance of sediment transport in mangrove systems with waves is affected by the vegetation in several ways. Mangroves and their roots trap sediment, causing reduced sediment transport (Furukawa et al., 1997). The presence of vegetation increases the bed roughness of the system, causing extra drag force. This increases the tidal asymetry, causing more ebb dominance (Horstman et al., 2019). This process has only been observed in channelized mangrove systems in literature, which are not present in our model because it is a one-dimensional model. However, the model results show it to be present even in this one-dimensional setting. This effect can be seen in the velocity, bed shear stress and sediment concentration (Figure 15). This ebb dominance causes sediment to be transported away from the coast, inhibiting coastal progradation. This can be seen in the change of the boundary over time (Figure 21) in the scenarios without waves, where the coastline progrades more when there are no mangroves present. Pneumatophores have shown to affect the turbulence dissipation under waves in mangrove systems (Norris et al., 2017; Norris et al., 2019). How these factors contribute to the sediment transport in mangrove systems depends on the wave height (Figure 36b). Without waves, the presence of vegetation causes more sediment to be transported away from the coast due to increased tidal asymmetry (Horstman et al., 2019). This is shown in the more positive sediment fluxes when vegetation is absent (Figure 19). This causes less coastal accretion to occur when vegetation is present (Figure 20). For small waves with H_s = 0.3 m, there is little to no significant difference between the net sediment fluxes of scenarios with and without vegetation (Figure 19). For medium-sized waves with H_s = 0.5 m, the presence of vegetation causes less sediment to be transported away from the coast compared to when vegetation is absent. This shows that under medium-sized waves, the sediment-trapping properties of mangroves have a larger influence than the increased ebb-flow properties. Under small waves the influence of both properties are nearly equal, while without waves the ebb-flow increasing properties have a larger influence. These results lead to the conclusion that whether mangrove vegetation causes more or less seaward sediment transport depends on the wave height, with an increasing wave height causing less seaward sediment transport.

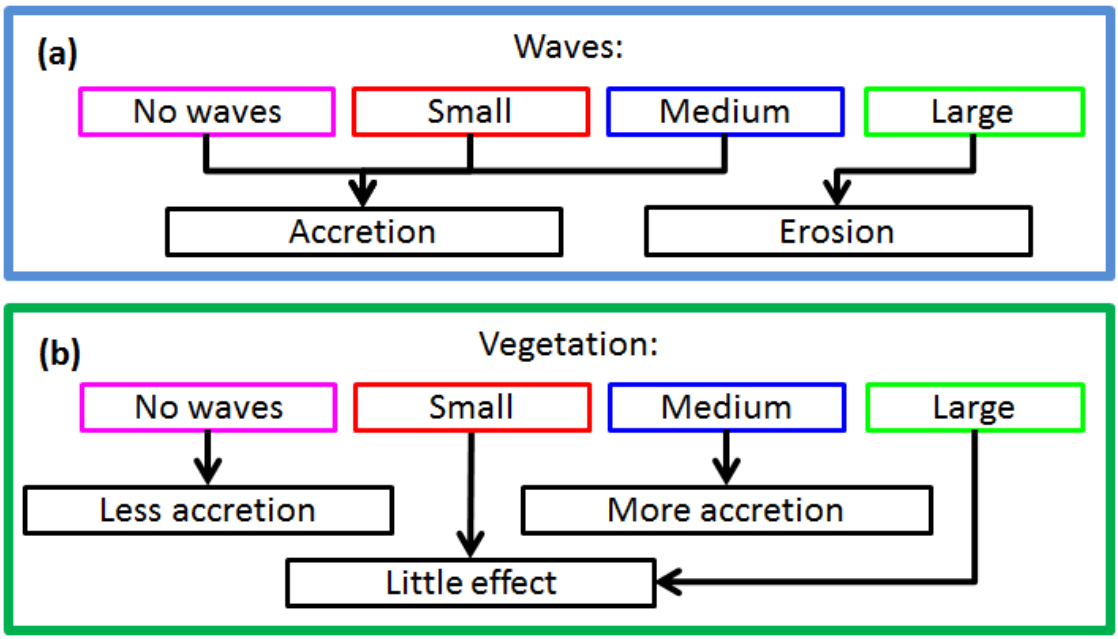

Figure 36: Schematic chart showing the relations between wave height, vegetation presence and coastal accretion/erosion. (a): Whether the different wave heights cause coastal accretion or erosion compared to the initial profile. (b): The effect of adding vegetation to the different wave height scenarios.

In the model scenarios with vegetation, the coastal progradation does not seem to start until the vegetation is more mature. Without vegetation, coastal progradation starts right away. This contrast leads to the conclusion that young vegetation mostly causes the effect of increasing drag force, while this balances out with more mature vegetation trapping more sediment. This is related to the different roughness formulations in the model between $h > h_v$ and $h \leq h_v$. To answer research question 1b, the question of whether sediment gets transported towards the coast or away from it depends on a complicated balance between wave height, tidal currents and vegetation presence.

Research question 1c concerned the effect of wave height on the coastal evolution of the system. The tidal asymmetry created by the addition of waves, which causes enhanced flow velocities during ebb but inhibited flow velocities during flood, causes more total seaward transport of sediment. This enhances negative sediment fluxes, promoting coastal regression. Conversely, waves transport sediment towards the coast through Stokes drift, promoting coastal progradation. With a constant sediment concentration at the seaward boundary, there is a constant input of sediment into the system. This is the largest contribution of wave action to the coastal evolution of the system. Comparing the amount of coastal accretion observed in the H_s = 0.3 m and the H_s = 0.5 m scenarios to that in the scenario without waves leads to the conclusion that the scenarios with wave action have a far greater amount of sediment input. As there is a constant sediment concentration of 0.02 kg/m^3 at the seaward boundary, Stokes drift allows this sediment to be continuously transported into the system.

The coastal morphodynamics depend on the balance between bed shear stress and the sediment concentration to deposit or erode sediment. Because wave action affects the balance between bed shear stress and suspended sediment concentration, with the change in the balance depending on the wave height, this results in more coastal progradation or in more coastal regression. The model results show that the balance between erosion and sedimentation is affected by the vegetation and by the wave height. Since the waves break very close to the seaward boundary for the H_s = 1.0 m scenario (Figure 17), the sediment is transported out of the system during ebb, which also causes coastal regression. This is shown in the very large negative net sediment fluxes (Figure 19). For the H_s = 0.3 m and H_s = 0.5 m scenarios, the waves break further landward, which prevents the sediment from being transported as far out to sea. Instead, they carry sediment from the seaward boundary towards the coast before they break, which is something the H_s = 1.0 m waves do not get the chance to do. This gives a reason for the stark difference between the development of the coast between the H_s = 0.5 m and H_s = 1.0 m scenarios. To answer research question 1c, small and medium-sized waves cause coastal progradation, while large waves cause coastal regression. The coastal progradation with small and medium-sized waves can be attributed to the large amount of sediment transported into the system by Stokes drift, while the coastal regression with large waves can be attributed to coastal erosion. All final profiles for the scenarios with waves show similar shapes to those found in *Avicennia* dominated coasts in nature, with flat platforms and steep edges (Bryan et al., 2017) (Figure 3). However, this is also observed in the scenarios without vegetation, leading to the conclusion that this coastal behavior is primarily caused by wave action and only secondarily by mangrove-induced processes. An interesting property of all final bed profiles with waves is that the lateral edge erosion described by Best et al. (2018) can clearly be observed. While Best et al. (2018) studied salt marshes instead of mangrove systems, using a different vegetation model, the same hydro-morphodynamic was used in this study, including the roller model simulating waves. This explains why the morphological evolution behaves in a similar manner. There are other differences

between the model set-up to explain the observed differences. The model described in Best et al. (2018) used a two-dimensional grid, which integrates cross-shore processes. This model grid differed in resolution, using grid cells of 10 m by 10 m, while this study used grid cells of 50 m by 50 m. The two-dimensional approach is mainly responsible for the differences between the model results, allowing for the generation of creeks in the salt marsh platform, which have been shown to affect the hydro-morphodynamics in coastal wetland systems through altering the flow velocities (Mazda et al., 1995; Horstman et al., 2019). Best et al. (2018) also found more landward transport due to waves, steeper marsh edge transitions under higher waves and larger platforms under lower waves. However, whether the landward transport is due to Stokes drift is not mentioned.

The results show that wave height does not always have a linear relation with the examined parameters. For some, the effect of wave height is clear, such as the final vegetation number, which decreases as wave height increases. However, for many factors, the effect of wave height is not as linear. Initially, the higher wave heights correspond with higher sediment concentrations and bed shear stresses. However, morphological change incurred by wave action will have its own effect on further hydrodynamic and morphodynamic change. These changes are not linearly related to the wave height. Because larger waves break with shallower water depths, the surf zone is located closer to the seaward boundary. Breaking waves are the main driver for increased suspended sediment concentration (Figure 17). The seaward shift of the surf zone with increasing wave height changes the sediment dynamics on a spatial scale, moving the peak suspended sediment concentration seaward. Since higher waves increase the near-shore bed shear stress during ebb and flood, it exceeds the critical value for erosion for a longer period of time during each tidal cycle. To offset this, a higher amount of suspended sediment is needed during high and low tide to promote sedimentation. With high waves (H_s = 1.0 m), the seaward movement of the peak suspended sediment concentration causes the near-shore area to not receive enough sediment with which to offset the increased erosion. This causes the coast to regress instead of prograde, whereas this is not the case with small and medium-sized waves.

5.2 Vegetation dynamics

Mangrove forests are of great economic and ecological value. Because of the value of healthy mangrove forests, an important factor to discuss is how they get affected by wave action. The parameters we use to judge the vegetation dynamics are the total vegetation number, total vegetation biomass and the average tree biomass over time. These fulfill different functions. The total vegetation biomass shows the health of the mangrove forest, with a declining total biomass showing a decline in health. The vegetation number and average tree biomass show the maturity of the forest, with an older, more developed forest having lower vegetation number and higher average tree biomass. The reason for this is that a young mangrove forest, shortly after colonization, consists of a relatively large amount of saplings, which compete more with each other as they grow. As mangrove trees mature, they exert a larger amount of competition stress on each other, as this is based on the diameter of the tree, which increases as the tree ages. This competition stress causes some of the saplings to die, decreasing the vegetation number without necessarily decreasing the total vegetation biomass.

The other factor controlling the vegetation development is the fitness ability, also called inundation stress. This is controlled by the relative hydroperiod of the grid cell on which the mangroves are located. Ellison & Farnsworth (1993) found that *Avicennia germinans* survives best around mean water level, and has trouble surviving at highest high water and lowest low water. This leads to the conclusion that *Avicennia germinans* needs a relative hydroperiod between 0.25 and 0.75 to survive, with its ideal relative hydroperiod being 0.50. Because this study models a symmetric tide, this means that (without sea level rise) the fitness ability of the species would be highest at z = 0 m, and decrease further away from that. However, the extended ebb period due to enhanced tidal asymmetry can shift this position of ideal hydroperiod.

Research questions 2a and 2b are on the effect of wave height on vegetation number and vegetation biomass, respectively. As discussed in section 5.1, waves cause an increased rate of morphological change. This higher rate of morphological change affects the vegetation. As mangrove vegetation has shown to be very sensitive to variations in their hydrological or tidal regimes, the large amount of wave energy has a noticeable effect on the resilience of mangroves (Blasco et al., 1996). Mangrove vegetation needs time in order to establish itself and grow in areas of suitable relative hydroperiod, as seedlings are very vulnerable and sensitive to disturbances (Balke et al., 2013). The relative hydroperiod depends on the elevation of the grid cell, since the elevation and the tide determine the amount of time a grid cell is inundated. Because of the faster morphological change, the elevation of a grid cell changes faster. This causes the relative hydroperiod in the grid cell to change faster, which causes the fitness ability of a grid cell to remain above 0.5 for a shorter amount of time. This creates less favorable colonization and growth conditions for mangroves, which results in a decrease in vegetation number. Because grid cells contain favorable growth conditions for a shorter amount of time, fewer mangroves mature, causing a lower total biomass, a lower average tree mass and a lower amount of grid cells covered by vegetation. This corresponds with the findings of Riis & Hawes (2003), who found the vegetation cover to be lower in systems with waves. The model results show a clear connection between wave height and vegetation, with an increase in wave height being related to lower vegetation number and total vegetation biomass. However, the evolution of these parameters is not the same through time, and the effect of wave height on the average vegetation biomass is not as linear. While large waves with H_s = 1.0 m don't allow for any vegetation development, all other scenarios show a unique progression of average vegetation biomass through

time. These are linked to the morphological development, since our results have shown that the vegetation is more influenced by changes in morphology than the other way around. To answer research questions 2a and 2b, higher waves cause a decrease in vegetation number and total vegetation biomass. However, the relationship between wave height and the average vegetation number is more complex, and dictated by the morphological evolution. The difference in the average vegetation biomass between the different wave height scenarios is smaller than the difference in vegetation number and total vegetation biomass, and which wave height scenario causes a higher average vegetation biomass fluctuates through time. However, when looking at the final vegetation parameters, scenarios with small and medium-sized waves show a higher average vegetation biomass than without waves. This shows that while waves decrease both vegetation number and total vegetation biomass, the former gets more affected than the latter. This reaffirms that waves mostly affect smaller trees, which are more vulnerable and thus die off (Balke et al., 2013), while larger trees survive.

For the scenario without waves, the average vegetation biomass decreases over time due to an increasing vegetation number while the total vegetation biomass stays relatively stable (Figure 25). If the morphology would not change, the vegetation number would decrease through time as the vegetation matures and exerts an increasing amount of biomass stress on the smaller trees. However, since the coast progrades, the mature vegetation at the landward edge of the forest continuously dies off due to the changing hydroperiod, while it gets replenished with young trees at the seaward edge. This causes large fluctuations in vegetation number and average tree biomass on short timescales, while causing relative stability on large time scales.

Research question 2c is on the effect of wave height on the vegetation development through time. For the scenario with small waves with H_s = 0.3 m, the morphology changes significantly faster than without waves (Figure 26). As the coastal boundary moves seaward at a constant rate, the average vegetation biomass stays relatively stable. This leads to the conclusion that small waves, while changing the morphology significantly faster than when waves are absent, do so at a rate that allows the vegetation to keep up with the changing hydroperiod. Then, as the morphological change slows down slightly in the last 75 years, this is reflected in the vegetation dynamics, with the average tree biomass immediately increasing due to vegetation having more time to mature, exerting more biomass stress on younger trees.

For the scenario with medium-sized waves with H_s = 0.5 m, because the presence of waves has a larger influence on the sediment-trapping ability of mangroves than on the ebb-flow enhancing ability, the presence of vegetation affects the balance between sedimentation and erosion in such a way that causes the coast to prograde more than without vegetation (Figure 20). Since an increased amount of coastal progradation has a negative effect on vegetation development, this creates a negative feedback loop. When coastal progradation slows down, the vegetation has time to mature (Figure 27). This alters the balance between sedimentation and erosion further, causing the coast to accrete vertically instead of horizontally (Figure 28), while the average vegetation biomass increases. This changes the hydrodynamics, causing the coast to accrete horizontally again, which causes the vegetation to die off, which allows for more relatively rapid coastal progradation. This fits the findings of Blasco et al. (1996), who found that even minor variations in hydrological regimes cause noticeable mortality. Eventually, coastal progradation slows down again, allowing the vegetation to mature again.

To answer research question 2c, the effect of wave height on the vegetation development through time depends on the relation between wave height, morphological change and vegetation dynamics. The vegetation dynamics are dictated by morphological change, which is dictated by the hydrodynamics. As the hydrodynamics are influenced by the vegetation, this creates complex feedback loops. These feedback loops are dependent on the wave height. For the scenarios without waves and with small waves, these feedback loops are positive, where the coastal development and the resulting vegetation development promote each other, leading to more of the same behaviour through time. For medium-sized waves, these feedback loops are negative, causing for more variable coastal development and vegetation development through time.

5.3 Sea level rise

Sea level rise has a small yet significant effect on the development of the mangrove system. Because there is a constant supply of sediment on the seaward boundary, there is a constant input of sediment into the system. Because of this constant sediment input and the lack of an obstruction on the landward boundary, the mangrove system can gradually shift landwards as the sea level increases. Most studies on the connection between sea level rise and mangrove systems have found the sediment accretion rate, which is dependent on the sediment supply, to be the deciding factor on whether or not the mangroves can survive sea level rise (Ellison J. C., 1993; Krauss, et al., 2013; Lovelock, et al., 2015; Woodroffe, 1990). This leads to the conclusion that the current sediment concentration of 0.02 kg/m^3 is enough to allow the mangrove system to keep up with sea level rise if no coastal barrier exists. Would the sediment concentration at the seaward boundary be lower, the effect of sea level rise on the vegetation is expected to have more significant impacts. Verification of this expectation requires further research.

Research question 3a was on the effect of wave action on the hydro-morphodynamics of the system in the presence of sea level rise, while research question 3b was on the effect of wave action on the vegetation number and biomass in the presence of sea level rise. When first looking at the scenarios without waves, it is clear that the coastal progradation suffers under the sea level rise. As established in section 5.1, Stokes drift plays an important role in transporting sediment from the seaward boundary into the system. Because Stokes drift is caused by wave action, the scenario without waves lacks this sediment transport mechanism, causing a lower amount of sediment input into the system. The limited supply of suspended sediment in these scenarios needs to be distributed over a larger area, since a larger part of the profile is submerged, during either the entire tidal cycle or part of it. Sediment is deposited further landward when sea level rise is present, but the amount of bed level change over the rest of the profile is decreased. For the vegetation, this mostly affects the most seaward part of the mangrove forests, which is typically populated by saplings. Because the bed level is comparatively lower, while the water level is comparatively higher, these are under increased inundation stress, which causes them to die. This causes the vegetation number to go down and the average tree mass to go up when sea level rise is introduced to the system. However, the impact of sea level rise on the vegetation dynamics is lessened because vegetation presence has a positive feedback with sea level rise. Because increased tidal inundation causes more frequent and longer periods of mineral sediment settling and enhanced vegetation growth, vertical accretion is increased (Kirwan et al., 2016). This, especially when no natural or human-made barriers prevent the vegetation from migrating inland, allows the vegetation to compensate for the negative effects of sea level rise, which allows the vegetation to survive.

With waves, the situation is different. The coastal boundary, which is defined as the grid cell where the bed elevation is closest to 0, progrades more when sea level rise is introduced to the system. This can be explained by looking at the final bed profiles. As the sea level rises, because of the high sediment concentration that is transported by waves, the highest point of the beach follows it. This causes the rest of the coastal slope to follow it as well, which causes the z = 0 m point to move seaward. The amount with which the bed level increases corresponds with the amount of sea level rise. However, as there is no change in sediment input between the different sea level rise scenarios, the sediment needed for this increase in bed level must lead to a relative decrease in sediment at another location. Because of this, the highest point of the coastal profile is located further landward. This causes the coastal slope to become less steep. This leads to a larger area with favorable relative

hydroperiod. This affects the vegetation of the system, causing a higher vegetation number consisting mostly of saplings, decreasing the average tree biomass. The development of the vegetation through time is also affected by sea level rise. As described in section 5.1, the H_s = 0.5 m scenario develops uniquely because the presence of waves affects the influence of the mangrove vegetation on the sediment trapping more than its influence on the ebb-tidal flow velocities. This balance is also affected by the sea level rise, which changes the hydrodynamics through the increased water depth. This changes the points in time where coastal progradation slows down, and the points in time where it speeds up. As described in section 5.1, this also affects and is affected by the vegetation dynamics. These also change with the addition of sea level rise, with the points in time where the vegetation starts maturing and the points in time where it dies off change due to the increased water depth.

To answer research question 3a, the increased water depth due to sea level rise gives a larger area over which the sediment can be deposited. Without waves, the extra landward sedimentation leads to less sedimentation over the rest of the profile, leading to lower bed levels. With waves, because Stokes drift transports enough sediment towards the coast for it to keep up with the sea level rise, the highest point of the profile becomes situated further landward. To answer research question 3b, without waves sea level rise has a negative effect on the resilience of the mangrove system, while it has a positive effect when waves are present.

Research question 3c was on the influence of different rates and types of sea level rise on the effect of wave action on mangrove system resilience. In this study, the rates of sea level rise considered are 1.32 m and 2.22 m over three centuries, called “slow” and “fast” sea level rise respectively. The types of sea level rise considered are linear and exponential (Figure 13). The effect of sea level rise can be seen in all wave height scenarios. While the different types and rates of sea level rise seem to have a similar effect without waves, the differences become more apparent with increasing wave height (Figure 31). In general, the rate of sea level rise affects the amount of morphological change, with higher rates of sea level rise showing a larger amount of boundary shift. The influence of the type of sea level rise, in comparison, is almost negligible. However, the type of sea level rise has a more significant effect on the resulting beach profile, when small or medium-sized waves are included (Figure 30). While the scenarios without sea level rise result in a flat platform, the linear sea level rise scenarios results in a straight-sloped platform, while the exponential sea level rise scenarios result in a curved-sloped platform. As this corresponds with the shape of the sea level rise curves (Figure 13), it can be concluded that the shape of the platform at the landward edge of the coastal slope follows the water level.

The vegetation is less affected by sea level rise than the morphology, with an exception for the H_s = 0.5 m scenario. Here, sea level rise’s effect on the hydrodynamics affects the balance between sedimentation and erosion affects the cycle of vegetation maturation and die-off. While this cycle of affected by all sea level rise scenarios, it is more significantly affected by the exponential sea level rise scenarios. This shows that the points in time where coastal progradation speeds up and where it slows down are more significantly affected by the change of the rate with which water depth increases than the rate with which water depth increases itself. To answer research question 3c, the rate of sea level rise affects the amount of morphological change, while the type of sea level rise affects the shape of the final bed profile, and the vegetation development through affecting the balance between sedimentation and erosion.

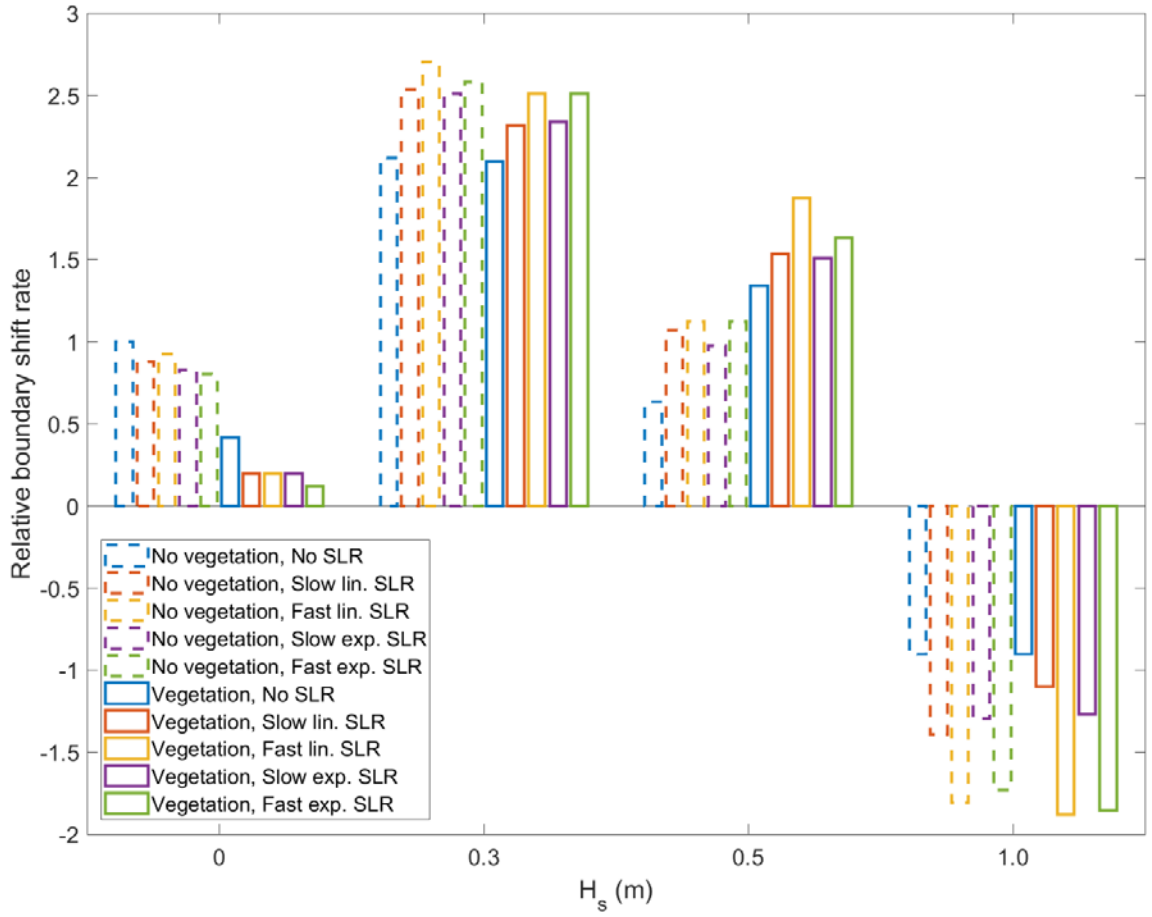

Figure 37: Relative boundary shift rate for all different scenarios.

The difference between sea level rise scenarios for a given wave height is significantly less than the difference between wave height scenarios for a given sea level rise. For morphological change, this can be determined by looking at the relative boundary shift rate, which is calculated by dividing each scenario's average boundary shift rate by the average boundary shift rate of the scenario without waves, vegetation or sea level rise. This shows that the differences between the different wave height scenarios and the different vegetation scenarios are more significant than the difference between the different sea level rise scenarios (Figure 37). A similar method can be used to calculate the relative vegetation number, relative total vegetation biomass, relative vegetation coverage and relative average tree mass (Figure 38). These all show larger differences between the different wave height scenarios than between the different sea level rise scenarios. However, this is possibly because of the sediment supply being sufficient for the mangrove vegetation to keep up with the rising sea level. Studies have shown that waves can prove beneficial in helping coastal wetlands keep up with sea level rise through increased sediment supply, through lateral edge erosion and resuspension of this sediment on the top of the platform (Hopkinson et al., 2018). If the sediment concentration at the seaward boundary would be decreased or eliminated, this mechanism could prove more relevant and could cause a bigger difference between the different sea level rise scenarios.

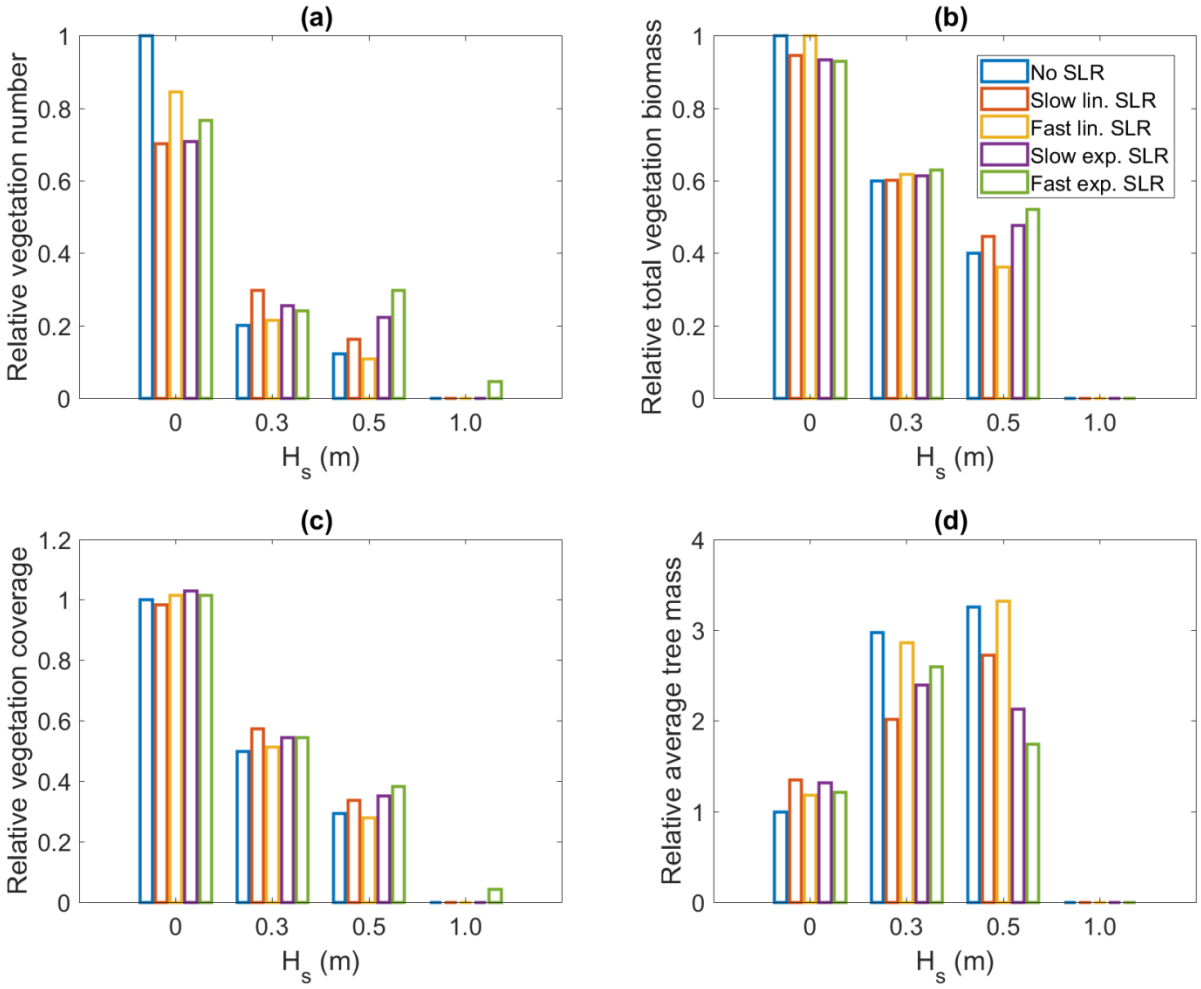

Figure 38: Relative vegetation number, relative total vegetation biomass, relative vegetation coverage and relative average tree mass for all different scenarios.

Since wave height has a far larger influence on the morphodynamics and vegetation dynamics than sea level rise does, and since both of these factors are subject to climate change, it might be advisable for policy makers to give priority to the change in wave height when researching the impacts of climate change on a mangrove system. At subtropical latitudes, wave heights are most likely to decrease with the changing climate (Hemer et al., 2013). At tropical latitudes, this is more regionally dependent. For example, the west coast of South America is likely to see increasing wave heights, while South-East Asia is likely to see decreasing wave heights (Figure 7). As mangroves primarily inhabit coastlines at tropical and subtropical wave heights, this is generally a positive change for mangrove populations. However, policy makers in charge of tropical mangrove systems should be more careful of increasing wave heights than those in charge of subtropical mangrove systems. All policy makers should also keep in mind that sea level rise might also itself be a cause of increasing wave heights, which might counteract the wave height decreasing effects of climate change (Vu et al., 2018). They should also keep in mind regional changes in the wind climate, which may have a significant impact on wave action under climate change (Charles et al., 2012). Since these different factors, many of which are regionally dependent, make the potential changes in wave height less clear than the changes in sea level, policy makers in charge of coastal mangrove systems are advised to invest more resources in investigating local changes in the wave climate.

5.4 Model limitations and suggestions for future research

There are a few clear limitations to the current model set up. The length of the model is a clear limiting factor, especially with H_s = 1.0 m. Because of the waves breaking so close to the boundary in that scenario, results could be very different if the seaward boundary was further away. Another limiting factor is the 50 m by 50 m grid cell size. Especially for vegetation, this grid cell size might lose a lot of the gradual variation within one grid cell. A smaller grid size would allow the model to capture a smoother transition in relative hydroperiod, allowing for more realistic model results.

Another large limitation is the roller model. The lack of short waves means the model does not calculate waves or their effect as accurately as the full-fledged Delft3D-WAVE model would. Another big limitation is that the roller model does not incorporate wave dampening effects by vegetation. Because this is a study on the interactions between waves, morphodynamics and vegetation, not incorporating one significant interface between these factors compromises the accuracy of the results. Not including vegetation's wave dampening effects causes the waves to have relatively more energy and thus relatively large effects on the coastal hydrodynamics, compared to if the effects would have been included. It would show a larger difference between the scenarios with and the scenarios without waves.

One more limitation is the frequency with which the model saves the map output. For this model, this is once every hour. The model uses this data to calculate the relative hydroperiod, which would be more accurate if the map data was to be saved more frequently.

Based on the results of this study, many different changes can be made to the model set-up to obtain more information about the different factors. The following paragraphs will give suggestions on changes to the model set-up that could provide more insight into the development of coastal mangrove systems under the effects of wave action.

The cross-shore length of the model could be changed to see if it is really the problem of breaking close to the seaward boundary which causes the distinctive shape of the H_s = 1.0 m bed profiles. If the distance between the seaward boundary and the location of wave breaking increases, this could cause the sediment to remain in the system instead of being transported out of it. This would cause the coastal erosion to decrease. The fast sea level rise scenarios cause the high water level to exceed 4 m, which is the initial bed level at the landward boundary. The limitations this causes is most clearly seen in the H_s = 1.0 m scenarios, where the vertical cliff eventually migrates to be located on top of the landward boundary. Expanding the cross-shore length of the model would allow the initial bed level at the landward boundary to exceed the water level at high water level combined with fast sea level rise, allowing more space for this vertical cliff to migrate.

More runs should be done with different wave heights, in order to find the gradual change of processes between H_s = 0.0 m and H_s = 1.0 m. This would prove useful in pinpointing the wave height where the effect of vegetation switches from decreasing to increasing coastal accretion, which is expected to lie somewhere around H_s = 0.3 m. It would also prove useful in pinpointing the wave height where the change in coastal morphology switches from net accretion to net erosion, which is expected to lie somewhere between H_s = 0.5 and H_s = 1.0 m.

Runs should be done with the Delft3D-WAVE module, both including and excluding the roller model. This way, the impact of this different way of calculating waves can be accurately observed, especially

considering the roller model does not include the vegetation in its calculations. While these calculations would take significantly longer, they would be more accurate. Because these calculations would include the wave-dampening effect of vegetation, the amount of wave energy would be reduced. This would lead to less morphological change due to waves.

More vegetation species could be included to observe how these species would interact with each other, and whether zonation will occur as found in literature (Alongi, 2002; Liu et al., 2018). This can be used to study how this zonation changes under wave action. This would likely increase the amount of sediment trapping (Kathiresan, 2003), which would increase the amount of coastal accretion. With species with different ideal relative hydroperiods, they would be able to cover a larger area of the model domain, influencing the hydro-morphodynamics on a larger scale.

The sediment concentration at the seaward boundary could be decreased or eliminated, to observe how the system behavior changes when there is a more limited amount of sediment. The coastal accretion in scenarios with small or medium-sized waves can be largely attributed to the continuous sediment input. Stokes drift transports sediment from the seaward boundary towards the coast, causing large amounts of coastal accretion. Limiting the sediment concentration at the seaward boundary removes this mechanism, which will probably have a large impact on the coastal evolution of the system. It can also be used to study what happens to the mangroves when the sediment accretion does not keep up with the sea level rise. This will most likely have large impacts on the survival of the mangrove system (Woodroffe, 1990; Ellison, 1993; Lovelock, et al., 2015).

The map data save frequency could be increased from once every hour in order to make the hydroperiod calculations more accurate. The vegetation model currently takes twelve points in time into account per tidal cycle, and uses the inundation at these moments to calculate the relative hydroperiod. A higher map data save frequency would increase the accuracy of these calculations.

The initial slope of the bed could be varied, in order to study the effect of steeper and gentler transitions in bed level on the coastal hydrodynamics and on the relative hydroperiod. As a steeper slope would create a smaller area in which the mangroves could grow, this would have significant effects on the vegetation dynamics and thus on the hydrodynamics. The opposite effect would result from using a gentler slope.

The model could be expanded to a two-dimensional grid in order to incorporate long-shore processes, which would make the model significantly more realistic. However, this would also make the model more computationally intensive and complicated. An important process that could be captured by changing the model to a two-dimensional grid is the forming of mangrove creeks and the possibility of measuring how the flow velocities in these creeks change with the addition of wave action. Multiple studies found that mangrove vegetation enhances the tidal asymmetry in tidal creeks by increasing the ebb-tidal dominance (Mazda et al., 1995; Horstman et al., 2019). While these tidal creeks are not present in the current model set-up because of the one-dimensional grid, this effect has still been observed in the model results. Changing to a two-dimensional grid could provide more insight into this process and wave action affects it. Changing the model set-up to a two-dimensional grid also allows the model results to be more accurately compared to the results found by Best et al. (2018), which would allow the differences between mangrove and salt marsh systems to be more closely investigated.

6 Conclusions

The introduction of waves to a mangrove system has a large effect on the hydrodynamics of the system, which affects the morphodynamics, which in turn affects the vegetation dynamics and development. Waves affect the hydrodynamics through altering the bed shear stress and suspended sediment concentration of the system, which affect the morphodynamics through altering the balance between sedimentation and erosion. Increased bed shear stresses enhance erosion, while increased suspended sediment concentrations cause enhanced sedimentation. This affects coastal progradation and recession, which affects the coastal morphology and the rate at which it changes. This affects the relative hydroperiod of the grid cell, which affects the vegetation dynamics. Vegetation affects the hydrodynamics, which creates a feedback loop between the change in vegetation and the change in morphology.

Small and medium-sized waves overwhelmingly cause enhanced coastal progradation, while large waves cause coastal regression. Because of this enhanced morphological change, the bed level at a location changes faster when waves are present than when they are not. This causes the relative hydroperiod to change, which forces additional stress upon the vegetation. This causes the vegetation number and total vegetation biomass to decrease. Because this primarily affects smaller trees, the average vegetation biomass increases.

The interaction between vegetation presence, wave height and coastal development is complex, with vegetation inhibiting coastal progradation without waves but promoting it with medium-sized waves. This is attributed to two properties of mangrove forests: the trapping of sediment and the enhancement of ebb-tidal flows. The former promotes accretion of sediment and thus coastal progradation, while the latter promotes erosion and thus coastal regression. As the wave height increases, the tidal asymmetry, bed shear stress and suspended sediment concentration also increase. These all get affected by vegetation in different amounts, causing the relation between vegetation and coastal progradation to change with increasing wave height.

Sea level rise has a noticeable effect on the development of a mangrove coast. Sea level rise causes an increase in water depth, which affects the hydrodynamics through the flow velocity, the current-related bed shear stress, the wave related bed shear stress and the Stokes drift. The rate of sea level rise affects the rate of morphological change, with faster sea level rise causing faster morphological change. Linear and exponential sea level rise scenarios show different morphodynamic behavior. The final bed profile shape depends on the type of sea level rise. Without sea level rise, a flat platform forms at the high water level. Linear sea level rise results in a straight-sloped platform and exponential sea level rise scenarios result in a curved-sloped platform. Because the sediment supply is large enough for the mangroves to keep up with sea level rise, the impact of sea level rise on the vegetation dynamics is small, especially when seen relative to the impact of wave height.

While wave action, mangrove vegetation and sea level rise all affect the development of the coastal system, their contributions are not equal. Wave action affects the coastal dynamics the most, followed by the mangrove vegetation and sea level rise. Understanding the complex relationships between coastal hydrodynamics, wave action, vegetation dynamics, morphodynamics and sea level rise will prove essential in providing adequate governance of mangrove systems. The knowledge that the effect of sea level rise is smaller than the effect of wave height on coastal mangrove systems will prove useful for policy makers in charge of coastal mangrove systems who are preparing for the

consequences of climate changes. When policy makers have limited resources to spend on climate change adaptation, it is more important to focus on the changing wave climate than on the changing sea level.

7 References

Airoldi, L., Abbiati, M., Beck, M. W., Hawkins, S. J., Jonsson, P. R., Martin, D., . . . Åberg, P. (2005). An ecological perspective on the deployment and design of low-crested and other hard coastal defence structures. *Coastal Engineering, 52*(10-11), 1073-1087.

Alongi, D. M. (2002). Present state and future of the world's mangrove forests. *Environmental Conservation, 29*(3), 331-349.

Alongi, D. M. (2008). Mangrove forests: Resilience, protection from tsunamis, and responses to global climate change. *Estuarine, Coastal and Shelf Science, 76*, 1-13.

Alongi, D. M. (2012). Carbon sequestration in mangrove forests. *Carbon Management, 3*(3), 313-322.

Anthony, E. J. (2004). Sediment dynamics and morphological stability of estuarine mangrove swamps in Sherbro Bay, West Africa. *Marine Geology, 208*(2-4), 207-224.

Asbridge, E., Lucas, R., Ticehurst, C., & Bunting, P. (2016). Mangrove response to environmental change in Australia's Gulf of Carpentaria. *Ecology and Evolution, 6*(11), 3523-3539.

Augustinus, P. G. (1995). Chapter 12 Geomorphology and Sedimentology of Mangroves. *Developments in Sedimentology, 53*, 333-357.

Balke, T., Bouma, T. J., Herman, P. M., Horstman, E. M., Sudtongkong, C., & Webb, E. L. (2013). Cross-shore gradients of physical disturbance in mangroves: implications for seedling establishment. *Biogeosciences, 10*, 5411-5419.

Baptist, M. J. (2005). *Modelling floodplain biogeomorphology.* PhD Thesis, Delft University of Technology.

Bärenbold, F., Crouzy, B., & Perona, P. (2016). Stability analysis of ecomorphodynamic equations. *Water Resources Research, 52*(2), 1070-1088.

Barloventomagico. *Mangle negro, rosado, prieto o algarrobo [Black mangrove] (Avicennia germinans).* Unare Lagoon, Anzoátegui, Venezuela. Retrieved from https://www.flickr.com/photos/barloventomagico/2578620629

Beach, R. A., & Sternberg, R. W. (1996). Suspended-sediment transport in the surf zone: response to breaking waves. *Continental Shelf Research, 16*(15), 1989-2003.

Berger, U., & Hildenbrandt, H. (2000). A new approach to spatially explicit modelling of forest dynamics: spacing, ageing and neighbourhood competition of mangrove trees. *Ecological Modelling, 132*(3), 287-302.

Best, Ü. S., van der Wegen, M., Dijkstra, J., Willemsen, P. W., Borsje, B. W., & Roelvink, D. J. (2018). Do salt marshes survive sea level rise? Modelling wave action, morphodynamics and vegetation dynamics. *Environmental Modelling & Software*.

Bird, E. C. (1986). Mangroves and intertidal morphology in Westernport Bay, Victoria, Australia. *Marine Geology, 69*(3-4), 251-271.

Blasco, F., Saenger, P., & Janodet, E. (1996). Mangroves as indicators of coastal change. *Catena, 27*, 167-178.

Bremer, T. S., & Breivik, Ø. (2017). Stokes drift. *Philosophical Transactions of the Royal Society A: Mathematical, Physical and Engineering Sciences, 376*(2111), 23.

Bryan, K. R., Nardin, W., Mullarney, J. C., & Fagherazzi, S. (2017). The role of cross-shore tidal dynamics in controlling intertidal sediment exchange in mangroves in Cù Lao Dung, Vietnam. *Continental Shelf Research, 147*, 128-143.

Charles, E., Idier, D., Delecluse, P., Déqué, M., & Le Cozannet, G. (2012). Climate change impact on waves in the Bay of Biscay, France. *Ocean Dynamics, 62*(6), 831-848.

Chen, R., & Twilley, R. R. (1998). A gap dynamic model of mangrove forest development along gradients of soil salinity and nutrient resources. *Journal of Ecology, 86*, 37-51.

Chmura, G. L. (2009). Tidal Salt Marshes and Mangrove Swamps. In F. I. Isla, & O. Iribarne, *Coastal Zones and Estuaries* (pp. 379-392). Oxford, United Kingdom: UNESCO-EOLSS.

Christie, M. C., Dyer, K. R., & Turner, P. (1999). Sediment Flux and Bed Level Measurements from a Macro Tidal Mudflat. *Estuarine, Coastal and Shelf Science, 49*(5), 667-688.

Coco, G., Zhou, Z., van Maanen, B., Olabarrieta, M., Tinoco, R., & Townend, I. (2013). Morphodynamics of tidal networks: Advances and challenges. *Marine Geology, 346*, 1-16.

Danielsen, F., Sørensen, M. K., Olwig, M. F., Selvam, V., Parish, F., Burgess, N. D., . . . Suryadiputra, N. (2005). The Asian Tsunami: A Protective Role for Coastal Vegetation. *Science, 310*(5748), 643.

Das, S., & Vincent, J. R. (2009). Mangroves protected villages and reduced death toll during Indian super cyclone. *PNAS, 106*(18), 7357-7360.

Davidson-Arnott, R. G., & Greenwood, B. (2009). Waves and Sediment Transport in the Nearshore Zone. In F. I. Isla, & O. Iribarne, *Coastal Zones and Estuaries* (pp. 43-61). EOLSS Publications.

Deltares. (2014). *Delft3D-FLOW, User Manual.* Delft: Deltares.

Det Norske Veritas. (2011). *Recommended Practice DNV-RP-H103.*

Dronkers, J. (1986). Tidal asymmetry and estuarine morphology. *Netherlands Journal of Sea Research, 20*(2-3), 117-131.

Ellison, A. M., & Farnsworth, E. J. (1993). Seedling survivorship, growth, and response to disturbance in Belizean mangal. *American Journal of Botany, 80*(10), 1137-1145.

Ellison, A., Farnsworth, E., & Moore, G. (2010). *Avicennia germinans.* The IUCN Red List of Threatened Species.

Ellison, J. C. (1993). Mangrove retreat with rising sea-level, Bermuda. *Estuarine, Coastal and Shelf Science, 37*(1), 75-87.

Francalanci, S., Solari, L., Toffolon, M., Siviglia, A., & Bertoldi, W. (2013). Effects of Bar Morphology and Vegetation on Flow Resistance in Gravel-Bed Rivers. *The 8th Symposium on River, Coastal and Estuarine Morphodynamics*, (p. 137). Santander, Spain.

Furukawa, K., & Wolanski, E. (1996). Sedimentation in Mangrove Forests. *Mangroves and Salt Marshes, 1*(1), 3-10.

Furukawa, K., Wolanski, E., & Mueller, H. (1997). Currents and Sediment Transport in Mangrove Forests. *Estuarine, Coastal and Shelf Science, 44*(3), 301-310.

Galvin, C. J. (1968). Breaker Type Classification on Three Laboratory Beaches. *Journal of Geophysical Research, 73*(12), 3651-3659.

Giardino, A., van der Werf, J., & van Ormondt, M. (2010). *Simulating coastal morphodynamics with Delft3D: case study Egmond aan Zee.* Deltares Delft Hydraulics.

Giri, C., Ochieng, E., Tieszen, L. L., Zhu, Z., Singh, A., Loveland, T., . . . Duke, N. (2011). Status and distribution of mangrove forests of the world using earth observation satellite data. *Global Ecology and Biogeography, 20*, 154-159.

Göltenboth, F., & Schoppe, S. (2006). 10: Mangroves. In F. Göltenboth, S. Schoppe, K. H. Timotius, & J. Margraf, *Ecology of Insular Southeast Asia* (pp. 187-214). Elsevier.

Hemer, M. A., Fan, Y., Mori, N., Semedo, A., & Wang, X. L. (2013). Projected changes in wave climate from a multi-model ensemble. *Nature Climate Change, 3*, 471-476.

Héquette, A., Hemdane, Y., & Anthony, E. J. (2008). Sediment transport under wave and current combined flows on a tide-dominated shoreface, northern coast of France. *Marine Geology, 249*(3-4), 226-242.

Hogarth, P. J. (2007). *The biology of mangroves and seagrasses.* Oxford: Oxford University Press.

Hogarth, P. J. (2015). Chapter 2: Mangroves and their Environment. In *The Biology of Mangroves and Seagrasses* (pp. 8-41). Oxford Univesity Press.

Hopkinson, C. S., Morris, J. T., Fagherazzi, S., Wollheim, W. M., & Raymond, P. A. (2018). Lateral Marsh Edge Erosion as a Source of Sediments for Vertical Marsh Accretion. *Journal of Geophysical Research: Biogeosciences, 123*, 22.

Horstman, E. M., Bryan, K. M., Mullarney, J. C., & Pilditch, C. A. (2016). Model versus nature: Hydrodynamics in mangrove pneumatophores. *Coastal Engineering Proceedings, 1*(35), 19.

Horstman, E. M., Mullarney, J. C., & Bryan, K. R. (2019). Tidal currents in a mangrove creek system quantified. *Abstract from NCK-DAYS 2019*, (pp. 51-51). Enkhuizen, the Netherlands.

Intergovernmental Panel on Climate Change. (2014). *Climate Change 2014: Synthesis Report.* Geneva, Switzerland.

Iribarren, C. R., & Norales, C. (1949). Protection des ports. *Proceedings XVIIth International Navigation Congress, Section II, Communication, 4*, 31-80.

Kathiresan, K. (2003). How do mangrove forests induce sedimentation? *Revista de Biología Tropical, 51*(2), 355-360.

Kathiresan, K., & Bingham, B. L. (2001). Biology of mangroves and mangrove Ecosystems. *Advances in Marine Biology, 40*, 81-251.

Kathiresan, K., & Rajendran, N. (2005). Coastal mangrove forests mitigated tsunami. *Estuarine, Coastal and Shelf Science, 65*(3), 601-606.

Kirwan, M. L., & Megonigal, J. P. (2013). Tidal wetland stability in the face of human impacts and sea-level rise. *Nature, 504*, 53-60.

Kirwan, M. L., Temmerman, S., Skeehan, E. E., Guntenspergen, G. R., & Fagherazzi, S. (2016). Overestimation of marsh vulnerability to sea level rise. *Nature Climate Change, 6*, 253-260.

Komiyama, A., Ong, J. E., & Poungparn, S. (2008). Allometry, biomass, and productivity of mangrove forests: A review. *Aquatic Botany, 30*(3), 128-137.

Krauss, K. W., Cahoon, D. R., Allen, J. A., Ewel, K. C., Lynch, J. C., & Cormier, N. (2010). Surface Elevation Change and Susceptibility of Different Mangrove Zones to Sea-Level Rise on Pacific High Islands of Micronesia. *Ecosystems, 13*(1), 129-143.

Krauss, K. W., McKee, K. L., Lovelock, C. E., Cahoon, D. R., Saintilan, N., Reef, R., & Chen, L. (2013). How mangrove forests adjust to rising sea level. *New Phytologist, 202*, 19-34.

Laffoley, D., & Grimsditch, G. (2009). *The management of Natural Coastal Carbon Sinks.* IUCN.

Leong, L. F., Kwan, C., Chong, V. C., & Sasekumar, A. (2005). Chapter 17 - Resource Valuation of Kuala Selangor Mangrove Forest. In A. Sasekumar, & V. C. Chong, *Ecology of Klang Strait* (pp. 237-259). Kuala Lumpur: University of Malaya.

Liu, M., Zhang, H., Lin, G., Lin, H., & Tang, D. (2018). Zonation and Directional Dynamics of Mangrove Forests Derived from Time-Series Satellite Imagery in Mai Po, Hong Kong. *Sustainability, 10*(6), 16.

Lovelock, C. E., Cahoon, D. R., Friess, D. A., Guntenspergen, G. R., Krauss, K. W., Reef, R., . . . Triet, T. (2015). The vulnerability of Indo-Pacific mangrove forests to sea-level rise. *Nature, 526*, 559-563.

Maa, P.-Y., & Mehta, A. J. (1987). Mud erosion by waves: a laboratory study. *Continental Shelf Research, 7*(11-12), 1269-1284.

Mazda, Y., Kanazawa, N., & Wolanski, E. (1995). Tidal asymmetry in mangrove creeks. *Hydrobiologia, 295*, 51-58.

Mazda, Y., Magi, M., Kogo, M., & Hong, P. N. (1997). Mangroves as a coastal protection from waves in the Tong King delta, Vietnam. *Mangroves and Salt Marshes, 1*, 127-135.

Mazda, Y., Magi, M., Nanao, H., Kogo, M., Miyagi, T., Kanazawa, N., & Kobashi, D. (2002). Coastal erosion due to long-term human impact on mangrove forests. *Wetlands Ecology and Management, 10*, 1-9.

McIvor, A., Möller, I., Spencer, T., & Spalding, M. (2012). Reduction of Wind and Swell Waves by Mangroves. *Natural Coastal Protection Series: Report 1*.

Meyer, R. E. (1972). *Waves on Beaches and Resulting Sediment Transport.* New York: Academic Press.

Montgomery, J. M., Bryan, K. R., Horstman, E. M., & Mullarney, J. C. (2018). Attenuation of Tides and Surges by Mangroves: Contrasting Case Studies from New Zealand. *water, 10*, 16.

Montgomery, J. M., Bryan, K. R., Mullarney, J. C., & Horstman, E. M. (2019). Attenuation of storm surges by coastal mangroves. *Geophysical research letters, 46*(5), 2680-2689.

Ng, P. K., & Sivasothi, N. (2002). *A Guide to Mangroves of Singapore 1: The Ecosystem & Plant Diversity.* Singapore Science Centre.

Norris, B. K., Mullarney, J. C., Bryan, K. R., & Henderson, S. M. (2017). The effect of pneumatophore density on turbulence: A field study in a Sonneratia-dominated mangrove forest, Vietnam. *Continental Shelf Research, 147*, 114-127.

Norris, B. K., Mullarney, J. C., Bryan, K. R., & Henderson, S. M. (2019). Turbulence Within Natural Mangrove Pneumatophore Canopies. *JGR Oceans, 124*(4), 2263-2288.

Okamato, T., Fortes, C. J., & Basco, D. (2011). Bore propagation speed at the termination of wave breaking. *Coastal Engineering Proceedings, 1*(32), 7.

Peregrine, D. H. (1983). Breaking Waves on Beaches. *Ann. Rev. Fluid Mech., 15*, 149-178.

Perona, P., Crouzy, B., Mclelland, S. J., Molnar, P., & Camporeale, C. (2014). Ecomoprhodynamics of rivers with converging boundaries. *Earth Surface Processes and Landforms, 39*(12).

Phuoc, V. H., & Massel, S. R. (2006). Experiments on wave motion and suspended sediment concentration at Nang Hai, Can Gio mangrove forest, Southern Vietnam. *Oceanologia, 48*(1), 23-40.

Pinet, P. R. (2008). Chapter 7: Waves in the Ocean. In P. R. Pinet, *Invitation to Oceanography* (pp. 230-261). Jones & Bartlett Learning.

Pye, K., & Neal, A. (1994). Coastal dune erosion at Formby Point, north Merseyside, England: Causes and Mechanisms. *Marine Geology, 119*(1-2), 39-56.

Reniers, A. J., Roelvink, J. A., & Thornton, E. B. (2004). Morphodynamic modeling of an embayed beach under wave group forcing. *Journal of Geophysical Research, 109*(C1), 1-22.

Riis, T., & Hawes, I. (2003). Effect of wave exposure on vegetation abundance,richness and depth distribution of shallow water plantsin a New Zealand lake. *Freshwater Biology, 48*, 75-87.

Roelvink, J. A. (1993). Dissipation in random wave groups incident on a beach. *Coastal Engineering, 19*, 127-150.

Schuerch, M., Vafeidis, A., Slawig, T., & Temmerman, S. (2013). Modeling the influence of changing storm patterns on the ability of a salt marsh to keep pace with sea level rise. *Journal of Geophysical Research: Earth Surface, 118*(1), 84-96.

Shugart, H. H. (1984). *A Theory of Forest Dynamics: The Ecological Implications of Forest Succession Models.* New York: Springer-Verlag.

Steffens, B., & Rasmussen, A. (2016). The Physiology of Adventitious Roots. *Plant Physiology, 170*, 603-617.

Stokes, G. G. (1847). On the theory of oscillatory waves. *Transactions of the Cambridge Philosophical Society, 8*, 441-455.

Svendsen, I. A., Madsen, P. A., & Hansen, J. B. (1978). Wave characteristics in the surf zone. *Proc. 16th Coast. Engrg. Conf., 1*, 520-539.

Tajziehchi, M. (2006). *Experimental and numerical modelling of wave-induced current and wave transformation in presence of submerged breakwaters.* PhD Doctorate Thesis, University of New South Wales, Faculty of Engineering.

Temmerman, S., Meire, P., Bouma, T. J., Herman, P. M., Ysebaert, T., & De Vriend, H. J. (2013). Ecosystem-based coastal defence in the face of global change. *Nature, 504*, 79-83.

Thampanya, U., Vermaat, J. E., Sinsakul, S., & Panapitukkul, N. (2006). Coastal erosion and mangrove progradation of Southern Thailand. *Estuarine, Coastal and Shelf Science, 68*(1-2), 75-85.

Toffoli, A., & Bitner-Gregersen, E. M. (2017). Types of Ocean Surface Waves, Wave Classification. In J. Calrton, P. Jukes, & C. Yoo-Sang, *Encyclopedia of Maritime and Offshore Engineering* (pp. 181-188). John Wiley & Sons, Ltd.

UNEP-WCMC. (2015). Global distribution of saltmarsh (ver. 2.0) Unpublished dataset. Cambridge, United Kingdom: UNEP World Conservation Monitoring Centre.

Valiela, I., Bowen, J. L., & York, J. K. (2001). Mangrove Forests: One of the World's Threatened Major Tropical Environments. *BioScience, 51*(10), 807-815.

van Maanen, B., Coco, G., & Bryan, K. R. (2015). On the ecogeomorphological feedbacks that control tidal channel network evolution in a sandy mangrove setting. *Proceeding of the Royal Society A, 417*(2180).

van Oorschot, M., Kleinhans, M., Geerling, G., & Middelkoop, H. (2016). Distinct patterns of interaction between vegetation and morphodynamics. *Earth Surface Processes and Landforms, 41*, 791-808.

Van Rijn, L. C. (1993). *Principles of sediment transport in rivers, estuaries and coastal seas.* Amsterdam: Aqua Publications.

Van Rijn, L. C. (1993, 2012). *Principles of sediment transport in rivers, estuaries and coastal seas.* Amsterdam, the Netherlands: Aqua Publications.

Van Rijn, L. C. (2011). *Principles of Fluid Flow and Surface Waves .* Amsterdam: Aqua Publications.

Van Santen, P., Augustinus, P. G., Janssen-Stelder, B. M., Quartel, S., & Tri, N. (2007). Sedimentation in an estuarine mangrove system. *Journal of Asian Earth Sciences, 29*(4), 566-575.

Vu, M. T., Lacroix, Y., & Nguyen, V. T. (2018). Investigating the effects of sea-level rise on morphodynamics in the western Giens tombolo, France. *OP Conference Series: Earth and environmental Science, 167*, 8.

Waisel, Y. (1972). *Biology of Halophytes.* New York: Academic.

Wiegel, R. L. (1964). *Oceanographical Engineering.* Englewood Cliffs, N. J.: Prentice-Hall.

Willemsen, P. W., Horstman, E. M., Borsje, B. W., Friess, D. A., & Dohmen-Janssen, C. M. (2015). *Decreased resilience of mangroves stressed by human interference (Master's Thesis).* University of Twente.

Woodroffe, C. D. (1990). The impact of sea-level rise on mangrove shorelines. *Progress in Physical Geography: Earth and Environment, 14*(4), 483-520.

Xie, D. (2018). Research intro of Dynamic Mangrove Model - Regular Meeting with MANs. Utrecht University.

Yuvaraj, E., Dharanirajan, K., Jayakumar, S., & Saravanan. (2014). Geomorphic settings of mangrove ecosystem in South Andaman Island: A geospatial approach. *Journal of Earth System Science, 123*(8), 1819-1830.

Zhao, Z.-D., Lian, J.-J., & Shi, J. Z. (2006). Interactions among waves, current, and mud: Numerical and laboratory studies. *Advances in Water Resources, 29*(11), 1731-1744.

Zhou, Z., Ye, Q., & Coco, G. (2016). A one-dimensional biomorphodynamic model of tidal flats: Sediment sorting, marsh distribution, and carbon accumulation under sea level rise. *Advances in Water Resources, 93*, 288-302.

8 Appendix

Appendix A: Morphodynamic model settings

Parameter	Setting	Unit
Grid cell size	50 x 50	m
Grid cells in M-direction	240	-
Grid cells in N-direction	1	-
Reference date	01 01 2017	dd mm yyyy
Simulation start time	01 01 2017 00 00 00	dd mm yyyy hh mm ss
Simulation stop time	01 01 2027 00 00 00	dd mm yyyy hh mm ss
Time step	0.5	min
Boundary location	West	
Boundary quantity	Water level	
Boundary forcing type	Harmonic	
Thatcher-Harleman time lag	120	min
Gravity	9.81	m/s^2
Water density	1000	kg/m^3
Roughness formula	Chézy	
Chézy's coefficient	65	$m^{½}/s$
Stress formulation due to wave forces	Van Rijn (2004)	
Horizontal eddy viscosity	1	m^2/s
Horizontal eddy diffusivity	10	m^2/s
Sediment type	Cohesive	
Initial sediment concentration	0	kg/m^3
Sediment concentration at boundary	0.02	kg/m^3
Reference density for hindered settling	1600	kg/m^3
Initial sediment layer thickness at bed	10	m
Specific density	2650	kg/m^3
Dry bed density	500	kg/m^3
Fresh settling velocity	0.5	mm/s
Saline settling velocity	0.5	mm/s
Critical bed shear stress for sedimentation	1000	N/m^2
Critical bed shear stress for erosion	0.2	N/m^2
Erosion parameter	5e-5	$kg/m^2/s$
Morphological scale factor	30	-
Spin-up interval before morphological changes	1440	min
Minimum depth for sediment calculation	0.1	m
Threshold depth	0.1	m
Marginal depth	-999	m
Smoothing time	60	min
Advection scheme for momentum	Flood	

Threshold depth for critical flow limiter	1000	m
Advection scheme for transport	Cyclic	
Wave direction (Nautical)	270	°
Directional spreading	0	°
Bottom friction factor	0.02	-
Wave height to water depth ratio	0.55	-

Appendix B: Vegetation model parameters

Parameter	Value	Unit
Species name	Avicennia germinans	
Maximum age	300	yr
Critical value for mortality	0.5	-
Initial stem diameter	1.37	cm
C_d of stems	1.5	-
Root diameter	1	cm
Root height	15	cm
C_d of roots	1	-
Maximum number of pneumatophores	10000	-
Constant describing the increasing rate of the amount of pneumatophores, f_i	0.1	-
Maximum stem diameter	140	cm
Maximum shoot height	3500	cm
Constant controlling the decreasing rate of biomass fitness, d	-0.00005	-
Growth constant 1, G	162	cm/yr
Growth constant 2, b_2	48.04	-
Growth constant 2, b_3	0.172	-
Fitness ability constant 1, a	-16	-
Fitness ability constant 2, b	16	-
Fitness ability constant c, c	-3	-
Above-ground constant 1, α	0.14	-
Above-ground constant 2, β	2.4	-